PROBING CELLULAR PROTEIN COMPLEXES USING SINGLE-MOLECULE PULL-DOWN

BY

ANKUR JAIN

DISSERTATION

Submitted in partial fulfillment of the requirements
for the degree of Doctor of Philosophy in Biophysics and Computational Biology
in the Graduate College of the
University of Illinois at Urbana-Champaign, 2013

Urbana, Illinois

Doctoral Committee:

Professor Taekjip Ha, Chair, Director of Research
Professor Jie Chen
Professor Martin Gruebele
Assistant Professor Sua Myong
Assistant Professor Supriya Prasanth

Abstract

Cellular processes result from dynamic interactions between biomolecules. The gold standard method for investigating interaction between biomolecules is the pull-down assay. We have extended the conventional pull-down assay to its ultimate limit: the analysis of single biomolecular complexes. We achieve this goal by performing the pull-downs directly on to the surface of microscope slides and visualizing the captured biomolecules at single-molecule resolution using total internal reflection fluorescence (TIRF) microscopy. We name this technology single-molecule pull-down or SiMPull.

In one reification biotinylated antibody against the protein of interest is immobilized on a flow chamber. The flow chambers are passivated using a polymer coating such that the cellular components do not bind, and the immobilized antibody specifically captures the target protein. Cell lysates are diluted to obtain isolated molecules suitable for single-molecule imaging. The target molecules are fluorescently labeled either using a genetically encoded fluorescent protein tag or using antibodies, and imaged using a single-molecule TIRF microscope.

Using SiMPull we are able to discriminate between multiple association states of a protein as well as determine the stoichiometry of interaction. This technology is widely applicable to an array of biological contexts, and is suitable to analysis of endogenous protein complexes from animal tissue. In particular, we have used SiMPull to investigate the architecture and assembly of mechanistic target of rapamycin complexes.

The complexes captured from cell extracts on to our imaging chambers retain their functional activities: thus SiMPull can be used as a preparatory tool for single-molecule biochemical analysis on proteins that cannot be readily purified or reconstituted. Finally, we have extended this approach to the analysis of lipid-protein interactions.

To my parents

Acknowledgements

It takes a village to raise a child. This dissertation would not have been possible without the help and support I received from my co-workers, friends and family. I would like to express my sincere gratitude to everyone who has made this journey possible.

Foremost, I would like to thank my advisor Prof. Taekjip Ha. I feel extremely fortunate to have worked under his mentorship that brought the best out of me. His enthusiasm for science, meticulous attention to detail and the broad perspective are some of the qualities I hope to carry forward. I am very grateful to Prof. Ha for nurturing me through the last 6 years, and in many ways, he is my role model as a scientist as well as a person.

Prof. Jie Chen and Prof. Kevin Xiang generously opened their labs at very preliminary stages of this work, and without their support and guidance, this project would not have succeeded. Ruijie Liu and Biswa Ramani played a formative role in setting up the SiMPull technology. I am particularly thankful to Edwin Arauz for our excellent ongoing collaboration, and for patiently explaining me the intricate details of the mTOR system.

I am profoundly grateful to Prof. Jie Chen, Prof. Supriya Prasanth, Prof. Sua Myong and Prof. Martin Gruebele for the immense career guidance and support I have received from them all through my PhD.

I am very thankful to the ever-helpful colleagues in the Ha lab. I thank Kaushik Ragunathan for the uncountable discussions about science and beyond. Reza Vafabakhsh and Yuji Ishitsuka, my senior colleagues in the lab were my immediate mentors. I heartily thank Kyung-Suk Lee, Prakrit Jena, Jaya Yodh, Sultan Doganay, Salman Syed, Ben Leslie, Kyu Young Han, Vasudha Aggarwal, Hajin Kim, Jingyi Fei, Xinghua Shi, Sinan Arslan, Ibrahim Cisse, Jeehae Park and Matt Comstock for their support and insightful discussions. I am grateful to Vasudha Aggarwal for experimental assistance.

Table of Contents

Chapter 1

Introduction

1.1 Background

Cellular processes are the result of dynamic interplay of proteins acting in macromolecular assemblies. Nearly every major biological process such as DNA replication is performed by an assembly of 10 or more proteins functioning in concert (Alberts, 1998). The activities of proteins (or protein assemblies) are orchestrated by dynamic interactions that allow cells to detect, transmit and respond to physical or chemical stimuli (Barrios-Rodiles et al., 2005; Yamada and Bork, 2009). Understanding how proteins interact and function in the context of interacting partners is central for understanding cell function and regulation.

Numerous large scale studies have aimed to define the network of protein interactions or the *interactome* of yeast (Ito et al., 2001; Ho et al., 2002; Krogan et al., 2006; Gavin et al., 2006), drosophila (Giot et al., 2003; Formstecher et al., 2005) and humans (Stelzl et al., 2005; Rual et al., 2005; Gandhi et al., 2006). Databases such as IntAct and BioGRID mine published data to keep track of newly identified interactions and verification of known ones and have logged ~332,000 and ~290,000 binary interactions respectively (as of July 2013). It can be argued for every cell type and cell condition (cell cycle, stimulus, stress, nutrition…) there exists a unique interactome that determines the status of the cell. Defining this interactome and understanding its dynamics is the next frontier of biology (Przytycka et al., 2010).

1.2 Limitations of ensemble pull-down assay

One of the most widely used techniques for studying interacting proteins is the pull-down or the co-immunoprecipitation assay (Puig et al., 2001; Gingras et al., 1999). In the classical pull-down assay, the protein of interest or bait is selectively isolated from cell or tissue extracts. The

physiological binding partners of the bait protein, or the prey, co-purify with the bait protein. The identity of the prey proteins is determined using western blot or mass spectrometry (Figure 1a, b). This conceptually simple method has been the work-horse for probing protein interactions for several decades.

Though instrumental in discovery of new binding partners, the data from ensemble pull-down assay represents an average of protein complexes. Inside the cell, the same protein can associate with multiple partner proteins to achieve different functional states. For example, let us consider a simple situation where a protein A forms protein complexes with proteins B and C. From ensemble pull-down of protein A, one can identify that A interacts with proteins B and C, however, it is not determined whether all the three proteins are present in the same physiological complex (ABC) or AB and AC are two mutually exclusive protein complexes. In reality, each protein can potentially bind to many more partner proteins: recent analyses have revealed that each protein on an average has 5 binding partners in yeast (Grigoriev, 2003), or 6.24 in humans cancer cells (Kar et al., 2009).

Furthermore, in the ensemble pull-down assays, information about the stoichiometry of protein complexes is lost. Many proteins achieve a functional state after a stimulus dependent change in the oligomerization state: a recent survey suggests that 35% or more of the proteins in a cell are oligomeric (Ali and Imperiali, 2005). Similarly, one can determine the pair-wise interaction partners using yeast two hybrid (Fields and Song, 1989) or the complementation assays (Kerppola, 2006), but the physiological assembly of these interactions is not deciphered.

In the last few years, several techniques have emerged to bridge the gap between protein interaction registry and understanding their physiological permutations. For example, electron microscopy has revealed the architecture of intact ribosomes, proteasome (Lander et al., 2012) and so on. Mass spectrometry is extended to analysis of intact protein complexes (Zhou et al., 2011; Rose et al., 2012). Computational biologists have pieced together the information available from numerous experimental techniques to build models of large multi-component assemblies such as the nuclear pore complex (Alber et al., 2007) and the HIV viral capsid (Zhao et al., 2013). However,

these methods portray a static picture of the protein interaction networks and dynamics of protein interactions as it occurs within the cell is not recapitulated.

1.3 Single-molecule fluorescence microscopy

Over the last two decades, single-molecule manipulation technologies have matured into powerful tools and have provided remarkable insights about mechanisms underlying biological processes. The ability to manipulate and detect single biomolecules confers several important advantages over the ensemble approaches. First, it allows direct detection of sub-populations and their dynamics. For example, single-molecule fluorescence analysis of protein folding revealed the transition states and transition path times (Chung et al., 2012). Rare or transient states are usually averaged out in the ensemble measurements but can be accessed in the single-molecule experiments. Second, single-molecule detection allows synchronization of otherwise non-synchronizable dynamics. The motion of molecular motors such as myosin on actin filaments or nucleic acid translocases on DNA or RNA cannot be readily synchronized and single-molecule imaging methods have been extensively applied to investigate these motor proteins (Ha et al., 2012; Veigel and Schmidt, 2011; Myong et al., 2005). Third, single-molecule detection allows correlation of multiple parameters: for instance, the force exerted by a helicase molecule can be correlated with its translocation activity (Lee et al., 2013). Finally, single-molecule experiments inherently require lower amount of sample as compared to ensemble methods.

However, these methods have been primarily limited to in vitro purified biomolecules or re-constituted protein complexes. Recent advancements have allowed application of single-molecule fluorescence microscopy (Reyes-Lamothe et al., 2010) and force spectrometry (Rai et al., 2013; Blehm et al., 2013) to live cells. However, these experiments are technically challenging and require significant expertise both in instrumentation as well as sample handling.

1.4 Conceptualization of single-molecule pull-down

We argued that if we can combine the conventional pull-down assays with single-molecule visualization, we will be able to detect the heterogeneity in protein interactions (Figure 1c). For the

proteins A, B and C, if each of the proteins B and C are labeled with fluorophores, single fluorophore co-localization will allow us to directly distinguish between AB, AC and ABC type configurations (Figure 1d). Second, photobleaching of fluorophores is a stochastic process. When the proteins are labeled at known ratio, by monitoring the fluorescence time trajectories of individual molecules, we can determine the copy number of each protein in the complex (Figure 1e) (Coffman and Wu, 2012; Ulbrich and Isacoff, 2007). Lastly, we will be able to extend single-molecule technologies to in vivo protein complexes.

We have successfully combined the pull-down assays with total internal reflection fluorescence microscopy based single fluorophore detection: we name this hybrid technology single-molecule pull-down or SiMPull. Briefly, using antibody against the protein of interest immobilized on a single-molecule fluorescence imaging chamber, we are able to specifically capture the target protein. The detailed methodology for performing the SiMPull assay is outlined in Chapter 2, and the proof-of-concept on model systems and advantages of SiMPull over ensemble pull-down are presented in Chapter 3. The SiMPull technology is widely applicable to proteins from variety of cellular contexts and organisms, and has provided novel stoichiometry information on numerous systems as we demonstrate in Chapters 4 and 5. SiMPull as a preparatory tool extends the reach of single-molecule imaging experiments to proteins that are not available in purified or reconstituted forms as exemplified in Chapter 6. Lastly, by using liposomes as baits for capturing proteins from cell extracts we have developed a new methodology to study lipid-protein interactions. This conceptually simple yet powerful approach can potentially provide far-reaching insights in understanding of biological systems.

1.5 Overview

Over the last couple of years, numerous technologies have been developed for single-molecule analysis of proteins and protein complexes in cell extracts, particularly using single-molecule fluorescence imaging. Hoskins et al. probed the assembly of spliceosomes using SNAP-tag labeled proteins in yeast extracts (Hoskins et al., 2011). Single-molecule experiments in frog oocyte extracts have revealed the dynamics of DNA replication (Yardimci et al., 2012). Yeom et al. used

immuno-purified TUT4 to investigate the kinetics of microRNA poly-uridinylation, while Lee et al. probed the dynamic interaction of Ras with Raf at 50 ms time-resolution. In single-molecule force spectroscopy, researchers were able to trap organelles within cell extracts and investigate the forces exerted by molecular motors. Experiments in cell extract may present the new frontier for single-molecule technologies: this semi-vivo approach may help bridge the gap between the in vitro and in vivo methodologies.

1.6 Figures

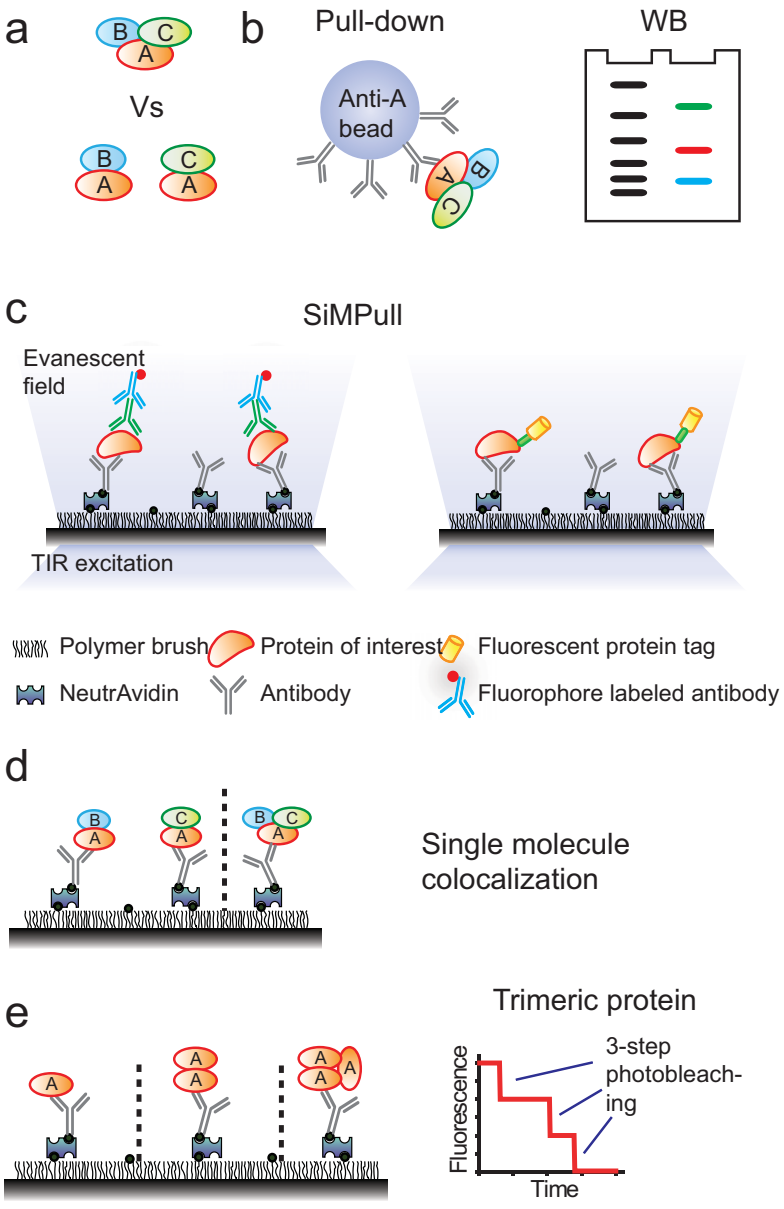

Figure 1.1 Comparison of conventional pull-down with SiMPull. (a, b) Ensemble pull-down cannot distinguish between different association states of protein A. (c) Schematic for SiMPull. (d) AB, AC and ABC type complexes can be discriminated by single-molecule co-localization. (e) Single molecule fluorescence photobleaching analysis reveals the stoichiometry of protein complex.

Chapter 2*

Experimental Strategy

In this chapter, I describe the general protocol for the SiMPull assay. I discuss the strategy we use to specifically pull-down the proteins of interest from crude extracts, fluorescent labeling of proteins, data acquisition and analysis. The protocol is designed for antibody based pull-down of cytosolic/soluble proteins. Modifications in sample preparation for proteins from other cellular contexts are discussed in Chapter 4. The advantages and potential pitfalls of SiMPull and the requisite control experiments to rule out false positives are listed.

2.1 Single fluorophore imaging

We use a prism-type total internal reflection fluorescence microscope (TIRFM) equipped with an electron-multiplying charge-coupled device (EM-CCD) for single-molecule imaging. The TIR illumination creates an evanescent field of excitation light that extends only 100–200 nm from the surface, and hence, almost exclusively excites the fluorophores tethered to the surface (Funatsu et al., 1995; Roy et al., 2008). Thus, TIR excitation significantly reduces the background from fluorophores in solution, and the technique has been widely applied for single-molecule microscopy (Joo et al., 2008). Although all experiments in this dissertation were performed using a prism-type TIRF microscope (Figure 2.1), several labs have successfully adopted SiMPull in commercial or home-built objective-type TIRFM systems (Kim et al., 2013b; Padeganeh et al., 2013) (Maximilian Ulbrich, personal communication).

*This work in Chapter 2 has been published as the following paper:

- Jain A, Liu R, Xiang Y and Ha T, "Single molecule pull-down for studying protein interactions", *Nature Protocols* **7**, 445-452 (2012).

TIRF microscopy

We adapted an inverted microscope to hold a trapezoid fused-silica prism on top of the microscope slide (Roy et al., 2008). Figure 2.1 depicts a schematic of the instrument used for SiMPull experiments. Briefly, the excitation laser beam is directed towards the objective through the prism at an incidence angle greater than the critical angle (68°). The prism is index matched with the flow chamber using immersion oil, such that the evanescent excitation field is created at the quartz-aqueous buffer interface. An x60 water immersion objective (NA = 1.2) is used to collect the fluorescence signal. The scattered light is rejected using suitable emission filters. The emitted light is imaged onto a 512 x 512 pixel EM-CCD after x2 image expansion. The final pixel size in the imaging place is ~140 nm. The excitation laser intensity is modulated using a half-wave plate and a polarizing beam splitting cube to achieve a final intensity of 0.5 – 3 $W\text{-}m^{-2}$ at the quartz-aqueous buffer interface, so as to obtain a 5-10 fold signal above the background noise. Multi-color imaging is achieved using different and spectrally separated fluorophores, and corresponding excitation sources and emission filters. For YFP (yellow fluorescent protein) excitation, we used a 488 nm laser and a band pass (535/30) emission filter; mCherry or red fluorescent proteins (RFPs) were excited either at 532 nm or 568 nm and fluorescence signal was collected using a 607/36 band pass filter.

Data acquisition and analysis

Fluorescence signal is recorded using custom software written in Visual C++ (written by Kyung Suk Lee, Ha lab). The software acquires movies as series of frames at specified time-resolution. Single molecule time trajectories are extracted from the movies using scripts written in IDL. The program creates an averaged image of the first 10-frames, and identifies single molecules as intensity maxima greater than a predetermined threshold. The algorithm also fits a Gaussian point-spread function to the identified molecules to avoid including multiple molecules or aggregations into the analysis. Next, the local background is subtracted and intensities from 7 by 7 pixels surrounding the peak are added to obtain intensities of single molecules, with or without a Gaussian weighing factor. The extracted single-molecule time trajectories and mean fluorophore count per movie are analyzed using custom MATLAB codes.

2.2 Surface passivation

A key aspect of any pull-down assay is the selective isolation of the proteins of interest on a matrix. The bait recruiting matrix should (1) specifically capture the target proteins and (2) be refractory to other biomolecules present in whole cell extracts. We achieve these goals by coating microscope slides and cover slips with methoxy polyethylene glycol (mPEG). PEG is a long chain biocompatible polymer, and a uniform PEG coating substantially reduces the binding of proteins to the glass surfaces (Roy et al., 2008; Fleminger et al., 1990). A small amount (2-5%) of biotinylated PEG is added during the slide preparation: biotin PEG functionalizes the surface and allows specific immobilization of biotinylated biomolecules using an avidin linker. I will briefly discuss the strategy commonly used in our lab to passivate quartz/glass surfaces. In the first part, the glass or quartz substrate is functionalized with an amine group using an aminosilane. Second, the amine group of aminosilane is reacted with NHS-ester PEG.

Surface silanization

Silanes are monomeric silicon compounds and have been extensively used to functionalize glass surfaces. The silicon atom in the silane is attached to four substituent groups that can be non-reactive or exhibit reactivity towards inorganic (glass) or organic compounds. Our silane of choice is N-(2-Aminoethyl)-3-aminopropyltrimethoxysilane that contains three hydrolyzable propyl groups and one non-hydrolyzable amine functional group.

The silica substrate (quartz or glass) is cleaned and activated by treatment with KOH. KOH etches glass surfaces and exposes the active hydroxyl groups. The silane reaction with an activated glass surface involves four steps (Figure 2.2): (1) Silane is hydrolyzed and forms the reactive silanol group. (2) The silanol groups condense together to form silanol oligomers. (3) The oligomers then hydrogen bond with OH groups of the substrate. (4) Finally, the surfaces are allowed to dry or are thermally cured during which a covalent linkage is formed between the surface and the organic group, and a water molecule is released. In a common protocol for PEG passivation, slides are burnt using a propane torch prior to silanization. Heating at higher temperature incrementally removes silanol groups from siliceous surfaces, thus deactivating them for reaction with silane (Emoto et al.,

1996; Wan et al., 2010). Moreover, heating at higher temperatures over 300°C may permanently deactivate the surfaces (Wan et al., 2010), and is not advisable.

PEG passivation

The amine functionalized surfaces are reacted with mPEG with an active N-hydroxysuccinimide (NHS) ester group. Instead of a direct linkage between mPEG and NHS ester, these two groups are connected via an alkyl chain. The alkyl chain provides a sterically hindered active ester group: reactivity of the ester group can be modulated by changing the length of the linker region (Roberts et al., 2002). Additionally, upon reaction with amine group, the alkyl chain linked NHS-ester yields a stable amide linkage. Our mPEG-NHS-ester of choice is mPEG-SVA (succinimidyl valerate) with a hydrolysis lifetime of ~10 min at pH 8.5 at room temperature (Revyakin et al., 2012). During surface preparation, mPEG-SVA is mixed with 2-5% biotin-PEG-SVA to yield biotin functionalization. The preferred molecular weight of PEG is 5,000 (~110 monomers).

2.3 Sample preparation

SiMPull is performed using the same samples (purified proteins, tissue or cell lysates) as used for a conventional pull-down analysis. Extracts are typically prepared by lysing cultured cells or tissues with detergents. We have tested a variety of detergents and cell types for SiMPull analysis (Jain et al., 2011) (see Chapter 3), as well as non-detergent lysis methods. Similar to the conventional pull-down assays, it is critical to use non-denaturing conditions in order to preserve the physiological interactions that may occur. We avoid SDS and other strong ionic detergents for lysis as they can potentially denature the immobilized antibodies or disassemble protein complexes. Sonication of samples leads to protein aggregation and is not recommended for cell lysis. For detergent sensitive samples such as membrane proteins, we typically use either a mild detergent (such as digitonin) or dounce homogenization.

2.4 Protein capture and detection

Protein pull-down

The selective capture of the bait protein is achieved using surface immobilized antibodies. We construct flow chambers on the PEG passivated slides (Figure 2.3). The biotin-doped surfaces are saturated with NeutrAvidin, and biotinylated antibody against the bait protein is immobilized at a concentration of 10-20 nM. It is often difficult to label the primary antibody with biotin. Many primary antibodies are supplied either as sera or in buffer with BSA as stabilizer and are hence, not suitable for labeling reactions. For immobilizing unlabeled antibodies, we use a biotinylated secondary antibody on the surface that can recruit the primary antibody against the bait protein. Secondary antibodies against one species can often cross-react with other species unless they have been specifically adsorbed to minimize cross-reactivity. For assays involving multiple antibodies, we use cross-adsorbed and affinity purified antibodies.

For imaging single molecules, the protein of interest must be immobilized at sufficiently low density such that the bait molecules are well separated on the slide surface. Cell lysates typically require dilution to obtain this low density. As the concentration of the protein of interest in the lysates is not known a priori, and also varies across preparations, it is difficult to predict the appropriate dilution factor for the lysate. We use an iterative approach: we choose a suitable starting point and then titrate the concentration of lysate to obtain 0.1 - 0.2 molecules-μm^{-2} imaging area upon 20 min incubation on the antibody coated surface. In this regime, the density of antibody molecules on surface is at least 100-fold higher than the concentration of immobilized bait/prey molecules and hence, the protein capture is not limited by the availability of binding sites. Figure 2.4 illustrates how this dilution factor is decided for a YFP tagged protein.

Protein detection

The target protein can either be chemically conjugated with a fluorophore, or labeled via antibodies (Figure 2.5). In one approach, the protein of interest can be expressed as fluorescent protein (FP) fused chimera and can be directly visualized under TIRFM. Labeling with FP tags ensures one-to-one labeling and we have utilized YFP tag for determining stoichiometry of a variety

of proteins (Means et al., 2011; Panter et al., 2012; Shen et al., 2012). However, FPs exhibit low photostability and cannot be used to monitor the temporal dynamics of proteins for extended period. Additionally, many FPs exhibit multiple emission states that may complicate stoichiometry analysis (Hendrix et al., 2008). So far, we have not been able to identify a suitable FP besides eYFP/eGFP for photobleaching analysis. Another approach is chemical conjugation of organic fluorophores using genetically encoded polypeptide tags: others and us have successfully utilized SNAP-tag (Hoskins et al., 2011) and aldehyde-tag (Shi et al., 2012) to specifically label proteins in whole cell extracts. Advances in genetically encoded fluorophore conjugation schemes such lipoic acid ligase mediated labeling (Yao et al., 2012) or FlAsH/ReAsH(Adams et al., 2002; Machleidt et al., 2007) chemistry should enable conjugation of bright and photostable organic fluorophores to target proteins using a relatively small epitope tags.

The immobilized proteins can also be detected via fluorophore conjugated antibodies in a sandwich assay scheme. Typically, 5-10 nM of primary detection antibody is incubated on the immunoprecipitated protein for ~20 min, followed by a fluorophore conjugated secondary antibody at 0.1-2 nM for 5 min. This approach allows detection of endogenous proteins without any modifications. However, antibodies may not bind to all the epitopes and this method does not ensure a stoichiometric labeling. We prefer to use antibodies suitable for immunoprecipitation or immunofluorescence applications as these antibodies generally recognize epitopes in folded proteins (unlike WB where the protein is unfolded). Antibodies are large (150 kDa) and the epitope may not be exposed due to surface immobilization. Advances in high-affinity single-chain antibody development, such as camelid nanobodies (Ries et al., 2012), or nucleic acid aptamer based detection may allow sensitive and stoichiometric detection of endogenous proteins (Gold et al., 2010; Loffredo et al., 2013).

2.5 Advantages of SiMPull

SiMPull allows direct detection of individual proteins and thus we can discriminate between multiple association states of a protein. It provides quantitative data on the bait and prey protein populations. Each molecule contributes only once irrespective of the excitation intensity or camera

gain, unlike WB where the intensity of the protein band is determined relative to a control and absolute quantification is difficult. SiMPull also allows us to determine the stoichiometry of the complexes by photobleaching step analysis (Ulbrich and Isacoff, 2007; Jain et al., 2011). The prepared complexes may also be used for biochemical analysis of their activities at the single-molecule level: thus, SiMPull can be used as a preparatory tool to study the functional activity of protein complexes that are not accessible through recombinant methods, as we demonstrate in Chapter 6. In addition, SiMPull promises improvement by orders of magnitude in cost, time and sensitivity over conventional western blotting. The method is generally applicable to a wide variety of cellular contexts and can be tailored to any alternative pull-down or fluorophore-labeling schemes.

2.6 Pitfalls of the SiMPull assay

Unlike western blot analysis, SiMPull does not separate biomolecules on the basis of their size, and it relies solely on fluorophore-based detection. Hence, in reality, SiMPull is similar to dot-blot or ELISA. Appropriate controls are necessary for correct interpretation of the data. We typically perform control experiments by replacing each of the capture or detection antibodies with the corresponding control antibodies and by using control lysates without bait or prey protein expression. As in conventional pull-down assays, additional controls (for example, mutations that prohibit binding between the bait and the prey proteins) may be performed, depending on the context.

The quality of passivation has an important role in determining the specificity of pull-down. Although the PEG surfaces substantially reduce the nonspecific binding, it will occur at protein concentrations >100 nM. Also, antibodies may bind nonspecifically to pulled-down proteins or may cross-react, leading to false positives, and suitable controls are essential to ensure that the observed fluorescence arises from the relevant interaction.

In its current form, SiMPull is applicable when one already knows the anticipated binding partners, and it cannot be used as a discovery tool. Lysates are typically diluted to obtain a

sufficiently low protein concentration for single-molecule imaging. Accordingly, weak interactions with dissociation rate constants of > 0.01 s^{-1} may not be suitable for the method (see Chapter 3).

2.7 Figures

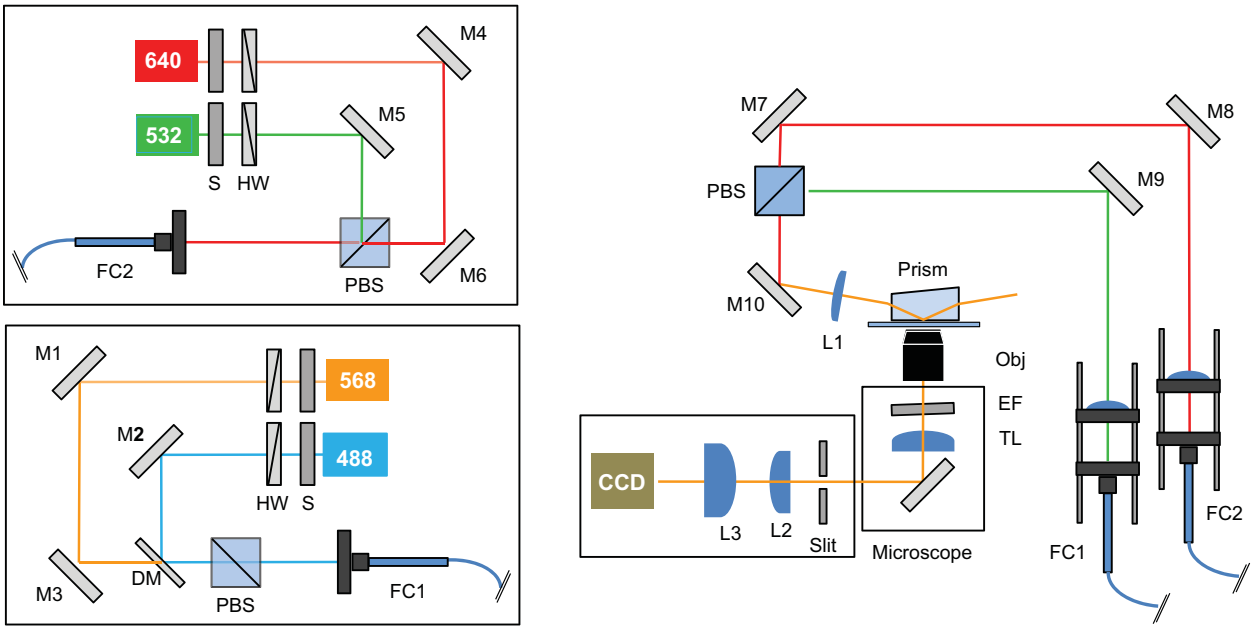

Figure 2.1 Optical lay-out for prism-type TIRFM used for SiMPull. DM: Dichroic mirror, EF: Emission filter, HW: Half-wave plate (λ/2), L1-3: Achromatic lens, M1-5: Mirror, Obj: Objective lens (water: NA 1.2, PBS: Polarizing beam-splitter, S: Shutter, TL: Tube lens, FC: Fiber optic beam coupler (Figure courtesy of Felix Tritschler).

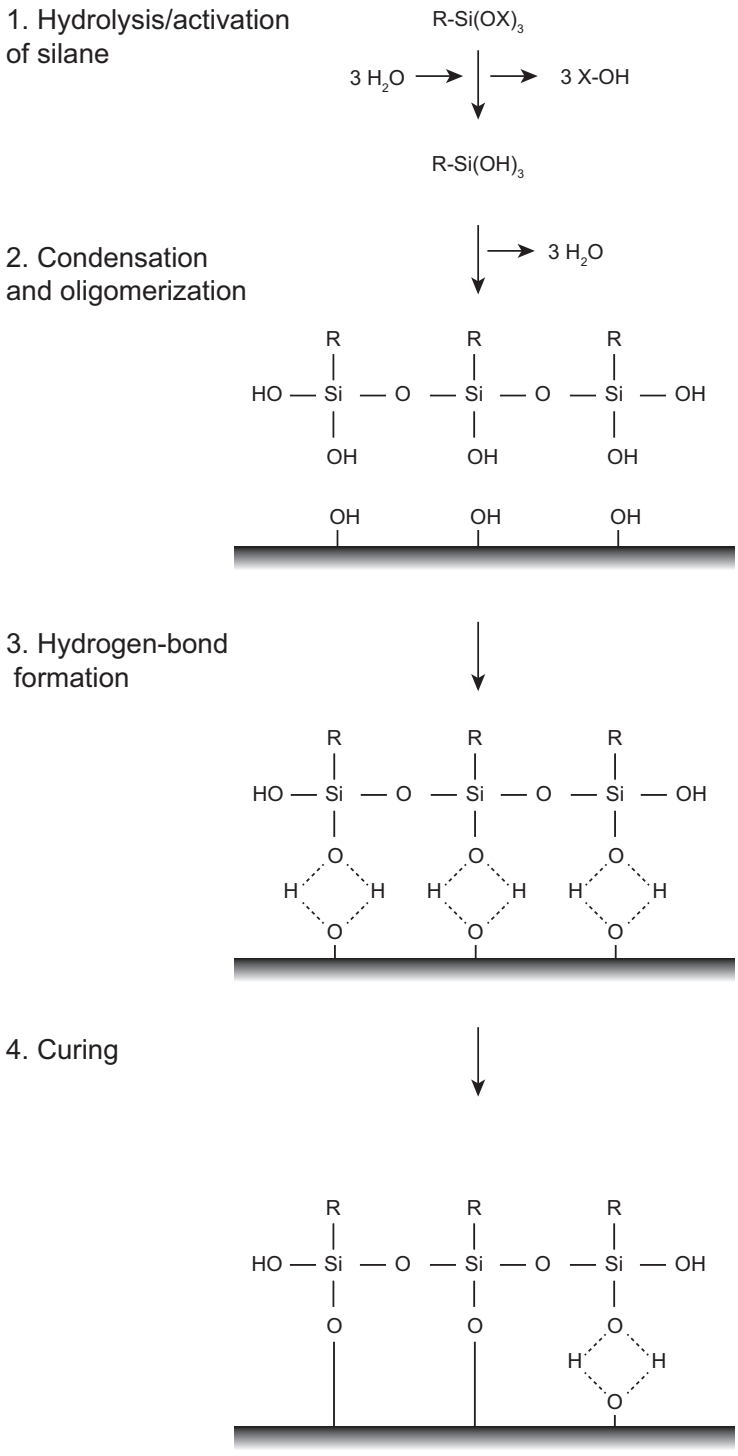

Figure 2.2 Schematic for the silanization of silica substrates.

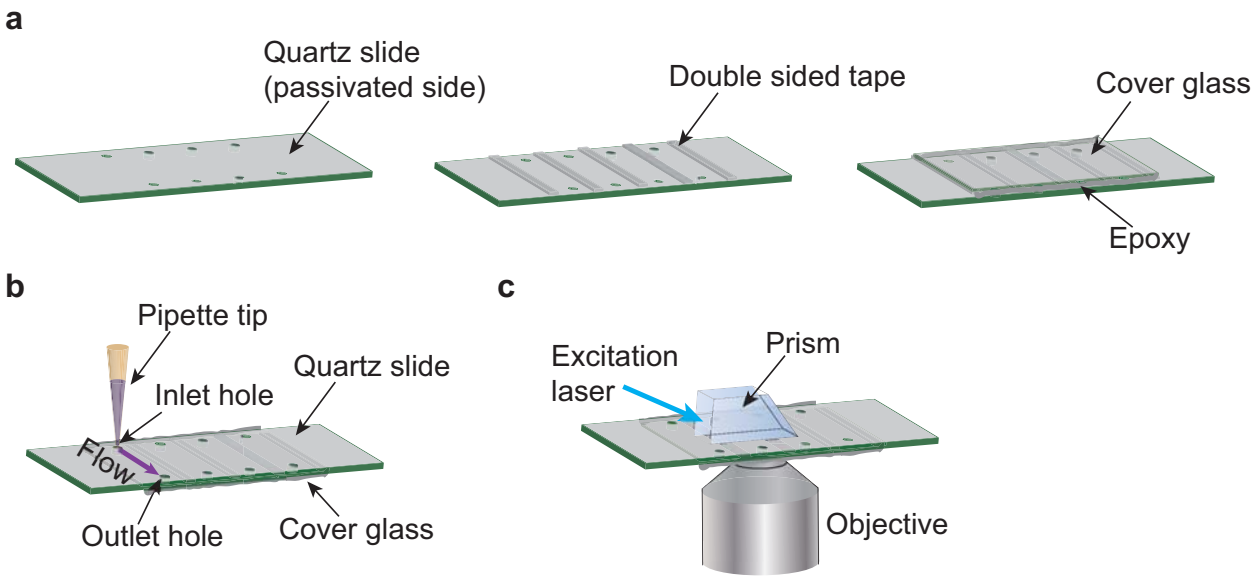

Figure 2.3 Preparation of flow chambers. (a) To assemble the flow chamber, place the quartz slide with the passivated side facing up. Put double-sided tape between the successive holes to create channels. Place the cover glass on top of the tape, and seal the edges with epoxy. (b) The holes on the slides are used for flowing solutions through the chamber using a pipette. (c) The prism is placed on top of the slide to create an evanescent excitation field at the quartz-aqueous buffer interface.

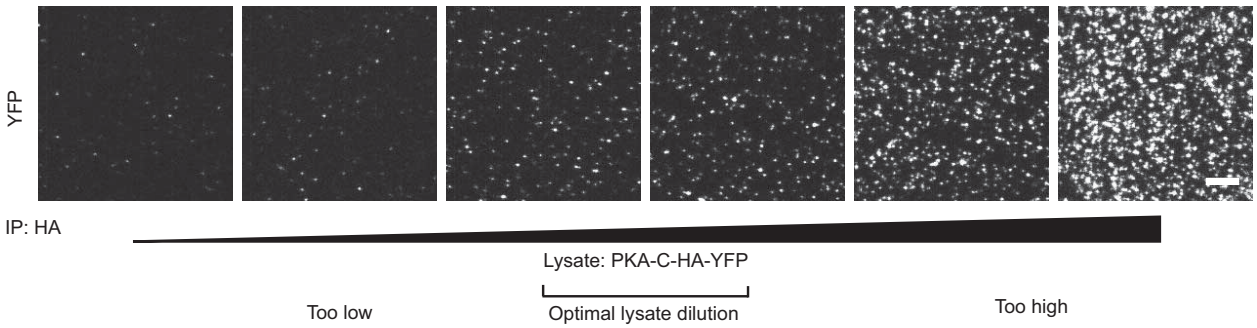

Figure 2.4 Determination of lysate dilution factor. The lysate concentration is serially increased starting with a 5,000-fold dilution (second from left), to a 250-fold dilution (right). Image in left depicts background. The optimal fluorophore density for resolving single fluorophores is 0.1 – 0.2 fluorophores per μm^2 as depicted in the center two images. Scale bar is 5 μm.

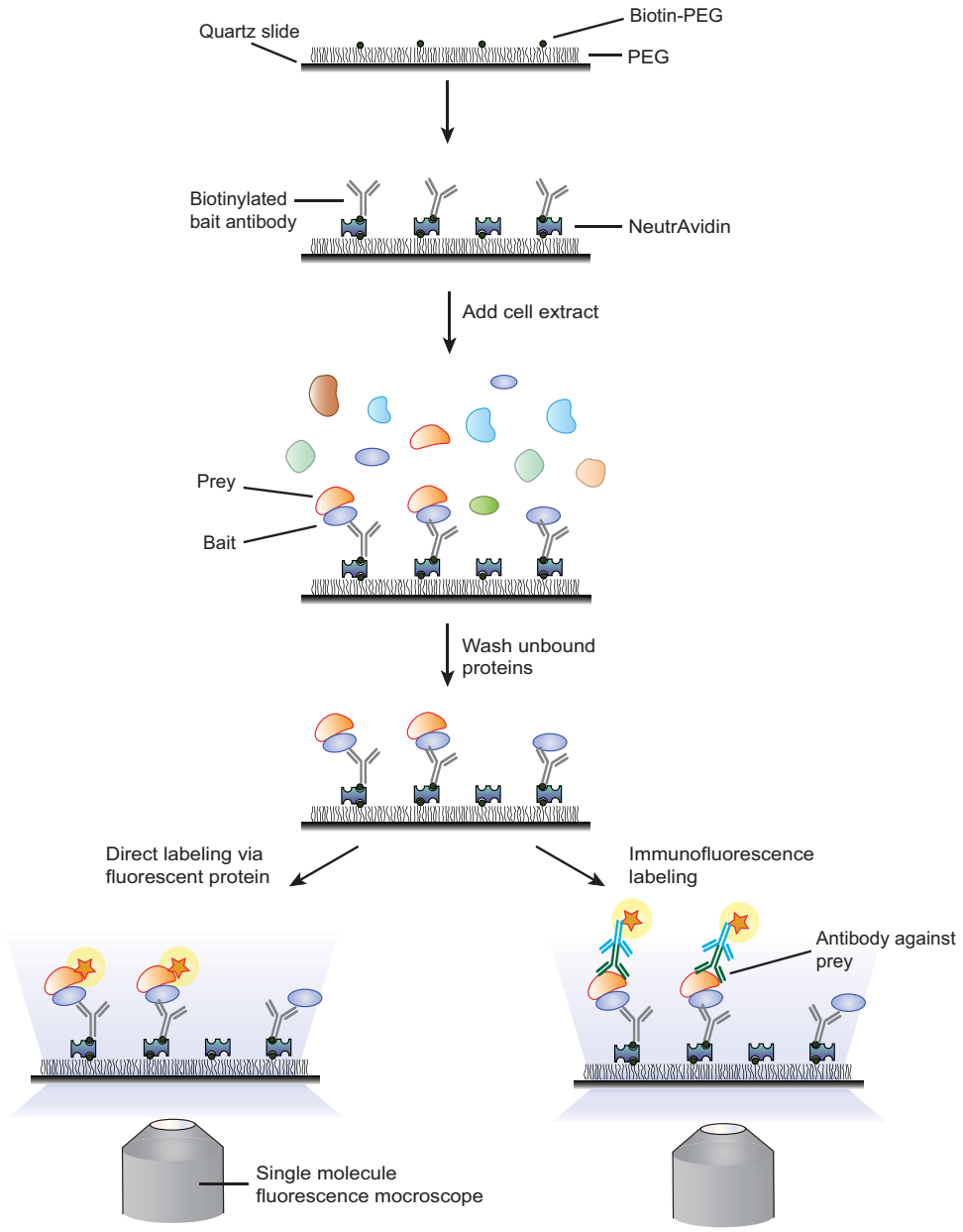

Figure 2.5 Schematic for single-molecule pull-down. Microscope slides and coverslips are passivated with PEG, doped with biotin-PEG. Antibodies against the bait protein are immobilized using NeutrAvidin. When cell extract is added to the chamber, the surface immobilized antibody captures the bait protein, together with the prey. Other cellular components do not bind and are washed away. When the prey protein bears a fluorescent protein tag, it can be directly visualized using a single-molecule fluorescence microscope. Alternatively, the pulled down complexes can be labeled via immuno-labeling for prey protein detection.

Chapter 3*

Proof-of-Concept

In this chapter, I present the initial experiments we performed to validate our SiMPull approach. Briefly, purified proteins were compared against lysates, and we performed single-molecule co-localization analysis on a well-characterized protein complex: protein kinase A (PKA). The advantages of SiMPull over conventional biochemical methods are discussed through these model systems.

3.1 SiMPull validation using YFP

We first validated SiMPull for specific capture of the protein of interest from cell extracts. As a proof-of-principle, we started with lysate from cells expressing YFP and compared it against the purified protein. YFP was poly-histidine tagged for affinity purification. When 100 pM purified YFP is applied to flow chambers coated with anti-His antibody, we observe YFP fluorescent spots (Figure 3.1). The number of observed spots increases on increasing the protein concentration. The slide surface without any immobilized fluorescent protein yields significantly fewer fluorescent spots per imaging area, 2500 μm^2 (~30 spots), possibly due to impurities during surface preparation. The binding is antibody specific and the number of fluorescent spots observed on the control antibody (anti-FLAG) is comparable to the blank slide surface.

Next, we expressed the poly-histidine tagged YFP in HEK293 cells. Cells were lysed using 0.5% NP-40 in the lysis buffer. When an appropriate dilution of this lysate is flowed through the

*This work in Chapter 3 has been published as the following paper:

- Jain A, Liu R, Ramani B, Arauz E, Ishitsuka Y, Ragunathan K, Park J, Chen J, Xiang Y, & Ha T, "Probing cellular protein complexes using single-molecule pull-down", *Nature* **473**, 484-488 (2011).

chamber coated with anti-His antibody, we observed single YFP molecules (Figure 3.2), similar to the purified protein. When YFP lysate was added to chamber coated with the control antibody (anti-FLAG), we observed minimal increase in fluorescence spots above background. Even lysates at10-fold higher concentration yielded ~30 additional spots above blank, implying less than 0.5% non-specific adsorption of protein. Control cell lysates, without YFP expression, yielded similar increment in fluorescent background. Thus, the fluorescent protein density of specific pull-down of proteins was 5-10 higher than the background, which was kept all throughout our experiments by suitably diluting the lysates. We verified that the binding of YFP to the antibody is stable over two hours and the pulled down proteins do not readily dissociate from the antibody even after multiple washes with physiological buffers (Figure 3.3). In summary, the PEG passivated surfaces exhibit minimal non-specific binding and can be used for specific immuno-precipitation of the protein of interest from whole cell extracts.

3.2 Direct quantification of proteins

One clear advantage of SiMPull is that it allows sensitive and quantitative detection of proteins. The protein quantification does not depend on the camera gain or the intensity of excitation light, as each immobilized molecule contributes just once. We asked if we can use SiMPull for determining the concentration of proteins in dilute whole cell extracts. The binding of purified YFP to anti-His antibody increases with increase in protein concentration (Figure 3.4). At low concentrations, the number of spots observed scales linearly with the protein concentration as we demonstrate for Alexa488 labeled purified SNAP protein immobilized via anti-SNAP antibody (Figure 3.5). Thus, the antibody coated slides can be calibrated using known concentrations of the protein of interest. When a lysate with unknown concentration of SNAP or YFP tagged protein is applied to these antibodies, we can determine the unknown concentration by comparing the number of observed spots against the calibration with the purified protein. The binding affinities of the antibodies vary widely and therefore, each antibody needs to be separately calibrated for concentration determination.

Finally, if the number of cells used for lysate preparation is known *apriori*, we can use SiMPull to determine the concentration of a given protein in the cell extract, and thus calculate the average copy number of the protein per cell. We have used this approach to determine the concentration of SNAP tagged proteins in *methanosarcina* (Chapter 4).

3.3 Characterization of SiMPull surfaces

The spot counts on SiMPull flow-chambers are reproducible. For the same antibody-antigen pair, when we apply equal concentration of antibody (~10 nM) and the protein of interest, the number of spots observed are within 20% of one another on different channels on the same flow chamber or between different slides (Figure 3.6). Thus, only the affinity of the antibody determines the efficiency of pull-down. Furthermore, the calibration curves are similar on different batches of slide: we calibrated different batches of slides for determining the concentration of a SNAP tagged protein. For two different batches, we observed a 3-fold change in the background fluorescence (possibly due to different amount of impurities during slide preparation) but the scaling factor from the concentration of the protein to the spots per imaging area were within 10% (Figure 3.7). In general, we are able to repeatedly use the same dilution of the lysate on different days of experiment, as long as the expression level is the same. The antibody concentration on the surface is in huge excess of the immobilized protein (Figure 3.8), and upon 15-30 min incubation, the binding of the protein is at equilibrium and does not significantly vary across experiments on different slides or days.

3.4 Stoichiometry determination

Single molecule fluorescence photobleaching analysis can be used to determine the stoichiometry of the labeled proteins (Ulbrich and Isacoff, 2007; Leake et al., 2006). When we analyzed the fluorescence time trajectories of YFP pulled down via anti-His antibody, we find that most molecules exhibited a constant fluorescence intensity level that bleached down to the background level in a single imaging frame. Sample monomeric YFP fluorescence traces are shown in Figure 3.9. A vast majority of the molecules (93%) bleached in a single photobleaching step

(Figure 3.10). Nearly 7% of the molecules bleached in two photobleaching steps. The observed 2-step bleaching events can be likely attributed to false-colocalization of two or more molecules. We ran a simulation where 400 molecules (working density) were randomly localized on a 256 by 512 pixel array (camera array size). Molecules lying within 2-pixel distance were said to be "co-localized", as the pixel size in our assays is ~140 nm: 2-pixel distance corresponds to the diffraction limit. If two or more molecules localize within 2-pixel distance, they will appear as a single spot that bleaches in multiple steps. From the simulation, the expected co-localization is 4 ± 1% at our molecule immobilization density (400 spots per imaging area). This matches to a reasonable degree with our experimental results of 7% two-step photobleaching.

We prepared a tandem dimeric YFP (tdYFP) construct where two YFP molecules are fused to each other at a genetic level. We performed similar experiments and analyzed the photobleaching behavior of tdYFP pulled down from cell extracts. A majority of tdYFP molecules (59%) bleached in two discernible steps, while about 37% exhibited one-step bleaching (Figure 3.9, 3.10). This distribution is consistent with previous reports (Ulbrich and Isacoff, 2007) indicating that only about 75% of YFP is actively fluorescent.

Corrections for photobleaching step analysis

If each YFP molecule is active with a probability of 0.75, for a dimer, the fraction of molecules with both YFP as actively fluorescent (and thus bleaching in 2-steps) is 0.75*0.75 or ~56%. Several corrections need to be applied to quantitatively determine the exact fraction of dimers: only the molecules with one active YFP (~94%) are visible; multiple molecules may bleach within the same imaging frame (~5%); a fraction of molecules (~10%) is the background spot count most of which bleach in a single photobleaching step and ~5-10% of molecules may exhibit false co-localization by chance. Finally, the exact fraction of actively emitting YFP also varies from one preparation to another, and is usually between 70-80% (Tombola et al., 2008). The traces are manually scored for the number of observed photobleaching steps. Each molecule is scored as having 1-4 steps. If the number of steps cannot be reliably identified, the trace is 'rejected' and a separate count is maintained. After scoring all the traces, the fidelity of the scoring is verified by plotting the

intensity of the molecules: on average, the molecules exhibiting two photobleaching steps should be twice as bright as the ones bleaching in a single step (Figure 3.10).

Again, only a small fraction (<5%) bleached with 3 or more steps, which reinforces the notion that we are pulling down single protein entities and not protein aggregates. The fluorescence time traces and the distribution of photobleaching step for proteins from cell extract were equivalent to those obtained from purified proteins (Figure 3.10). Thus, using SiMPull we are able to specifically capture the target protein and determine its stoichiometry.

3.5 Multi-color SiMPull of PKA complex

Next, we tested if we can use SiMPull to pull down single protein complexes from cell extracts. We used cyclic adenosine monophosphate (cAMP)-dependent protein kinase A (PKA) as our model system. PKA is a ubiquitous serine/threonine kinase that acts downstream of G-protein coupled receptor (GPCR) pathway (Collins et al., 1991). In the inactive state, PKA forms a tetrameric enzyme complex consisting of two regulatory (R) and two catalytic (C) subunits. In the presence of cAMP, the complex disassembles and the regulatory subunits release the catalytic subunits, thereby activating the enzyme. We used mCherry, a red fluorescent protein, as a second color in conjunction with YFP for our 2-color SiMPull experiments. We prepared C-HA-YFP and R-Flag-mCherry constructs and transfected these in HEK293 cells; using conventional biochemical analysis we ensured that the modified constructs assemble as the PKA complex and dissociate upon cAMP treatment (Figure 3.11a).

mCherry spectrum is shifted by ~100 nm as compared to YFP. We used different excitation wavelengths to independently excite YFP or mCherry: YFP was excited at 488 nm and emission was detected using a band pass filter (520 – 550 nm). mCherry was excited at 532 nm or 568 nm and mCherry emission channel was limited to 590 nm – 625 nm. Control experiments with samples containing C-HA-YFP did not show any detectable fluorescence above background in mCherry channel and vice versa (Figure 3.12).

When only C-HA-YFP was expressed in cells, using surface immobilized antibodies against HA- or YFP-epitope, we were able to pull down the protein specifically as detected via YFP fluorescence (Figure 3.11b). The control lysate or the C-HA-YFP lysate when applied to control antibodies (against a tag not present on protein), shows at least 10-fold reduced number of spots, comparable to the blank.

Single molecule co-localization

We co-expressed C-HA-YFP and R-Flag-mCherry in HEK293 cells. When the lysate from these cells was applied to SiMPull chambers with anti-Flag antibody, we observe mCherry fluorescence spots as expected (Figure 3.11c, d).We could also detect YFP fluorescence spots, implying that we are able to co-capture C-HA-YFP with R-Flag-mCherry. The number of fluorescent spots in mCherry and YFP channels was similar, indicating a one-to-one association between these two proteins on average. When we overlay the mCherry and YFP fluorescent images, we find that 57% of YFP molecules colocalized with a corresponding mCherry, within the same diffraction limited spots (Figure 3.11d). For colocalization analysis, mCherry was excited first to avoid any complexity arising due to FRET from YFP to mCherry. Incomplete colocalization may arise from basal tonic activation of PKA, or more likely, from fluorescently inactive fractions of YFP and mCherry as discussed below.

Adding cAMP analog, 8-bromo-cyclic AMP to the flow channel or pre-incubating the lysate with the analog resulted in greatly reduced number of C subunit (YFP spots) without a significant change in R subunit (mCherry spots) (Figure 3.11c, e); the colocalization between YFP and mCherry is reduced to 4%. Intracellular levels of cAMP can be modulated by activating GPCRs. When the cells over-expressing PKA complex were stimulated with forskolin, an agonist for adenylyl cyclase for cAMP production, the amount of C subunit (YFP molecules) was significantly decreased, indicating activation and dissociation of PKA holoenzymes (Figure 3.11c).

Active fraction for mCherry

Red fluorescent proteins are often found to have inferior photophysical properties when compared against GFP variants. mCherry is frequently used as the red fluorescent protein of choice

as it is monomeric and matures quickly (~30 min), but it has several drawbacks. Quantum yield of mCherry is low as compared to GFP (Yu et al., 2009). The protein exhibits complex photophysics (Hendrix et al., 2008) and multiple fluorescent states (Wu et al., 2009). Consequently, mCherry is not suitable for fluorescence photobleaching step analysis (Yu et al., 2009). Although mCherry is imperfect, we have not been successful at identifying a better red fluorescent protein for single-molecule studies.

The active fraction of YFP is ~75%. Given mCherry's poor photophysical properties, it is difficult to quantify the active population using the tandem-dimer approach we used for YFP. Dunne et al. (Dunne et al., 2009) report the active fraction of mCherry trimers to be 70-80% that of Citrine fluorescent protein trimers. Maeder et al. (Maeder et al., 2007) report that around 50% of mCherry is "active" in yeast cell imaging experiments. Both studies (Dunne et al., 2009; Maeder et al., 2007) were performed with a tandem trimeric mCherry fusion and may not represent the true active fraction in our experiments.

The low fraction of active mCherry would imply that a fraction of mCherry labeled complexes would not be detected. Assuming ~40% active fraction of mCherry, ~36% of PKA complexes would not have any fluorescently active mCherry partner, limiting the theoretical maximum colocalization to be around 64%. Thus, our observed colocalization of 57% is likely limited by the photophysical properties of mCherry, and can be improved by using a more active fluorescent protein or using booster antibodies (Ries et al., 2012).

Stoichiometry of PKA

We then explored the stoichiometry of PKA via photobleaching analysis. We expressed C-HA-YFP alone, and pulled it down using HA-antibodies. 91% of YFP traces exhibited one-step photobleaching indicating a monomeric population (Figure 3.11f). Next, we examined the stoichiometry of C-HA-YFP in complex with R-Flag-mCherry. C-HA-YFP and R-Flag-mCherry were co-expressed; and protein complexes were pulled down using antibodies directed against Flag epitope. 47% of immunoprecipitated C-HA-YFP molecules displayed two photobleaching steps (Figure 3.11g), while 51% molecules bleached in one step. The number of traces exhibiting higher

number of photobleaching steps (3 or 4) accounted only 2%. Assuming a 75% active fraction of YFP (Ulbrich and Isacoff, 2007) our results indicate that each PKA complex has two copies of C-HA-YFP. Thus SiMPull is applicable to intact protein complexes and can reveal their composition and stoichiometry.

3.6 Immunofluorescence labeling of pulled down complexes

So far we have implemented SiMPull assay for pull-down of proteins fused with fluorescent proteins. Fusion with a fluorescent protein tag may perturb the functional activity of the protein. We extended the assay for detecting immunoprecipitated single complexes using antibodies, using mammalian target of rapamycin complex 1 (mTORC1) as a model system. mTORC1 is a key signaling complex that regulates cell growth and metabolism in response to nutrient availability to the cells (Kim et al., 2002; Sabatini, 2006). In addition to mTOR (mammalian target of rapamycin), a defining component of mTORC1 is Raptor (regulatory associated protein of mTOR), which associates with mTOR at an equimolar ratio (Kim et al., 2002; Yip et al., 2010). We expressed Flag-mTOR and HA-Raptor at near endogenous levels in HEK293 cells. Flag-mTOR was pulled down using biotinylated Flag-antibody; Raptor was detected using HA-antibody followed by fluorescently labeled secondary antibody. When both Flag-mTOR and HA-Raptor were co-expressed, we observed detection antibody binding as fluorescent spots whereas only background level was detected when only one of the two proteins was expressed (Figure 3.13). Thus, SiMPulled complexes can be detected via immunofluorescence labeling.

The antibodies used in this assay may not bind to all the available epitopes. Moreover, binding of one antibody may preclude the binding of another antibody on the sample molecule owing to its large size and resultant steric hindrance. Therefore, immunofluorescence labeling scheme is currently not suitable for stoichiometry determination. With the ongoing advancements in high-affinity antibody development, advent of single chain camelid antibodies (nanobodies) (Ries et al., 2012) and the nucleic acid based aptamers (Gold et al., 2010), it should be possible in the future to fluorescently label pulled down proteins with higher efficiency, and determine their stoichiometry.

3.7 Comparison with WB

SiMPull is performed using the same samples and reagents as used for the convention pull-down followed by WB analysis. No additional sample preparation steps are required for SiMPull analysis. We have been able to use the same antibodies that work for conventional pull-down. For nearly all applications that we have tested so far (> 50), we find that if antibody works for ensemble immuno-precipitation, it works for SiMPull. In fact, as detection in SiMPull is significantly more sensitive than the conventional WB, we have been able to successfully use the antibodies that do not work for ensemble pull-downs.

We have directly compared the spot counts that are obtained from SiMPull and band intensity in WB, using the same detection antibody (Figure 3.14). On increasing the amount of plasmid used for transfection, we see an increase in protein expression level, as detected via WB. SiMPull-based protein count scales exactly as the WB-based quantification.

In addition to determining protein concentrations, SiMPull can reveal the multiple association states of the protein and provide information on the stoichiometry of the complex. SiMPull can be used for single-molecule functional analysis of protein complexes that cannot be produced by recombinant methods.

The conventional bulk WB analysis can be combined with mass spectrometry to identify unknown binding partners. Though we can successfully elute the bound proteins from SiMPull flow chambers, the sample is not sufficient for mass spectrometry analysis. Hence, SiMPull can only be applied when one already knows the anticipated binding partners. Furthermore, SiMPull lacks the sizing capabilities of WB and can result in false positives: appropriate controls are necessary to rule out false/non-specific binding of fluorophore labeled proteins/antibodies to verify that the observed binding arises from real interaction.

3.8 Dynamic range of binding strengths accessible to SiMPull

Cell lysates require dilution prior to application to the SiMPull chambers to obtain well-separated molecules on the imaging surface. One potential concern is that the single-molecule

imaging concentrations may be significantly below the physiological concentration of these proteins and hence, the protein complexes may fall apart. We typically dilute the lysates immediately before addition to the flow chambers. Hence, strength of interactions that can be studied is determined by the dissociation rate constant, k_{off}, of the interaction.

The lysates are diluted right before addition to the sample chamber and imaged immediately. The whole dilution and addition to sample chamber step can be completed in less than 1 minute. Time for data acquisition depends on the statistics desired and could be completed in 1-2 minutes. Figure 3.15 depicts pull-down of YFP from cell extracts performed in < 120 seconds. Hence, as long as the k_{off} for the reaction is smaller than 10^{-2} s^{-1}, we should be able to detect the physiological complexes.

Typically, in cell extracts, upon cell lysis, proteins are diluted by ~1000-fold as compared to intracellular protein concentrations. Hence, by decreasing the time require between cell-lysis and data acquisition to a few minutes, together with sensitive detection, we may be able to access weak interactions that are not observed in conventional pull-down assays that require 6 – 24 h for protein pull-down and analysis.

3.9 Sample requirement for SiMPull

The sensitivity of the SiMPull is determined by the affinity of the capture antibody: once a fluorescently labeled protein is immobilized, the detection efficiency is nearly 100% in single-molecule experiments, barring for the photobleaching or labeling efficiency of the protein. Typically, for purified proteins, we are able to perform our experiments with 20 – 200 pM of purified proteins (See Figure 3.4, 3.5). The volume of our SiMPull flow chamber is ~20 ul. Thus, typically, we require 0.4 – 4 femtomols or ~10^8 copies of the protein. The sample chambers used in our assay are fairly rudimentary and a significant improvement in the sample requirements can be achieved, even without the need for sophisticated microfluidics. For certain high-copy number proteins, we may already be in the regime for single cell analysis. In fact, using over-expressed proteins and combining SiMPull with flow-cytometry, we have been able to detect proteins from as low as 5 cells (Figure

3.16). Thus, in principle, by reducing the sample chamber volume, we should be able to analyze the protein contents from a single cell using SiMPull.

3.10 Figures

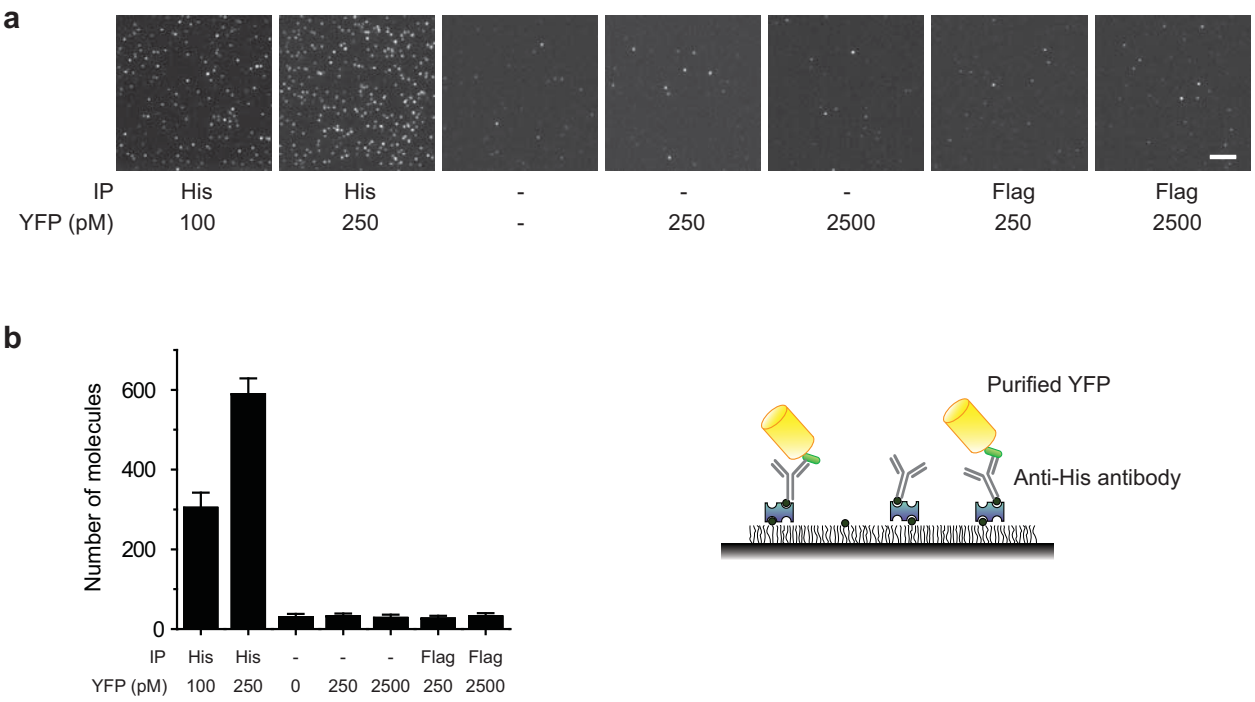

Figure 3.1 Purified YFP pull-down. (a) TIRF images of 100 pM/250 pM of purified YFP protein immobilized on chambers coated with anti-His antibody. No significant protein binding is observed when up to 2.5 nM of protein is added in the absence of antibody or on control (anti-Flag) antibody. Scale bar is 5 μm. (b) Bar graph of the average number of molecules per imaging area corresponding to images in (a). Error bars represent standard deviation of the mean across 20 or more images.

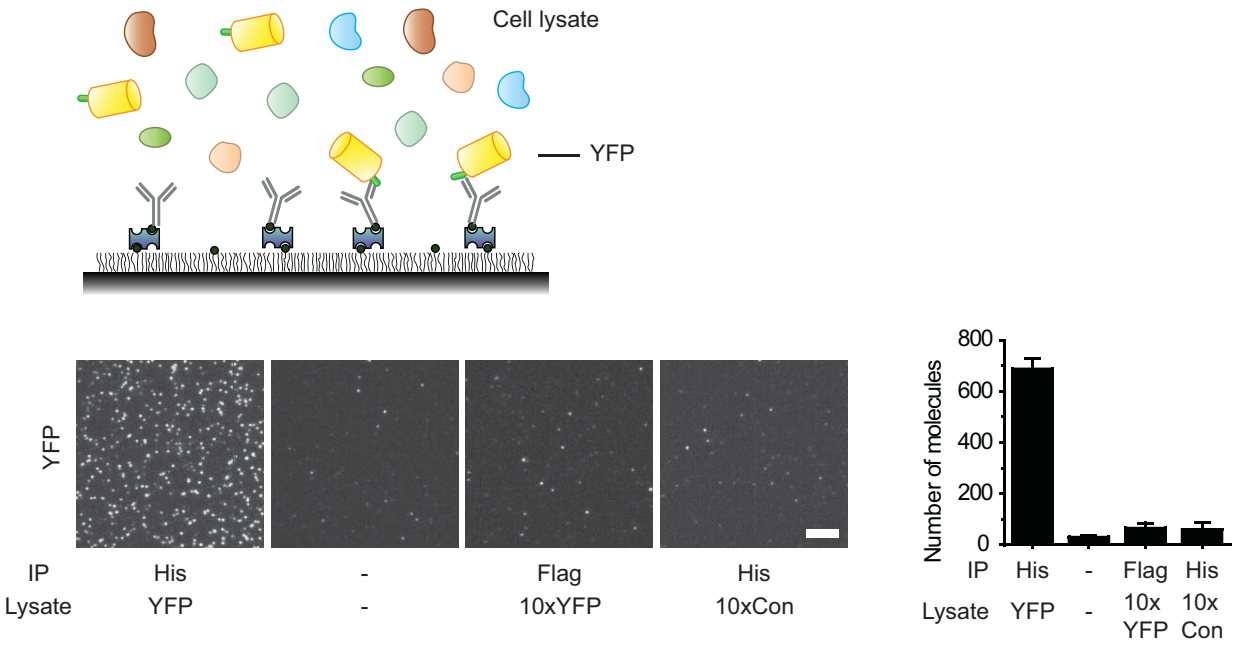

Figure 3.2 YFP pull-down from cell extracts. Schematic (top) and TIRF images of single YFP molecules pulled down from cell lysate. Lysate from cells over-expressing $(His)_6$-YFP (YFP) or control cells (Con) was infused onto a chamber coated with antibody against His-tag or a control antibody (Flag-tag). Dash (-) indicates no antibody or no sample was added. Scale bar is 5 μm. Bar graph of average number of molecules observed per imaging area (2500 μm^2). Error bars depict standard deviation of the mean across 20 or more images.

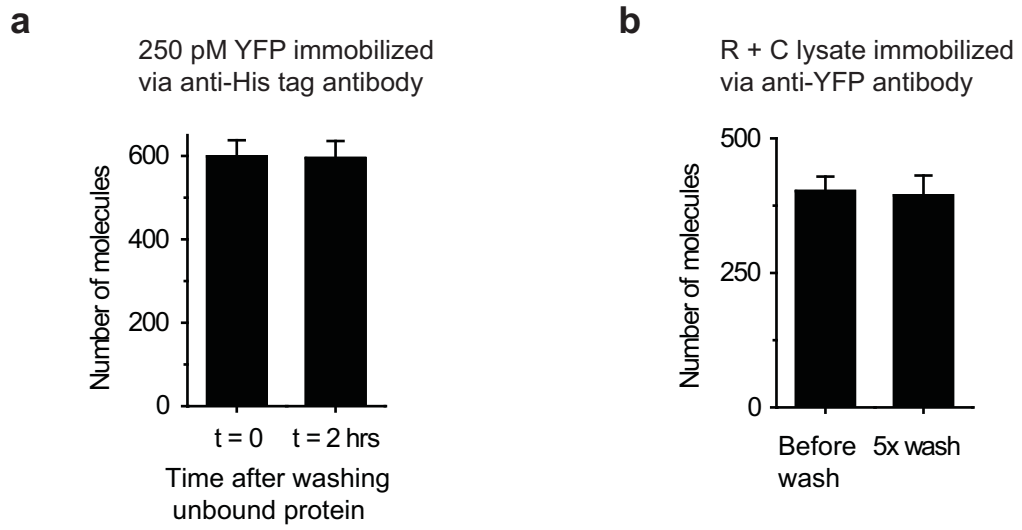

Figure 3.3 Stability of antibody binding. (a) 250 pM of purified YFP was immobilized via antibody against polyhistidine tag. Unbound protein was removed by washing the flow chamber. Average number of bound molecules was counted immediately, and 2 hours after wash. (b) PKA C-HA-YFP and R-Flag-mCherry were co-expressed. PKA complexes were immobilized via anti-YFP antibody. Number of pulled down YFP molecules was counted before and after 5 times wash with physiological buffer. Immobilized proteins do not dissociate from the surface during our imaging time-scale. Error bars represent standard deviation of the mean across 20 or more images.

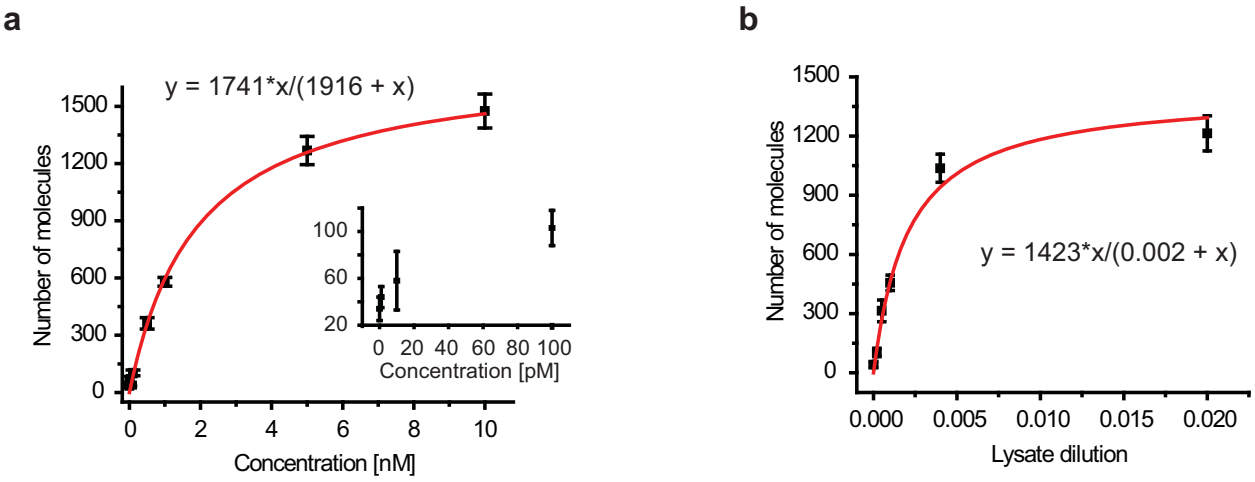

Figure 3.4 YFP concentration titration. Concentration titration of $(His)_6$-YFP (a) purified or (b) lysate on flow chamber coated with anti-His tag antibody, and corresponding fit to a first order Hill equation. Inset in (a) is a zoom into the low concentrations regime (1 pM – 100 pM) for purified YFP immobilization. By comparing the number of fluorescent molecules pulled down for cell extract against a purified protein standard, we can determine the protein concentration in cell extracts.

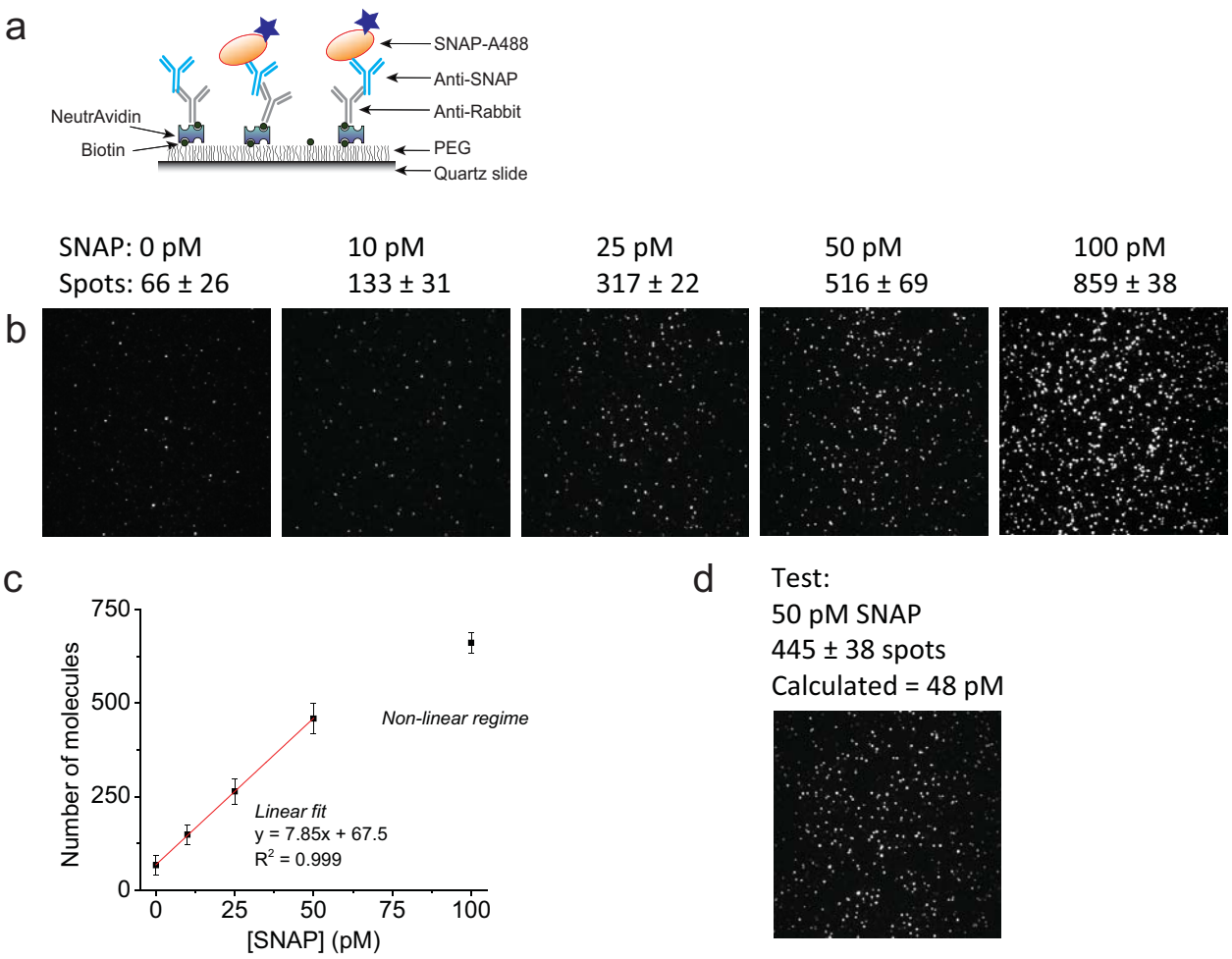

Figure 3.5 Protein binding linearly increases on SiMPull surfaces. (a) Schematic for immobilization of purified SNAP protein labeled with Alexa488. (b) As the concentration of SNAP protein is increased, the observed number of fluorescent spots increases (c) The spot count relates linearly to the protein concentration. At higher concentration (> 50 pM) molecule density is too high to resolve individual molecules. (d) The calibration curve in (c) can be used to measure unknown protein concentration. As a test, we applied 50 pM of purified SNAP protein on the SNAP antibody coated surfaces. From the calibration curve, the spot count corresponds to 48 pM SNAP, within 5% of the actual concentration.

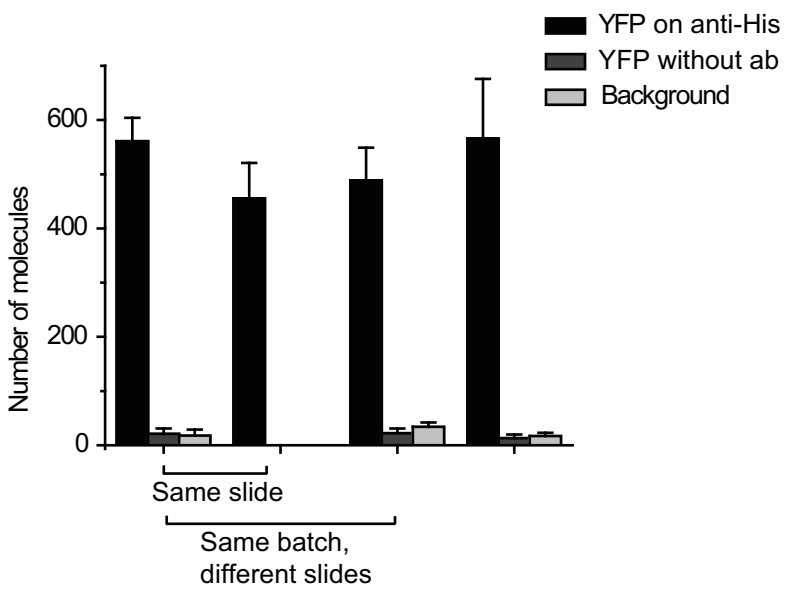

Figure 3.6 PEG slide reproducibility. Flow chambers were constructed on the same microscope slide (adjacent channels), on slides from same preparation batch, and on a slide from an independent preparation. Same amount of YFP lysate was added either with or without surface immobilized antibody against the protein. Fluorescence background (no immobilized FP) was also monitored. The mean YFP spot count is reproducible within 20% for all chambers. Error bars depict standard deviation of the mean across 20 or more images.

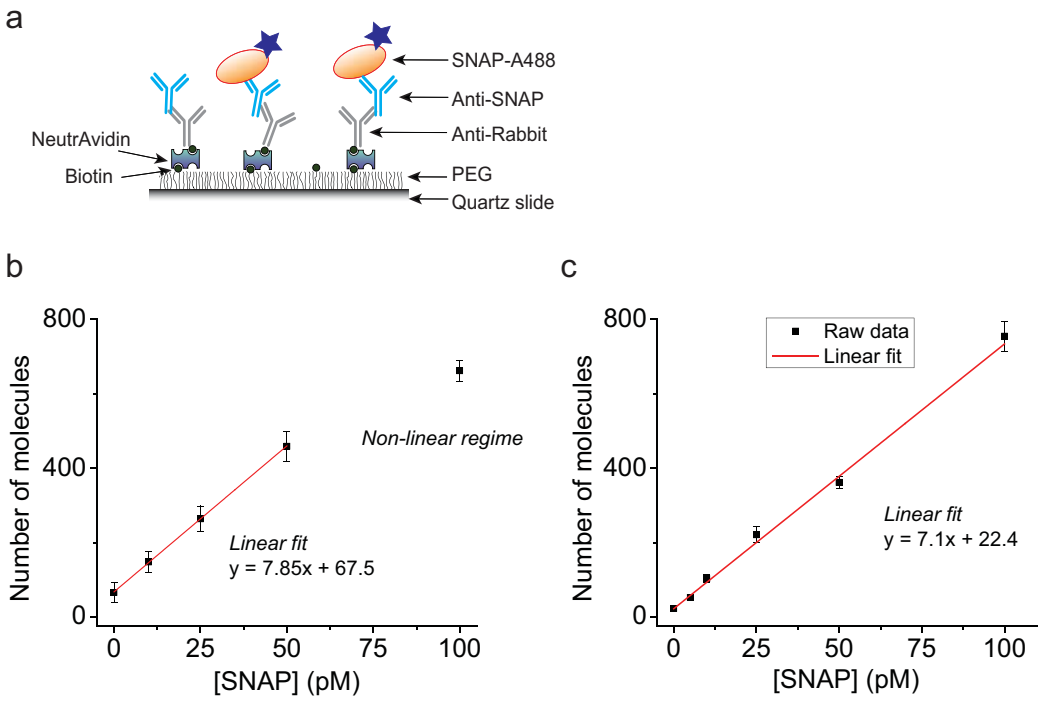

Figure 3.7 Slide reproducibility. (a) Schematic for SNAP capture. (b, c) The calibration curves obtained on different batches of slides are reproducible.

Figure 3.8 Density of binding sites. Biotinylated antibody from rabbit is immobilized on the surface and detected via Alexa647 labeled anti-rabbit antibody. As the white image indicates, there are so many rabbit antibodies on the surface that the image looks uniformly bright with the resolution of optical microscopy. Image on right depicts typical working density of single molecules immobilized on the surface.

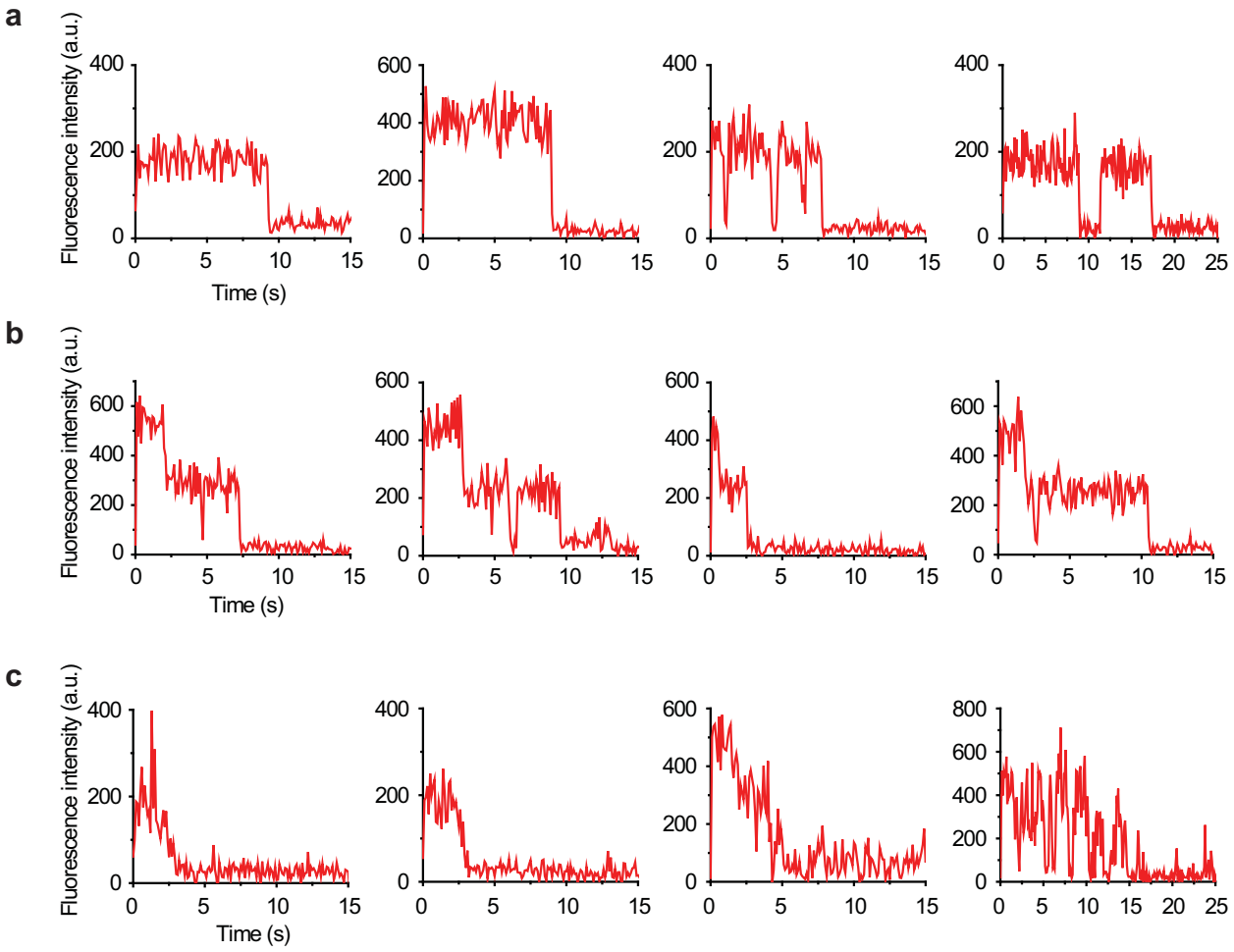

Figure 3.9 Sample YFP time traces depicting (a) one-, or (b) two- step photobleaching. For determining the stoichiometry, traces were manually scored for the number of bleaching steps. (c) For a fraction of molecules, clean fluorescent intensity levels and hence bleaching events could not be determined. This happened due to (1) low signal to noise ratio (2) unresolved bleaching steps (3) excessive photoblinking (4) molecules did not bleach completely. Such molecules were excluded from stoichiometry analysis. These molecules were scored under "rejected traces". The fraction of rejected traces was 20-25%

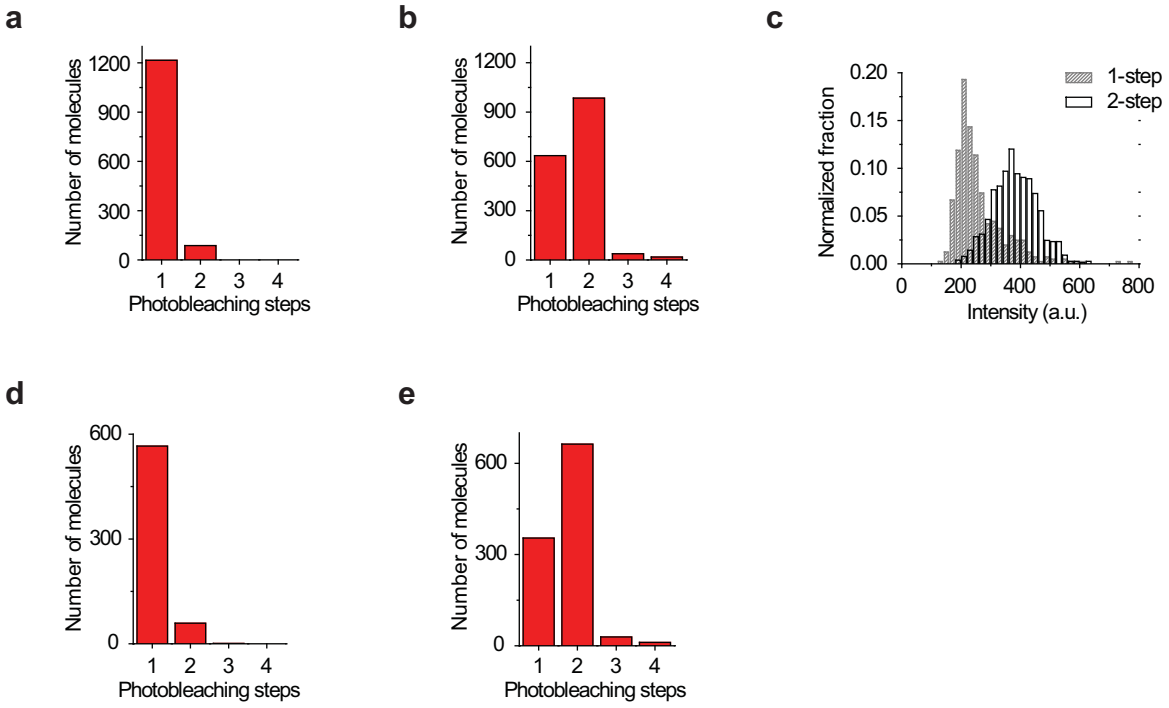

Figure 3.10 Photobleaching step distribution. Distribution of number of observed bleaching steps (a) for monomeric YFP and (b) for tandem dimeric YFP (tdYFP) pulled down from cell extracts. A vast majority (93%) of monomeric YFP molecules bleached with single photobleaching step, as expected. In contrast, analysis performed on tdYFP construct showed that a majority of tdYFP molecules (59%) bleached in two steps while about 37% exhibited one-step bleaching. Only a small fraction (< 5%) bleached with three or more steps. (c) Fluorescence intensity distribution of tdYFP molecules exhibiting 1-step (gray) and 2-step (black) photobleaching. As expected, the fluorescence intensity of 2-step bleachers was about double that of single step bleachers, and their relative populations were consistent with previous reports of about 75% of YFP being fluorescently active. The distribution of photobleaching steps for purified (d) monomeric YFP and, (e) tdYFP is comparable to that for proteins pulled down from lysate.

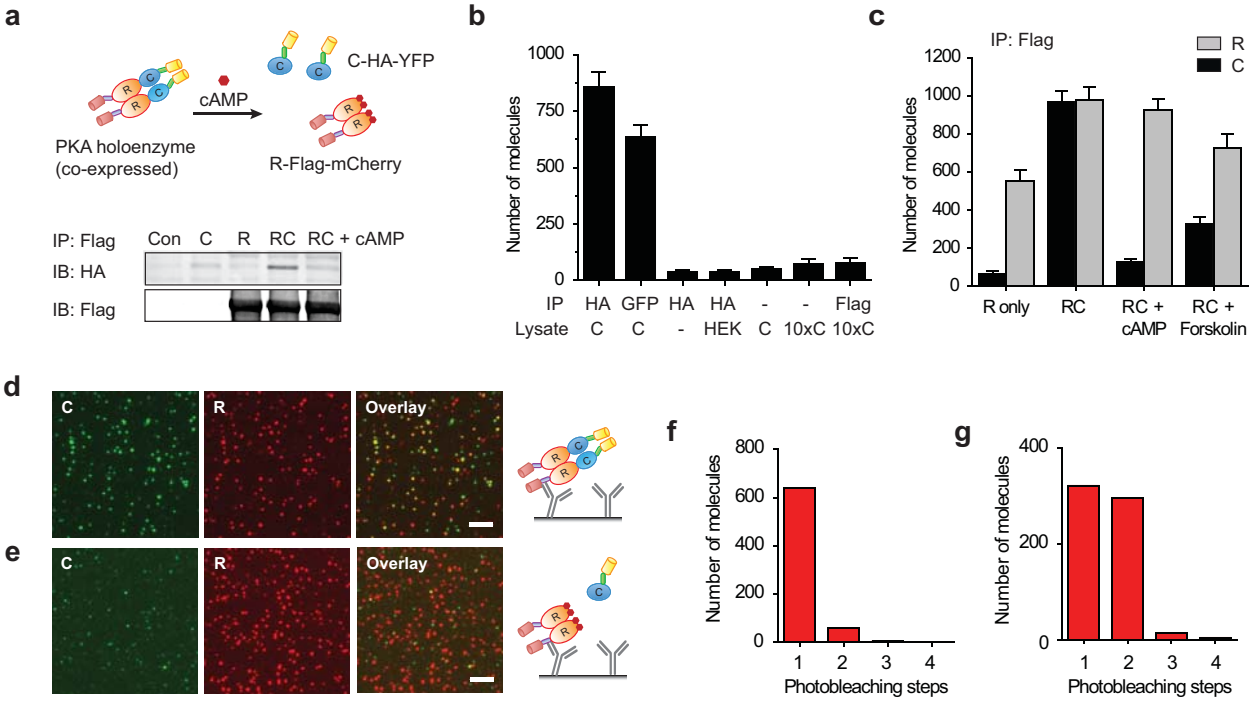

Figure 3.11 PKA complex pull-down. (a) Schematic of PKA construct: regulatory (R) subunit is tagged with Flag and mCherry tags. Catalytic (C) subunit bears HA and YFP tags. In WB (bottom), C is pulled down with R; on adding cAMP, the complex dissociates. (b) C-HA-YFP pull-down. When lysate from cells expressing C only is applied onto the surface with anti-HA or anti-YFP antibody, we see single YFP molecules. The lysate shows minimal binding without any antibody or on anti-Flag antibody even when 10-fold higher C-lysate (10xC) was added. Control HEK293 lysate (HEK) does not show any significant fluorescence above blank. (c-e) PKA complex pull-down. (c) Bar graph with average number of molecules observed per imaging area. (d) Single molecule co-localization of immunoprecipitated PKA complexes, imaging YFP (left), mCherry (center) and overlay (right). (e) On adding cAMP to the lysate, YFP spots are not observed. Photobleaching step distribution (f) for C only lysate directly immobilized via antibody against HA-tag and (g) for C pulled down with R. Error bars in (b, c) represent standard deviation of the mean across 20 or more images. Scale bars in (d, e) are 5 μm.

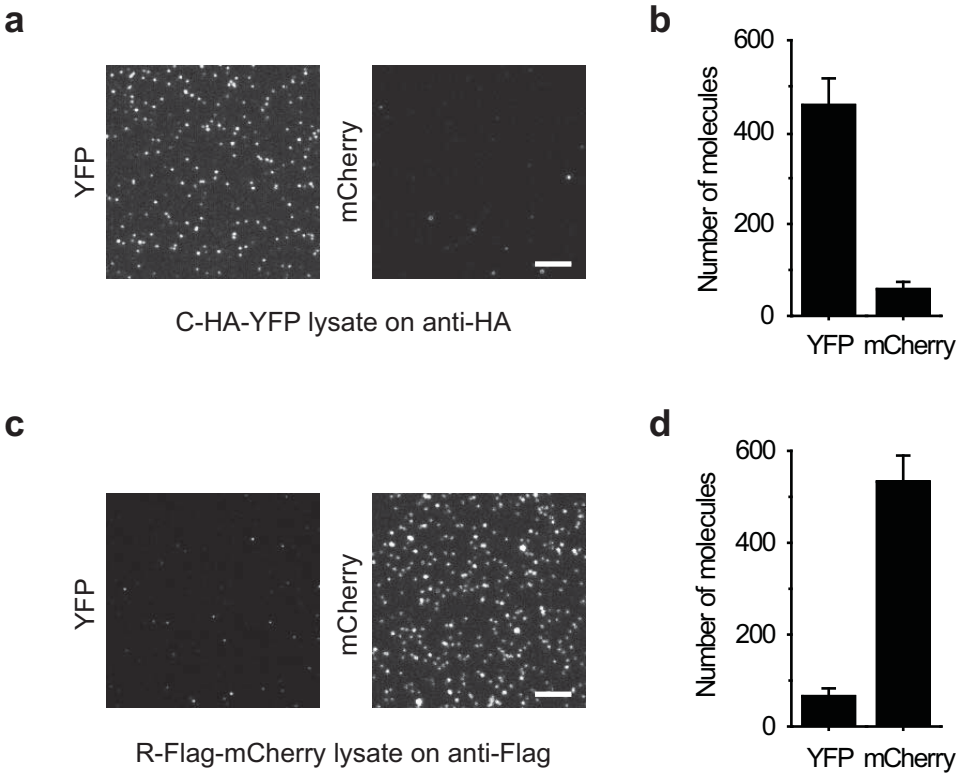

Figure 3.12 Cross-talk between YFP and mCherry channels. (a, b) C-HA-YFP lysate is immobilized via antibody against HA-tag and is imaged for YFP (left) and mCherry (right) fluorescence. mCherry channel shows background level of fluorescence. (c, d) Similarly, when lysate with R-Flag-mCherry only is immobilized, no significant fluorescence is observed on YFP imaging. Scale bars in (a, c) represent 5 μm. Error bars in (b, d) depict standard deviation of the mean across 20 or more images.

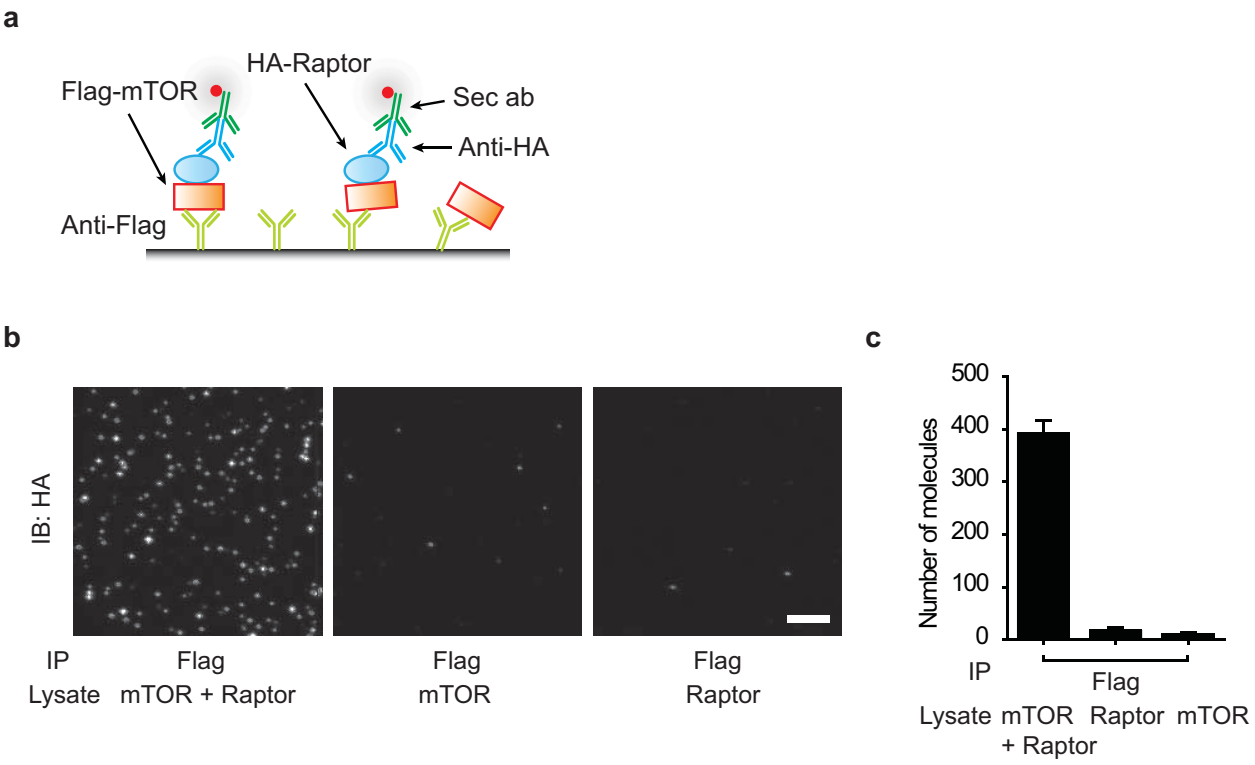

Figure 3.13 Single molecule immunofluorescence labeling of mTORC1. (a) Schematic. (b) Anti-Flag antibody was immobilized on surface. Lysate from cells expressing (b, center) Flag-mTOR alone, (b, right) HA-Raptor alone or (b, left) both proteins were added to the slide. Immunoprecipitated protein complexes were detected using antibody against HA-tag (IB: HA) and a corresponding secondary antibody labeled with Cy3. (c) Bar graph of number of Cy3 spots per image.

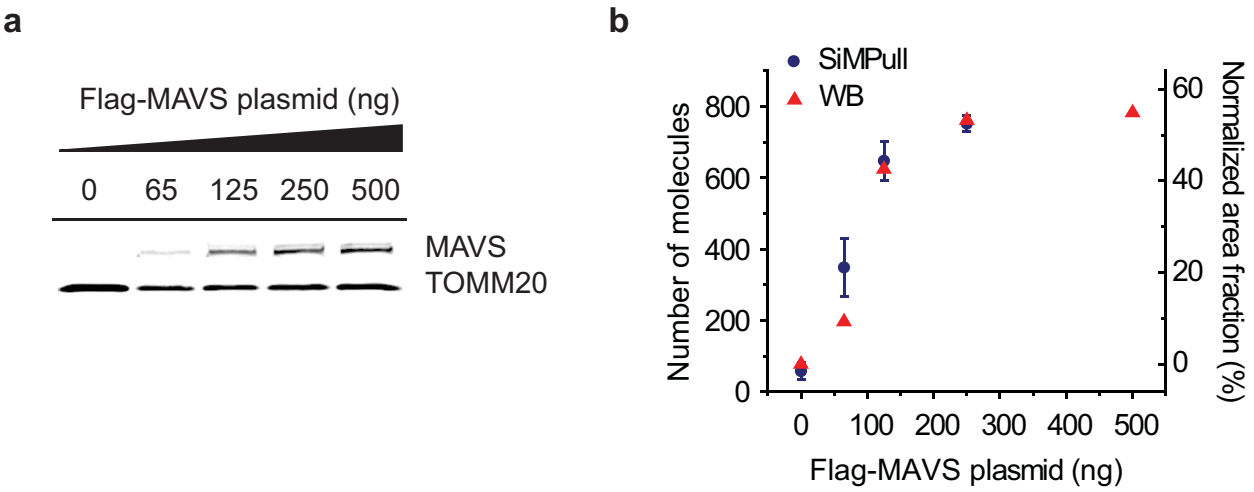

Figure 3.14 Quantitative comparison of SiMPull with WB. HEK293 cells were transfected with different amounts of Flag-MAVS plasmid. (a) WB was performed with anti-Flag antibody. (b) Comparison of WB with SiMPull. Area of the WB band for MAVS was normalized against TOMM20 (mitochondrial marker protein) and plotted in (b) (red triangle, axis on right). For SiMPull, Flag-MAVS was pulled down via biotinylated Flag antibody. A 50-fold dilution of the lysate was used for each plasmid concentration. MAVS was detected using anti-MAVS and corresponding secondary antibody labeled with Cy3. The number of Cy3 spots per imaging area (2500 μm^2) was determined and plotted in (b) (blue circle, axis on left). Error bars represent standard deviation of the mean across 20 or more images.

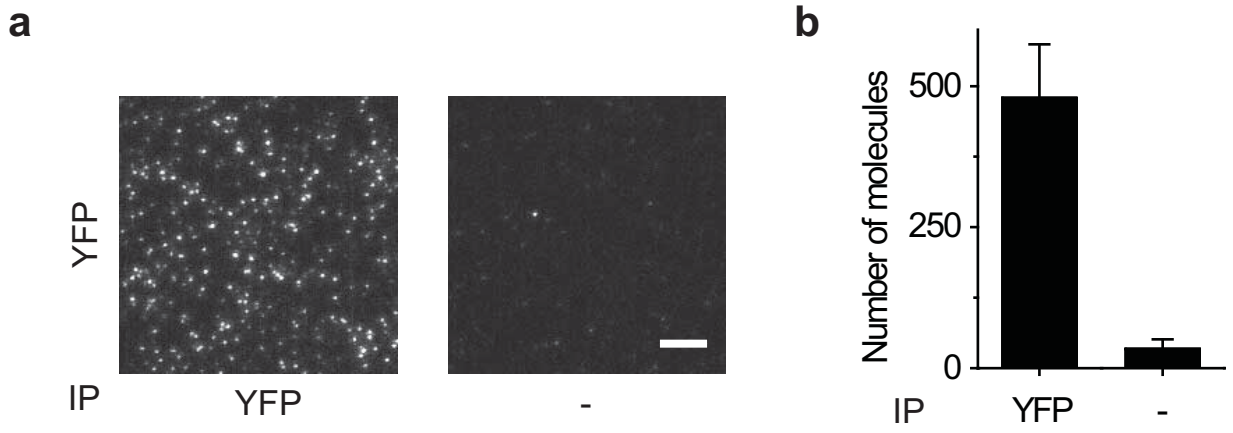

Figure 3.15 Range of k_{off} values accessible to SiMPull. Pull-down of YFP from cell extracts and single-molecule analysis can be completed in 150 s starting from crude cell extracts. (a) HEK293 cells were transfected with $(His)_6$-tagged YFP. Freshly prepared lysate was diluted by a factor of 100 and added to chamber coated with anti-His antibody. The dilution and addition to sample chamber step could be completed in less than 1 minute. Time for data acquisition depends on the statistics desired; acquisition of 20 movies for the data presented above required 1.5 minutes. Hence, as long as the dissociation rate constant, k_{off}, for the interaction is smaller than 10^{-2} s^{-1}, SiMPull can be used to detect the physiological interactions. Scale bar is 5 μm. (b) Bar graph for the average number of YFP molecules per image. Error bars represent standard deviation of the mean across 20 images.

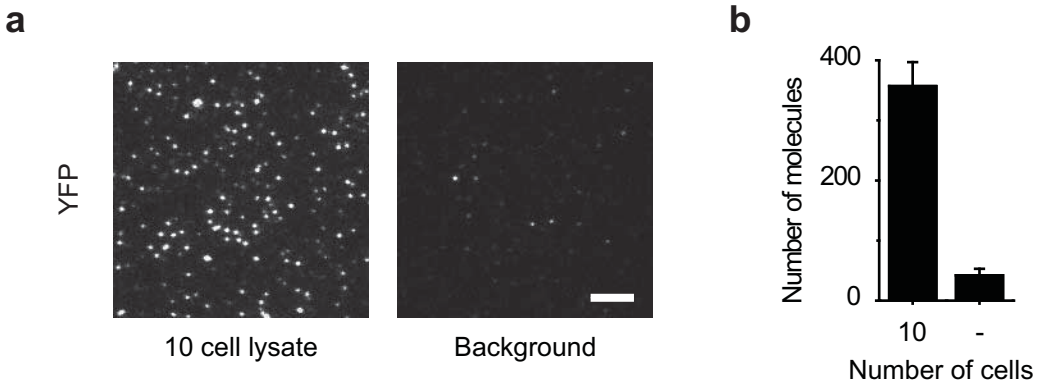

Figure 3.16 SiMPull analysis on lysate from 10 cells. (a) HEK293 cells expressing PKA (C-HA-YFP and R-Flag-mCherry) were sorted using fluorescence-assisted cell sorting at 10 cells per well in a 96 well plate. Cells were lysed in ~10 µl lysis buffer. The lysate from 10 cells was applied to flow chamber coated with antibody against HA-tag and imaged for YFP. Scale bar is 5 µm. (b) Bar graph depicts average number of YFP molecules per imaging area (2500 μm^2). Error bars represent standard deviation of the mean across 20 or more images.

Chapter 4*

Applications to Cellular Contexts

We have been able to apply SiMPull to a wide variety of systems and obtain new biological information. Our initial applications were primarily towards stoichiometry determination. The overall experimental scheme is similar though we had to suitably tailor the sample preparation and the protein capture scheme to fit the requirements for respective systems; these variations are discussed in depth together with the biological insights we were able to gain.

4.1 Cytosolic proteins

Cytosolic proteins are usually soluble and the lysates are prepared by suitable non-ionic detergent lysis methods such as NP-40 or CHAPS. I have already discussed two cytosolic proteins, PKA and mTOR in Chapter 3. Here, I will present one more example, together with functional analysis of SiMPulled protein.

*This work in Chapter 4 has been published as the following papers:

- Jain A, Liu R, Ramani B, Arauz E, Ishitsuka Y, Ragunathan K, Park J, Chen J, Xiang Y, & Ha T, "Probing cellular protein complexes using single-molecule pull-down", *Nature* **473**, 484-488 (2011).
- Means C, Lygren B, Langeberg L, Jain A, Dixon R, Vega A, Gold M, Petrosyan S, Taylor S, Murphy A, Ha T, Santana L, Tasken K, and Scott J, "An entirely specific type I A-kinase anchoring protein that can sequester two molecules of PKA at mitochondria", *Proceedings of the National Academy of Sciences*, **108**, E1227-E1235 (2011)
- Shen Z, Chakraborty A, Jain A, Giri S, Ha T, Prasanth K, and Prasanth S, "Dynamic association of ORCA with pre-RC components regulates DNA replication initiation", *Molecular and Cellular Biology*, **32**, 3107-3120 (2012)
- Panter M, Jain A, Leonhardt R, Ha T, and Cresswell P, "Dynamics of major histocompatibility complex class I association with the human peptide-loading complex", *Journal of Biological Chemistry*, **287**, 31172-31184 (2012)
- Patel J, Jain A, Chou Y, Baum A, Ha T and Garcia-Sastre A, "ATPase-driven oligomerization of RIG-I on RNA allows optimal activation of type-I interferon", *EMBO Reports* (In press)

4.1.1 Retinoic Acid Inducible Gene I (RIG-I)

RIG-I is a cytosolic innate immune receptor that recognizes pathogenic RNA in the cytosol of the cell and triggers an anti-viral immune response (Yoneyama et al., 2004). The innate immune receptors (such as RIG-I) are broadly expressed in most tissues and form the first line of defense against pathogenic invasion (Loo and Gale, 2011). These receptors recognize the molecular patterns associated with pathogenic invasion: for example, RIG-I in particular recognizes 5'ppp dsRNA which is typically absent in the cytosol of normal eukaryotic cells, as the 5'end of the messenger RNA is capped with 7-methylguanylate (Loo and Gale, 2011). Upon pathogen recognition, RIG-I triggers a signaling cascade leading to the expression of anti-viral genes such as inteferons that control infection and alert the specialized adaptive immune system.

Oligomerization of RIG-I is proposed to be required for activation of downstream signaling (Jiang et al., 2012). However, the exact nature of these oligomeric species is not known. We used SiMPull to investigate the formation of RIG-I oligomers, in the presence and absence of viral RNA.

RIG-I is largely monomeric

We fused RIG-I with a YFP-tag on the N-terminus. YFP-RIG-I was transfected in HEK293 cells, and the cells were infected with Sendai virus (SeV). RIG-I detects and mounts immune response to Sendai virus (SeV) infection; SeV has been widely used as a model system for understanding RIG-I mediated immune signaling (Rehwinkel et al., 2010). Twelve hours post infection cells were lysed in a physiological buffer (20 mM Tris pH 8, 100 mM NaCl) with 0.5% NP-40. RIG-I was pulled down on biotinylated anti-GFP antibodies. As shown in Figure 4.1, we are able to specifically capture YFP-RIG-I from cell extracts with and without infection. When we analyzed the fluorescence time-trajectories, we find that most molecules (~80%) bleach in a single-step; no difference is observed in the samples with and without viral infection.

Over-expression of RIG-I imparts immunity against virus infection to the cells and it is possible and in our experimental condition, the cells were not infected. A second possibility is that only a small fraction of RIG-I is oligomerizes: free and monomeric RIG-I is in excess and over-powers the detection of RIG-I oligomers.

Immuno-purified RIG-I oligomerizes on RNA

Owing to its large size (~100 kDa) and numerous post-translational modifications, it is difficult to purify functional full-length RIG-I from bacterial and insect over-expression systems. SiMPull requires significantly lower amount of samples as compared to the conventional biochemical assays: such quantities can be readily obtained from cultured mammalian cells. Additionally, homogenous purification is not essential as the surfaces are refractory to the binding of contaminants if any. Recently, Yeom et al. used immuno-purified TUT4 for single-molecule biochemical analyses (Yeom et al., 2011). We over-expressed and immuno-purified HA-RIG-I and YFP-RIG-I from HEK293 cells.

As a viral ligand, we used in vitro transcribed RNA corresponding to the defective interfering RNA of SeV, a 546-nt long copy-back, non-coding viral RNA, which is known to bind RIG-I (Baum et al., 2010). The in vitro transcribed RNA was fluorescently labeled by hybridizing it with 5 20-nt long DNA oligonucleotides conjugated to Cy5 dye. The oligonucleotide probes were designed against a region of the RNA with minimal secondary structure and hybridization was performed by mixing the RNA and the DNA in 1:1 ratio and heating it at 37°C for 10 min (Patel et al., in press).

First, we checked if the immuno-purified proteins retain RNA binding capacity. Immuno-purified HA-RIG-I or YFP-RIG-I were immobilized on the surface using antibodies against HA or YFP tags respectively. When the fluorophore labeled RNA is added, it binds only to the channel with RIG-I (Figure 4.2). Additionally, the oligonucleotide probes alone do not exhibit any binding to the immobilized proteins.

Next, we examined the oligomerization of RIG-I on the RNA. We mixed HA-RIG-I, YFP-RIG-I together with the RNA. We simultaneously added DNA oligonucleotides to the mixture. The formation of RIG-I/RNA complex was triggered by heating the mix at 37°C for 10 min; the oligonucleotide probes should anneal to the RNA during the same incubation. After the reaction, we captured the formed complexes using anti-HA antibody. We are able to observe RNA binding spots in the Cy5 imaging channel (Figure 4.3 b). The binding is specific to the HA-antibody, and without any RNA, the oligonucleotide probes do not exhibit any binding. Next, when we image the YFP

channel, we find that YFP-RIG-I is co-captured with HA-RIG-I (Figure 4.3 c). Without the RNA, the binding of YFP-RIG-I to anti-HA antibody is comparable to the blank (without anti-HA). Thus, HA-RIG-I and YFP-RIG-I oligomerize in the presence of viral RNA.

A likely mechanism is that individual RIG-I monomers first recognize and bind to the 5'ppp end of the dsRNA. Facilitated by ATP dependent translocase activity (Myong et al., 2009), the RIG-I monomers launch from the 5' end towards middle, freeing the 5'ppp for binding of the next RIG-I monomer, leading to multiple RIG-I molecules per RNA, that facilitate downstream signaling (Hou et al., 2011).

4.2 Membrane proteins

Membrane proteins are difficult to purify using conventional methods. The bound lipids are often essential for the structure and the activity of the proteins however lipids usually bind with low-affinity interactions that may not survive harsh biochemical purification steps (Marsh, 2003). In SiMPull, samples are gently treated: lysates are directly applied to the imaging chambers. No wash steps are required and the proteins can be directly imaged within a few minutes after cell lysis.

Many membrane proteins form multimers before they achieve a functional state. Several labs have now used TIRFM to determine the stoichiometry of membrane bound proteins using live cell single-molecule fluorescence imaging (Ulbrich and Isacoff, 2007; Tombola et al., 2008; Leake et al., 2006), however, the stoichiometry cannot be determined by photobleaching method unless the areal density of proteins is low enough for single-molecule detection (Ulbrich and Isacoff, 2007). SiMPull provides a simple solution to this problem where membrane patches can be solubilized in a suitable detergent, and then immobilized at a low density as desired by appropriately diluting the sample. An important consideration, however, is that the proteins should be homogenously solubilized. Incomplete solubilization may lead to a mixture of population while over-solubilization may disrupt the bound lipids. Of note, sonicated membrane preparations are often used for biochemical analysis of receptors. In our experiments, we found that membrane proteins are aggregated upon sonication;

these aggregates are unsuitable for photobleaching step analysis and sonication may lead to unwanted artifacts in biochemical analysis as well.

4.2.1 β_2-Adrenergic Receptor

We have used SiMPull to investigate the homo- and hetero-dimerization of beta-2 adrenergic receptor (β_2AR), a prototypical GPCR. HEK293 cells were transfected with Flag-YFP- β_2AR and cell surface proteins were isolated. Briefly, cells were harvested into hypotonic lysis buffer (10 mM Tris ph7.4, 1 mM EDTA) with 0.3% DDM (n-Dodecyl-beta-D-maltoside) for 30 min. The lysate was centrifuged for 10 min at 600g and the supernatant was collected. By flowing this preparation on anti-GFP or anti-Flag antibodies, we could specifically pull down the receptor (Figure 4.4). When we analyzed the stoichiometry of β_2AR via YFP photobleaching, we observed that nearly 38% of the traces displayed two distinct bleaching steps (Figure 4.5), indicating a ~70% dimer population. The fraction of traces exhibiting 3 and 4 step photobleaching steps was relatively low (4% and 1% respectively), and may represent higher order oligomeric species (Maurel et al., 2008). Our observation of β_2AR homo-dimerization is consistent with previous studies (Angers et al., 2000; Mercier et al., 2002).

We went on to see if β_1AR associates with β_2AR to form hetero-oligomers (Mercier et al., 2002). We co-expressed mCherry-β_1AR and YFP-β_2AR in HEK293 cells. Using antibodies against mCherry-β_1AR, we were able to pull down YFP-β_2AR and vice versa (Figure 4.5) and the two fluorophores colocalize (~42% colocalization). The expression level of proteins can influence the stoichiometry of GPCRs and further investigation and controls are needed to determine the true nature of association between ARs.

4.3 Organelle bound proteins

Proteins tethered to the intracellular membranes such as mitochondria, ER and lysosomes play important roles in spatial and temporal organization of the interior of the cell (Bernlohr et al., 1997). We have successfully applied SiMPull to numerous membrane proteins bound to the

intracellular organelles such as mitochondria and endoplasmic reticulum (ER) for stoichiometry determination.

4.3.1 Sphingosine kinase binding protein

A-kinase anchoring proteins (AKAPs) tether the cAMP-dependent protein kinase (PKA) to intracellular sites where they preferentially phosphorylate target substrates, thus spatially localizing PKA signaling (Edwards and Scott, 2000). As previously discussed, the PKA holoenzyme is a heterotetramer consisting of two regulatory (R) subunits that maintain two catalytic (C) subunits in an inhibited state. The R subunit genes are encoded by two different classes of genes that differ in sensitivity to cAMP and their sub-cellular localization.

Our collaborator, Prof. John Scott at the University of Washington at Seattle, identified that sphingosine kinase interacting protein (SKIP) pecifically anchors a subclass (class I) of PKA R subunits to the mitochondria (Means et al., 2011). We determined the stoichiometry of interaction of SKIP and PKA regulatory subunits. We co-expressed YFP-PKA-RI and Flag-SKIP in HEK293 cells. Cells were lysed using the buffer containing 20 mM Tris-HCl pH 7.6, 100 mM NaCl, 1% Triton X-100 with protease inhibitor cocktail, and Flag-SKIP was captured on the single-molecule imaging chambers using anti-Flag antibody (Figure 4.6).

We observed a range of fluorescence photobleaching steps, and nearly all (97%) of the YFP spots bleached in 4 or fewer steps (Figure 4.6 d, e), thus indicating the presence of up to tetramers or PKA-RI. To relate this distribution to the number of PKA-RI molecules per complex, one needs to account for the active fraction of YFP, typically 70-80%, resulting in a binomial distribution of number of photobleaching steps (Ulbrich and Isacoff, 2007). The observed distribution does not fit to a single binomial distribution and likely arises from a mixture of multiple stoichiometric states (Nakajo et al., 2010). The observed photobleaching step distribution was fit using least squares fitting to a sum of two binomial distributions (trimer + tetramer or dimer + tetramer) with two free parameters: the fraction of tetramers and the probability of YFP being fluorescently active. The distribution fits well to the sum of the two binomial distributions, corresponding to dimers and tetramers of YFP. The fit yields a dimer fraction of 59 ± 10%, and the probability of YFP being

active as 70 ± 3% (n = 4) (Figure 4.6 e); the active fraction of YFP is consistent with our previous experiments and published reports. Hence, each PKA-SKIP complex consists of either one or two PKA holoenzymes.

4.3.2 Mitochondrial antiviral signaling

MAVS (mitochondrial antiviral signaling) is an adaptor protein downstream of RIG-I, and is essential for innate immune defense against viruses. MAVS localizes at the mitochondrial outer membrane (Seth et al., 2005). Oligomerization of MAVS is known to be essential for its function: hepatitis C virus (HCV) encoded protein NS3/4A cleaves the oligomerization domain of MAVS, and thus eludes the immune system (Li et al., 2005). We investigated the oligomerization status of MAVS captured from mitochondrial preparations using SiMPull.

We expressed YFP-MAVS in HEK293 cells and isolated intact mitochondria using MITOISO2 kit (Sigma). The mitochondria were diluted in an isotonic buffer supplied with the kit before applying them to the SiMPull chambers. This isolation process preserves the integrity of mitochondria, and when the preparation is gently flowed on to chambers coated with anti-GFP antibody, we observe bright and extended fluorescent aggregates, likely arising due to multiple YFP-MAVS molecules held together by mitochondrial membranes (Figure 4.7). The stoichiometry of MAVS in these mitochondria (or mitochondrial patches) could not be determined as the spatial density of YFP-MAVS was too high for single molecules to be resolved. As a corollary, we are able to capture large organelles or organelle membrane patches on our SiMPull chambers.

Next, we solubilized the mitochondrial preparation using detergents. Upon pre-solubilizing the mitochondrial preparation using detergent, we observed well-isolated single YFP spots (Figure 4.7). These spots displayed single photobleaching step, suggesting that solubilized MAVS is monomeric. This contrast supports the notion that the fluorescent aggregates are due to immunoprecipitated mitochondrial membrane patches or whole mitochondria.

We activated MAVS mediate immune signaling by infecting cells with SeV. The detergent treatment may perturb the oligomerization of MAVS; we screened a variety of different detergent

conditions: 1% Triton X-100, 1% DDM and RIPA (1% NP-40, 1% sodium deoxycholate and 0.1% SDS) but in all cases, we observed predominantly a monomeric species (Figure 4.8) of MAVS.

More recently, Hou et al. demonstrated that MAVS indeed oligomerizes upon viral infection and forms multimeric prion-like aggregates (Hou et al., 2011). In retrospect, there could have been several reasons why we were not able to detect oligomerization of MAVS. First, YFP-conjugation may interfere with the functional activity of the protein and hinder oligomerization. Second, it is possible that the aggregates we observed are due to MAVS oligomers that fall apart under our detergent solubilization conditions or dilution or both. The prion-like MAVS aggregates are resistant to SDS solubilization (Hou et al., 2011), but YFP conjugation may weaken the interaction instead of abrogating oligomerization. MAVS prion formation may lead to assembly of proteins in a conformation such that these aggregates are not recognized by the antibody as was observe by Hou et al. (Hou et al., 2011). Finally, the excess of monomeric MAVS may also overpower any signal from a few oligomers. These caveats are potentially applicable to other systems as well and it is crucial to be aware of these limitations and to design the SiMPull experiments accordingly.

4.3.3 Peptide loading complex

The major histocompatibility complex (MHC) is responsible for presenting the antigen from the pathogen infected cells to the specialized immune cells such as the cytotoxic T-cells. The MHC class I receptors are found in all nucleated cells of the body and the antigen dependent interaction between MHC class I and the T-cell receptor is crucial for adaptive immune responses. Under the resting condition, the MHC class I molecules are loaded with self-peptides, derived from the cell's own 'house-keeping' proteins. In the event of pathogenic invasion or tumor transformation, the proteins derived from pathogen proteins may also be presented. The circulating T-cells continually sample the surface antigens presented via MHC class I and thus detect and eliminate the infected cells.

The MHC complexes are "loaded" with peptides at the ER and the process is mediated by multi-component protein complex called the peptide loading complex (PLC) (Peaper and Cresswell, 2008). The proteasome and other proteases in the cytosol of the cell generate small 8-20 amino acid

long peptides derived from endogenous or pathogen associated proteins. These peptides are transported to the lumen of the ER by the transporter associated with antigen processing (TAP) protein. The peptides are further processed and trimmed to 8-10 amino acid length, and loaded on to the MHC class I molecules by PLC consisting of a chaperon calreticulin, ERp57 and a key adaptor protein, Tapasin (Figure 4.9a). Upon binding of a high-affinity peptide, the MHC class I molecules are released from the PLC and reach the surface of the cell via the secretory pathway.

Although the functions of the PLC constituents are increasingly well understood, their stoichiometry is still controversial (Bangia and Cresswell, 2005).The ratio of TAP and MHC class I to tapasin, which is responsible for MHC class I recruitment and peptide binding optimization, is particularly critical for understanding the function of the PLC.

We transduced YFP-tagged tapasin into the tapasin-negative .220.B4402 cell line (Panter et al., 2012). Disulfide bond between tapasin and ERp57 is essential for stability and correct functioning of the peptide loading machinery: we used methyl methanethiosulfonate (MMTS) in the lysis and dilution buffers to stabilize the disulfide bonds. Cells were pretreated with 10 mM MMTS and lysed in 1% digitonin in a physiological buffer (150 mM sodium chloride, 25 mM Tris, pH 7.4) supplemented with 2 mM MMTS, 1 mM calcium chloride and protease inhibitors. The lysate was applied to chambers coated with a biotinylated monoclonal antibody against TAP1, a component of the TAP complex (Figure 4.9a) or an anti-GFP antibody. In both cases, we are able to specifically capture tapasin-YFP in comparison with slides coated with a control or no antibody (Figure 4.9b). We analyzed the fluorescence time-trajectories of tapasin pulled down with anti-TAP1. The nearly equal numbers of one- and two-step photobleaching events following TAP pull-down matched the binomial distribution predicted for a 1:2 TAP/tapasin-YFP ratio, given that only ~75% of YFP is fluorescently active (Figure 4.9c, d). Furthermore, the fluorescence intensity of the molecules exhibiting two-step photobleaching was twice that of the molecules photobleaching in a single step (Figure 4.9e), indicating accurate scoring of the fluorescence time traces, while the broad distribution of the 25% of traces that were not interpretable is consistent with a lack of scoring bias. In the past, the TAP/tapasin ratio has been suggested to be 1:2 (Rufer et al., 2007; Hulpke et al.,

2012) particularly due to the presence of one tapasin-binding site on each subunit of rat TAP (Rufer et al., 2007). Our SiMPull data confirm that the TAP/tapasin stoichiometry is 1:2 in human cells expressing human TAP.

Next, we investigated the stoichiometry of MHC class I at the PLC. We employed cell lines depleted of endogenous MHC class I, expressing YFP tagged MHC, HLA-A0201-YFP (A) and HLA-B-4402-YFP (B) (Panter et al., 2012). For both the cell lines, we were able to specifically capture the MHC class-I molecules using surface immobilized TAP1 antibody (Figure 4.10). When we analyze the stoichiometry, we find that a majority of the molecules (~90%) bleach in a single photobleaching step, indicating a monomer like behavior (Figure 4.10). Thus each PLC contains one MHC class I molecule at a time.

To further investigate the stoichiometry of MHC class I to tapasin, we utilized the antibodies PaSta1 and PaSta2 against tapasin that have been developed by the Cresswell lab (Panter et al., 2012). PaSta1 is reactive with all tapasin, while PaSta2 is unable to bind MHC class I-associated tapasin because its epitope is located at the MHC I-tapasin interface. On both biotinylated PaSta1 as well as PaSta2, we observed a monomeric stoichiometry of MHC class I (Figure 4.11). This result further supports the notion that at a time, only one molecule of MHC class I is associated with PLC. Finally, we treated cells with a proteasome inhibitor, lactacystin, to decrease the supply of peptides to the PLC. Lactacystin treatment stabilizes the interaction between MHC class I and the PLC but even after lactacystin treatment, we were not able to detect a substantial dimer population.

We were able to pull-down MHC class I even with PaSta2 antibodies, which block the binding site between MHC class I and tapasin (Figure 4.11): this result indicates that there are two potential binding sites, and possibly they are both functional in binding to MHC class I molecules. Even when one of the sites is blocked by the PaSta2 antibody, the second site can recruit an MHC class I molecule. Additionally, the cell lines we employed may still have residual MHC class I molecules (such as HLA-E) that are not labeled with YFP. Such endogenous molecules will not be visualized in our assay and incomplete depletion of untagged protein may hamper stoichiometry

determination with SiMPull. In fact, detailed biochemical analysis later revealed that a fraction of PLC (10-40%) indeed bind to two MHC class I molecules (Panter et al., 2012).

4.4 Nuclear proteins

4.4.1 Origin recognition complex

Eukaryotic DNA replication is initiated at thousands of origins of replication. To maintain the fidelity of the replicated DNA, the cell needs to ensure that each DNA fragment is replicated only once per cell-cycle. This fidelity or one-off origin licensing is partly achieved by regulating the assembly of the replication machinery on the origin by a conserved protein complex called the origin recognition complex (ORC) (Bell, 2002). ORC forms the scaffold for recruitment of the replication machinery and thus regulates DNA replication. In particular, binding of Cdt1 to the ORC leads to assembly of the replicative helicase, MCM2-7, promoting DNA replication. Cdt1 is inhibited by geminin, which ensures that the DNA is replicated only once, although the exact molecular details of this origin licensing are currently lacking (Aladjem, 2007). Prof. Supriya Prasanth's lab recently identified an ORC associated protein (ORCA) that modulates the binding of ORC to the chromatin and thus regulates replication initiation (Shen et al., 2010). In addition, ORCA also binds to Cdt1 and geminin, and is likely involved in recruiting these regulatory proteins to ORC (Shen et al., 2012).

We used SiMPull to investigate the interaction of ORCA with ORC, Cdt1 and geminin. To assess the stoichiometry of ORCA and ORC association, we co-expressed T7-ORCA and YFP-Orc1, a subunit of ORC. The lysate from these cells was added to a surface coated with T7 antibody (Figure 4.12a-c), while the lysate from cells that expressed only YFP-Orc1 served as the control. The control channel exhibited 5-fold lower binding of YFP-Orc1, indicating specific pull-down of ORC-ORCA complexes. Nearly 80% (864 out of 1,075) of YFP-Orc1 molecules pulled down with T7-Ocr1 bleached in a single step (Figure 4c), indicating that each complex has only one molecule of Orc1.

Similar analysis was performed on lysates expressing T7-ORCA and YFP-Cdt1; ~82% of the YFP-Cdt1 fluorescence spots bleached in a single photobleaching step, implying that each ORCA-Cdt1 complex has one molecule of Cdt1 (Figure 4.12d). Finally, we examined the stoichiometry of geminin in ORCA-geminin complexes. Previous studies have identified a dimerization domain in geminin that is essential for its activity (Benjamin et al., 2004). Our attempts to pull-down geminin with T7-ORCA were not successful; it is possible that geminin binding blocks the recognition by T7-antibody. Instead, we used a polyclonal antibody against ORCA immobilized via a biotinylated secondary antibody to pull-down OCRA-geminin complexes, while rabbit IgG was used as the control (Figure 4.12e). Lysate from cells expressing T7-ORCA and YFP-geminin were incubated in the chamber. There was a 5-fold enrichment of YFP spots in the anti-ORCA-coated chamber compared to the control. We find that nearly 54% of the YFP-geminin spots displayed two photobleaching steps, while 43% of them exhibited one-step photobleaching (Figure 4.12e). The intensity of the molecules bleaching in two steps was nearly twice the intensity of one step bleachers, thus confirming unbiased scoring. Our results are consistent with two geminin molecules per complex, given the ~75% of YFP is fluorescent. In summary, we demonstrate that each molecule of ORCA can interact with one ORC, one Cdt1, and/or two geminin molecules.

4.5 Archeal proteins

We have used SiMPull to determine the mean copy number of ribosomes and methyl-coenzyme M reductase (mcr) in a model methanogenic archea: *methanosarcina*. The endogenous gene locus of mcr and that of a ribosomal protein rpl were replaced with a SNAP-tagged version of these genes. The modified strains that showed similar growth rate and methane production as compared to the wild type were selected and used for SiMPull analysis.

Cells were grown in a medium supplemented with methanol; during the exponential growth phase, 10^8 cells were isolated. Cells were lysed and the proteins are labeled post-lysis with the Alexa-488 SNAP substrate, following the manufacturers' protocol. The free dye was removed by filtering the lysate 3 times with Amicon Ultra 10 kDa cut-off filters. The filtered lysate was used for SiMPull

with SNAP antibody. The SNAP antibody (NEB) was immobilized on the flow chambers using a biotinylated anti-Rabbit antibody at 10 nM concentration.

First, we calibrated the SNAP antibody coated surfaces using purified SNAP protein: on increasing the SNAP concentration, we obtain a linear increase in the number of observed fluorescent spots (Figure 4.13a, b). Thus, when an appropriate dilution of the lysate is applied to this antibody, the concentration of the protein in the lysate can be determined, assuming that the proteins in the lysate do not alter the binding affinity of the SNAP antibody to the SNAP tag, and the labeling efficiency is similar for the purified protein and the protein in the cell extract.

We find that the concentration of fluorescently labeled SNAP-mcr in the lysates is ~11 nM (Figure 4.13b). As these lysates are prepared by lysing 10^8 cells in 100 micro-liters of buffer, this concentration corresponds to a mean copy number of mcr as 6600 copies per cell. Similar analysis on the ribosomal protein, rpl yields a mean copy number of ribosomes as ~18,000 copies per cell (Figure 4.13c). Thus SiMPull is applicable to archeal proteins and can be used to determine the average copy number of proteins per cell. For a more accurate copy number determination, cells can be flow-sorted to get a better estimate of the number of cells. The amount of sample required for sample analysis is low (~10^2 - 10^6 cells depending on the copy number) and is not prohibitive for flow cytometry even at 100-1000 cells per second.

4.6 Animal tissue

Finally, we tested if we can use SiMPull to capture endogenous proteins directly from animal tissue. Pull-down of endogenously expressed proteins, although desirable, is challenging owing to low abundance, high background interaction with other cellular proteins, and general lack of high-affinity antibodies. As a model test system, we used AKAP interaction with PKA. AKAPs bind to PKA and confine it to discrete locations in the cell thus spatially organizing PKA signaling. Using ensemble pull-down we verified that AKAP150 can be co-immunoprecipitated with PKA from mouse brain extract (Figure 4.14).

Primary antibodies against proteins are often expensive and difficult to label with biotin or fluorophores. Thus, to keep our approach general, we used biotin-labeled secondary antibody to immobilize the antibody against the bait (PKA), and applied mouse brain extract (Figure 4.14a, b). On probing for the prey protein (AKAP150) using its primary antibody and fluorescently labeled secondary antibody, we observed ten-fold more fluorescent spots in the channel with PKA antibody as compared to the control channel. SiMPull required a 20-fold diluted sample as compared to 1 ml of undiluted extract that was used for the corresponding ensemble pull-down using the same antibodies (Figure 4.14b). This sensitivity allowed detection of PKA–AKAP binding from mouse heart tissue, which was below the detection limit of the conventional western blot under the same conditions (Figure 4.14c). Thus, SiMPull is applicable to endogenous proteins directly from animal tissue, and requires no additional sample preparation.

4.7 Figures

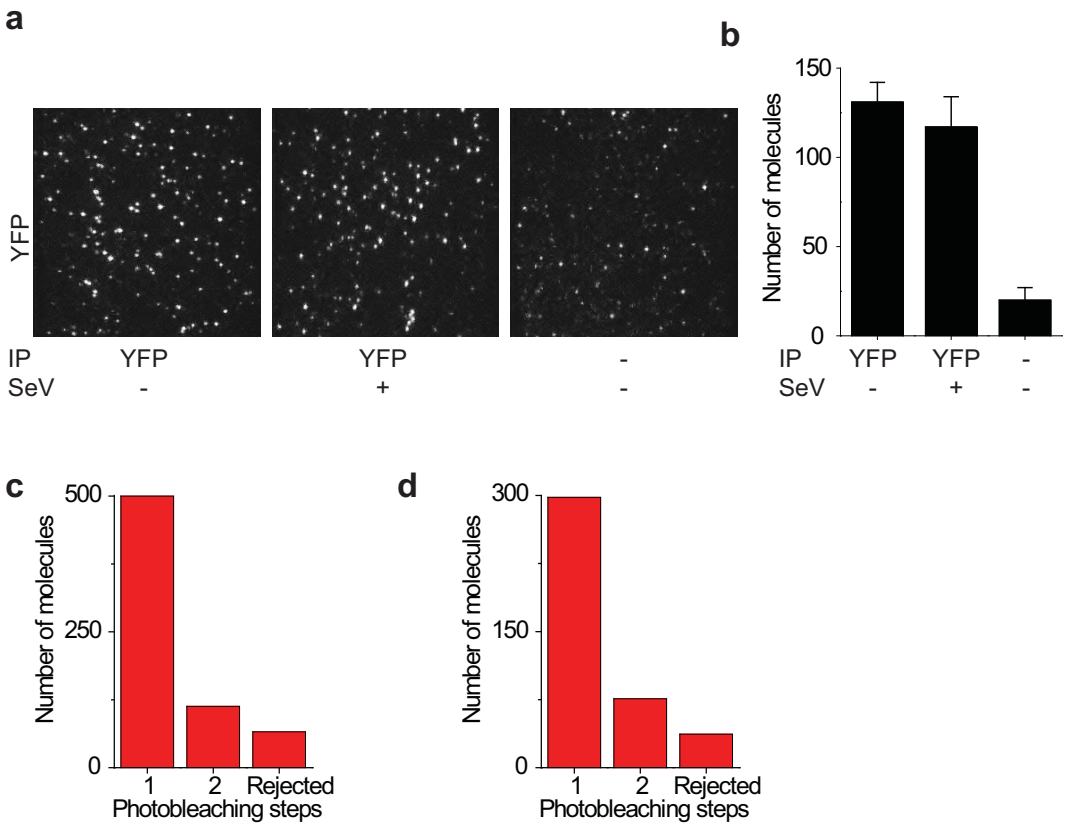

Figure 4.1 RIG-I pull-down. (a) Using surface immobilized GFP antibody, we are able to specifically capture YFP-RIG-I from HEK293 cells with or without SeV infection. (b) Bar graph for the number of observed YFP spots per imaging area (2500 μm^2). Photobleaching step distribution for YFP-RIG-I (c) before and (d) after SeV infection indicates that RIG-I is largely monomeric.

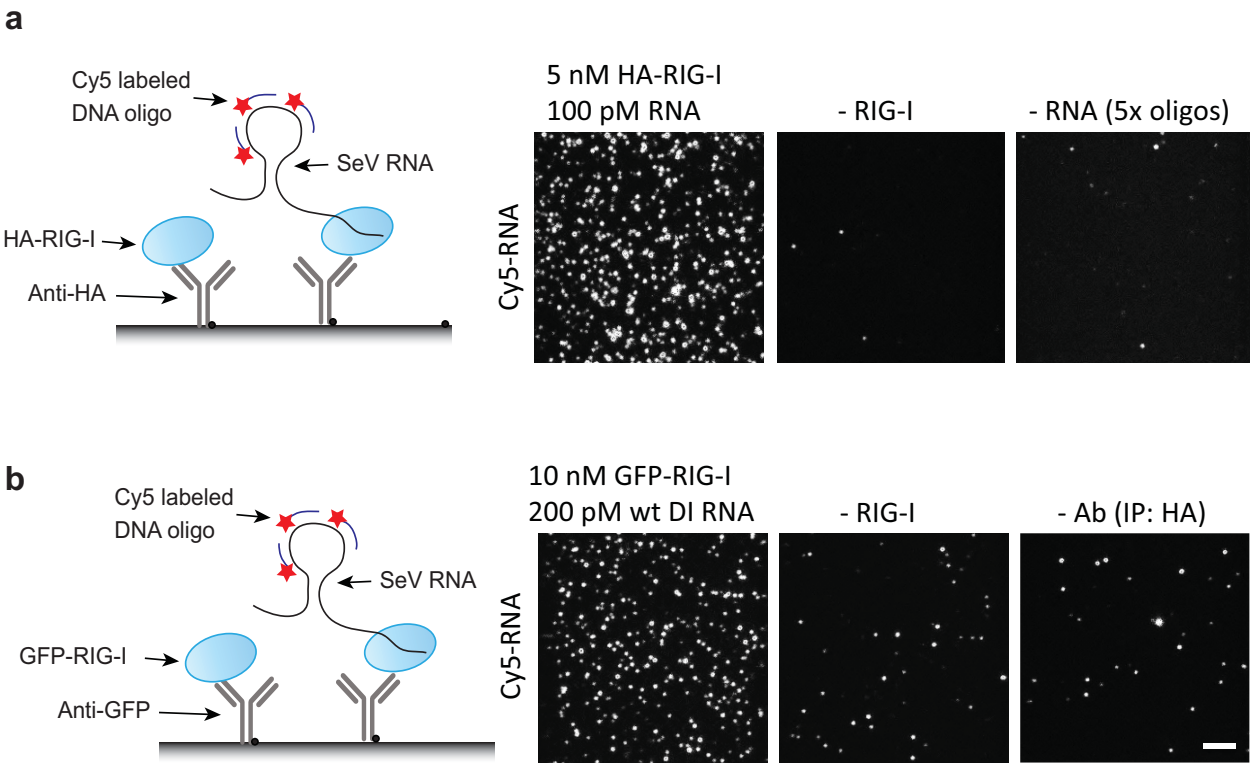

Figure 4.2 Immuno-purified RIG-I binds RNA. Immuno-purified (a) HA or (b) YFP tagged RIG-I is immobilized using antibodies against HA or YFP respectively. When a fluorophore labeled RNA is added to the channel, RNA binding is observed only in the channel with RIG-I. Fluorophore labeled oligonucleotide probes only or YFP-RIG-I added to the control antibody show significantly fewer Cy5 spots.

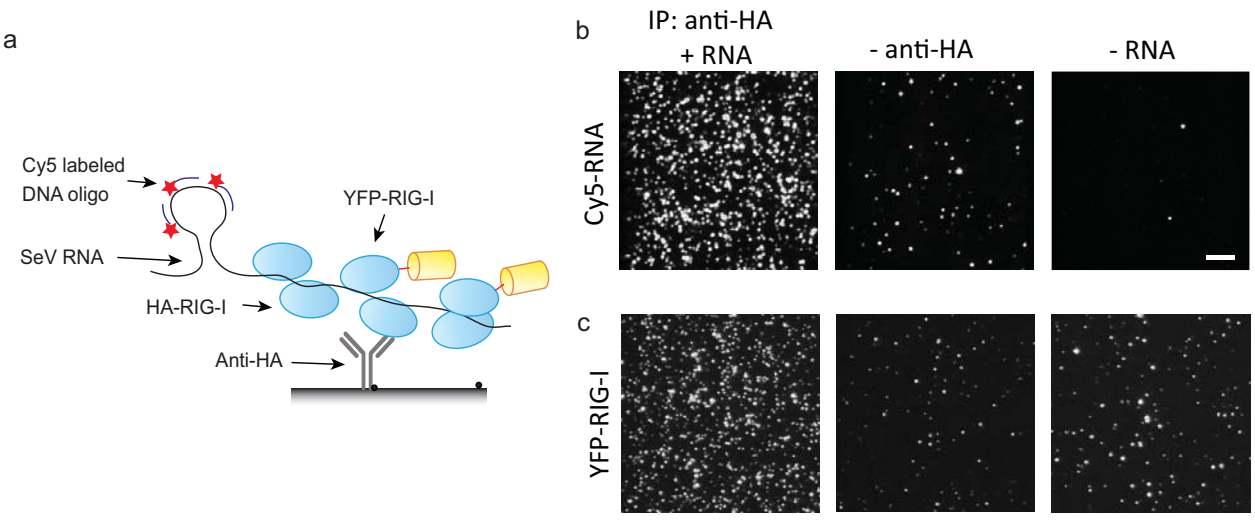

Figure 4.3 RIG-I oligomerization assay. (a) Schematic. Immunopurified HA-RIG-I and YFP-RIG-I are mixed with SeV RNA and Cy5 labeled probes against the RNA. (b) Upon applying this mixture to anti-HA antibody, we observe RNA binding only in the presence of anti-HA antibody. Background level of binding is observed in the control with anti-HA. (c) YFP-RIG-I binding is dependent on the RNA and HA antibody indicating RNA depending oligomerization of RIG-I. Scale bar is 5 microns.

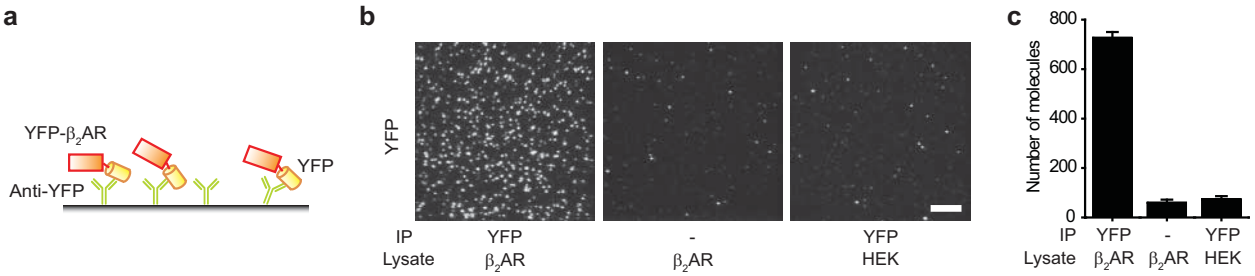

Figure 4.4 β_2AR pull-down from cells expressing Flag-YFP- β_2AR using antibody against YFP; (a) schematic, (b) typical TIRF images for YFP detection, and (c) average number of spots per image.

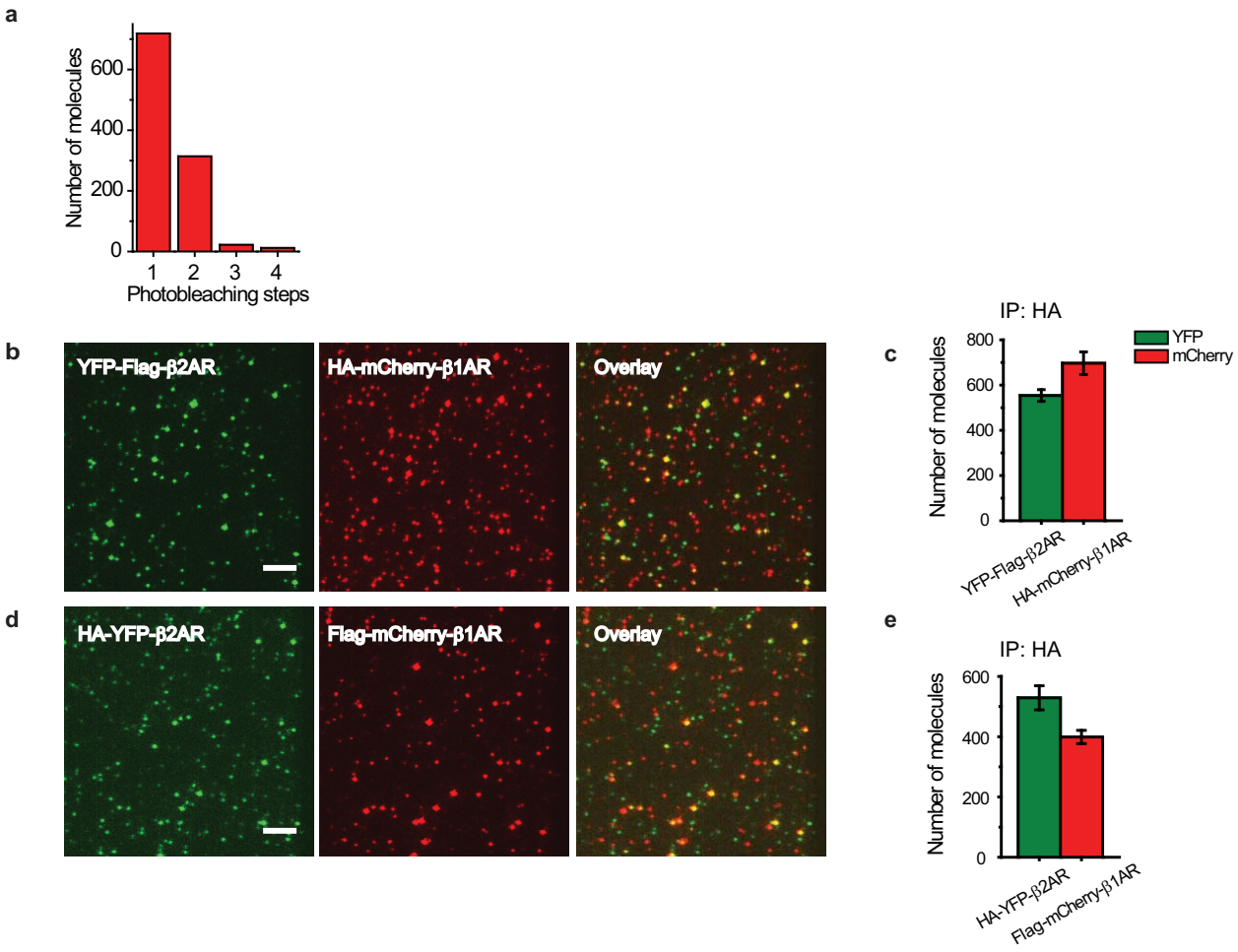

Figure 4.5 Oligomerization of adrenergic receptors. (a) Photobleaching analysis of YFP β2AR shows a mixture of one- and two-step photobleaching. (b, c) When YFP-Flag–β_2AR is co-expressed with HA-mCherry-β2A R, on pulling down β1AR, we are able to observe β2AR-YFP molecules (c). (b) TIRF images for YFP (left), mCherry (center) and their overlay (right). The fluorescence spots in the two channels co-localize. (d, e) Similarly, when β2AR-YFP is pulled down, we see corresponding β1AR-mCherry molecules. Scale bar in (b, d) is 5 μm. Error bars in (c, e) represent standard deviation of the mean across 20 or more images.

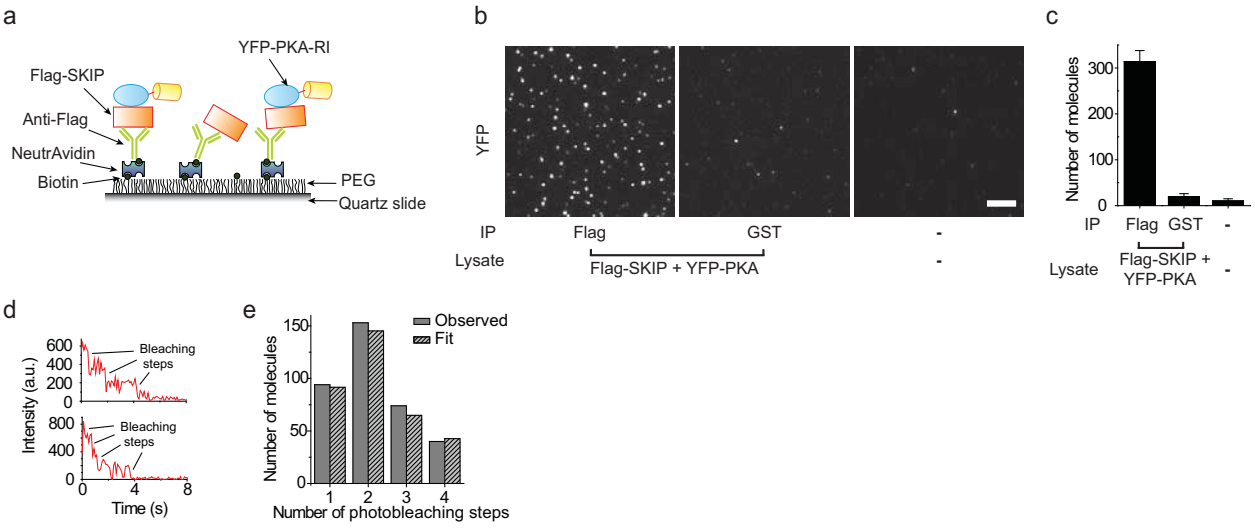

Figure 4.6 SiMPull analysis of PKA-SKIP complexes (a) Schematic: quartz slides are passivated with poly ethylene glycol (PEG) doped with biotin-PEG. Biotinylated antibodies against Flag tag are immobilized via a NeutrAvidin linker. On adding the lysate from cells co-expressing YFP-PKA-RI and Flag-SKIP, the surface immobilized antibody pulls down Flag-SKIP together with YFP-PKA-RI. (b) Typical TIRF images for YFP detection. Scale bar is 5 μm. (c) Average number of YFP spots per image. Error bars represent standard deviation of the mean across 20 or more images. (d) Representative YFP time-traces with step-wise photobleaching. (e) Observed distribution of number of photobleaching steps and corresponding fit to a sum of two binomial distributions.

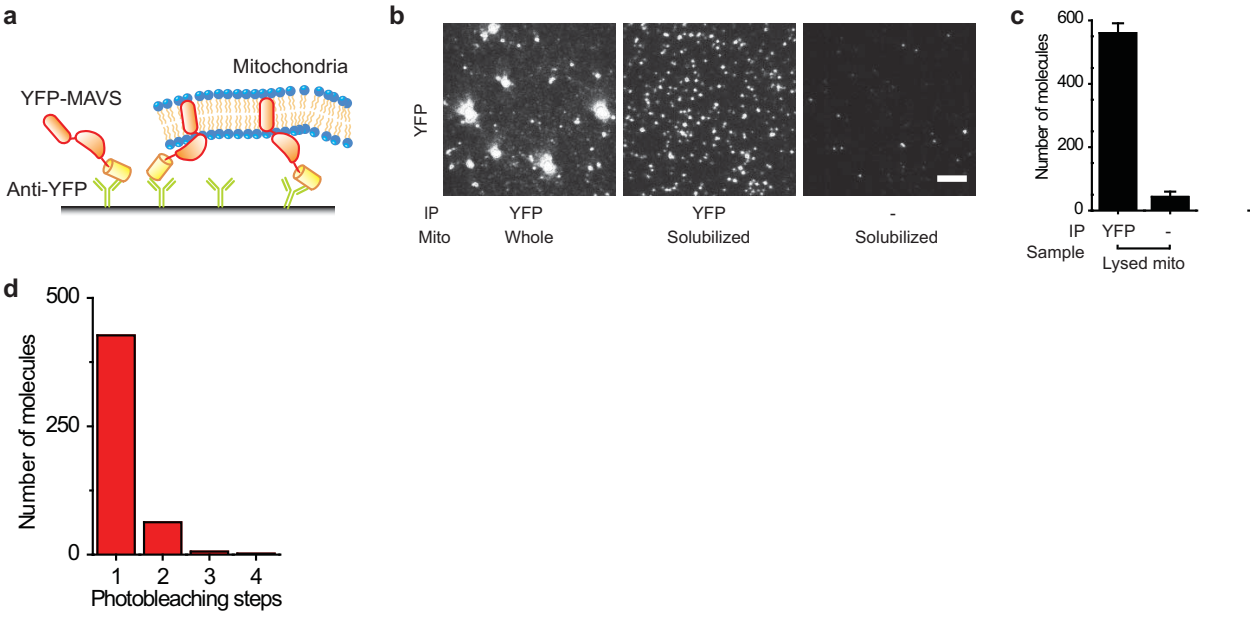

Figure 4.7 Mitochondria pull-down. Mitochondria were isolated from HEK293 cells over-expressing YFP-MAVS. This preparation was added either (b, left) directly or after detergent solubilization to flow chamber (b, center) with YFP antibody or (b, right) without YFP antibody. (c) Bar graph of the number of YFP molecules for solubilized mitochondrial preparations (d) Photobleaching analysis of solubilized MAVS. Most YFP molecules bleach with single photobleaching step, indicating that the majority of the solubilized MAVS is monomeric.

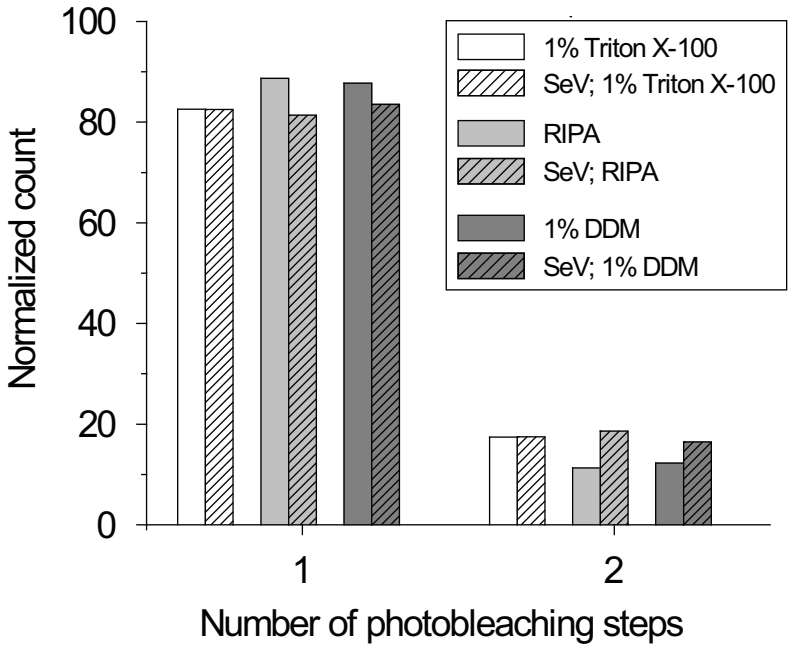

Figure 4.8 Photobleaching step distribution for YFP-MAVS from whole cell lysate. Cells expressing YFP-MAVS, with or without Sendai virus infection (SeV) were lysed using (a) 1% Triton X-100, 20 mM Tris-HCl (pH 7.5), 150 mM NaCl, 1 mM EDTA, (b) RIPA buffer (25 mM Tris-HCl (pH 7.6), 150 mM NaCl, 1% NP-40, 1% sodium deoxycholate, 0.1% SDS) or (c) 1% DDM, 20 mM Tris-HCl (pH 7.5), 150 mM NaCl, 1 mM EDTA. YFP-MAVS was pulled down using antibodies against YFP.

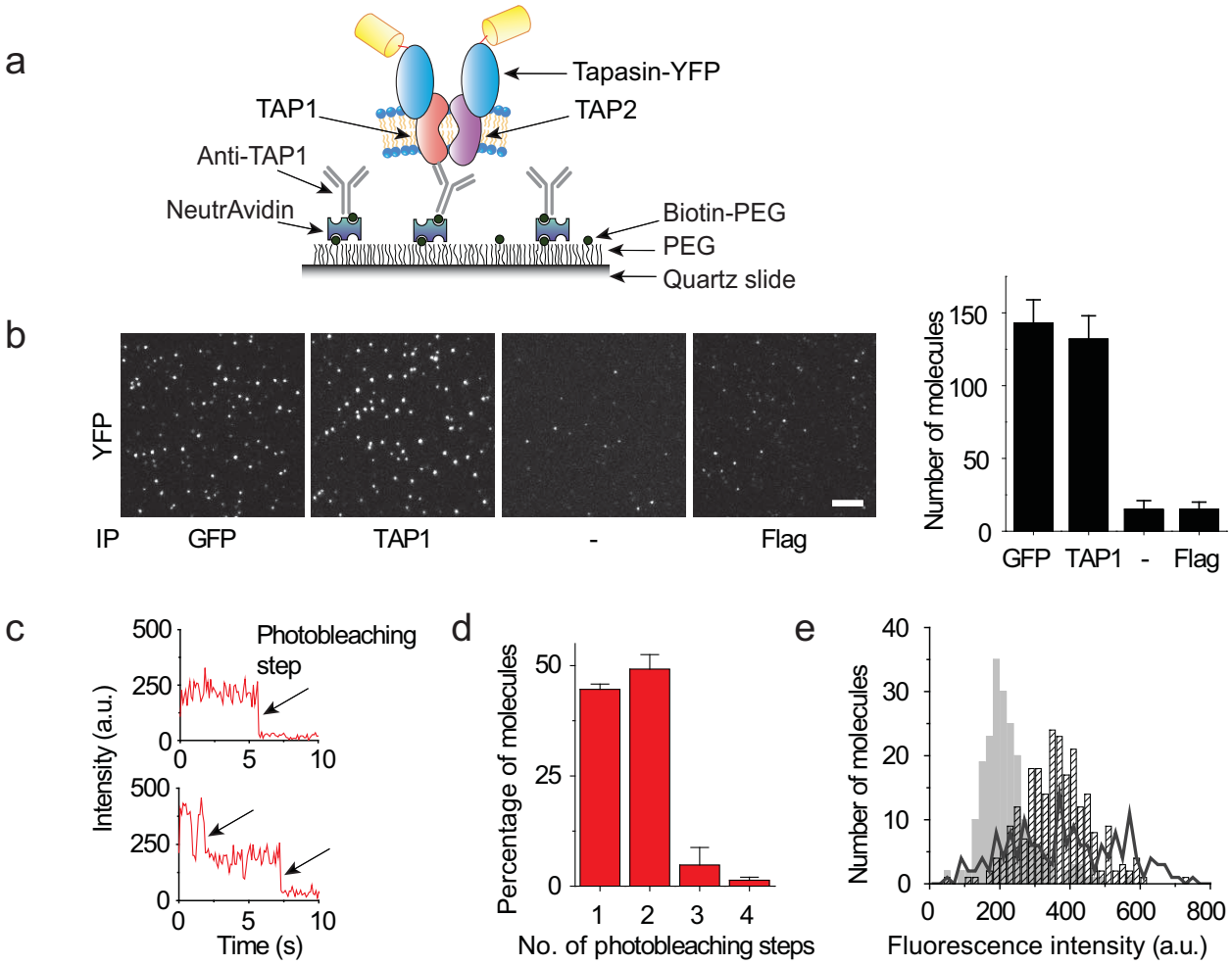

Figure 4.9 SiMPull of TAP-tapasin complexes. (a) Schematic depicting SiMPull analysis of .220.B4402.tapasin-YFP cells. Cells were lysed in digitonin and applied to an antibody-coated flow chamber, followed by imaging using a TIRF microscope. (b) representative fluorescent images (*left*) and quantitation (*right*) of tapasin-YFP pull-down in flow chambers coated with goat anti-GFP, the anti-TAP1 antibody 148.3, no antibody, or a control antibody (mouse anti-FLAG). The scale bar on the fluorescent images represents 5 μm. The quantitative results are expressed as the mean plus the standard deviation of at least 20 imaging areas (2500 μm^2 each) in one representative experiment. (c), representative fluorescence time traces of molecules exhibiting one-step (*top left*) and two-step (*bottom left*) photobleaching, photobleaching step distribution (*middle*), and fluorescence intensity distribution (*right*) for the observed tapasin-YFP photobleaching events.

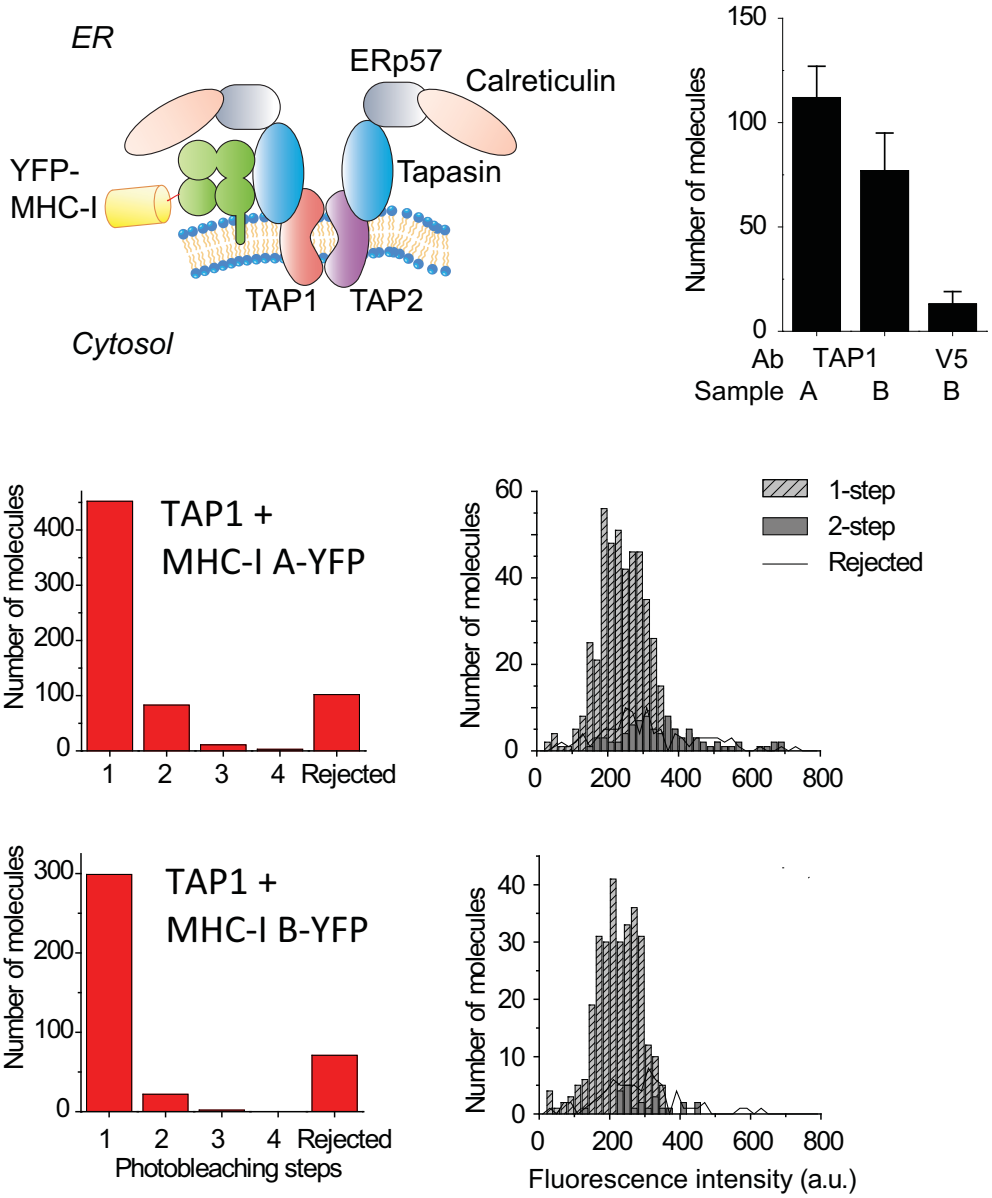

Figure 4.10 SiMPull of TAP-MHC class I complexes. MHC class I molecules are pulled down using surface immobilized anti-TAP1 antibody. For both samples A and B, the observed photobleaching step distribution indicates that only one copy of MHC class I molecule is bound per complex.

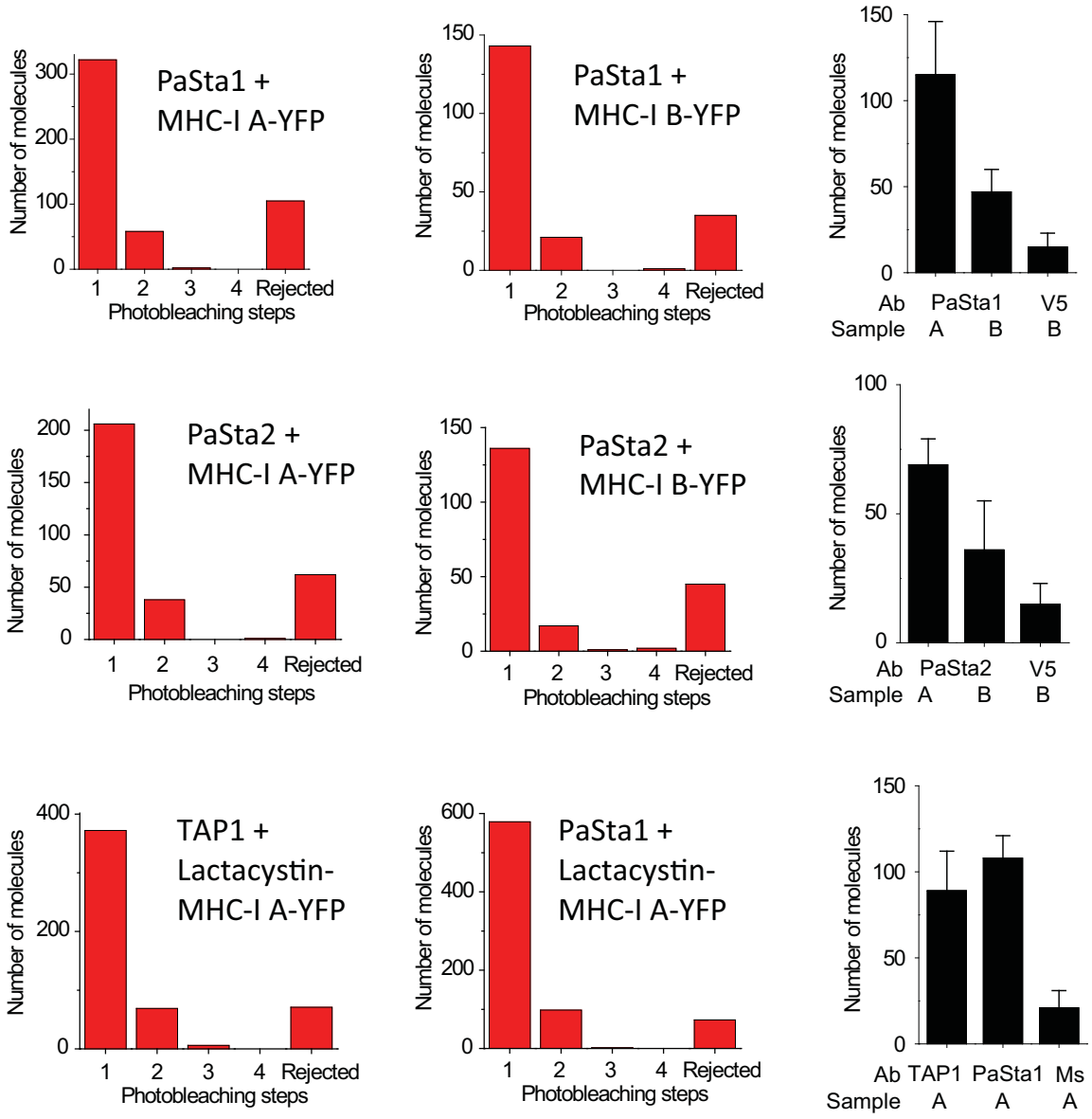

Figure 4.11 Stoichiometry of MHC class I-tapasin complex. MHC class I molecules pulled down with antibodies against tapasin, PaSta1 (a) or PaSta2 (b) are monomeric. Expression level was lower for B allele as compared to A. Blocking proteasome with lactacystin does not affect the observed stoichiometry of MHC class I molecules.

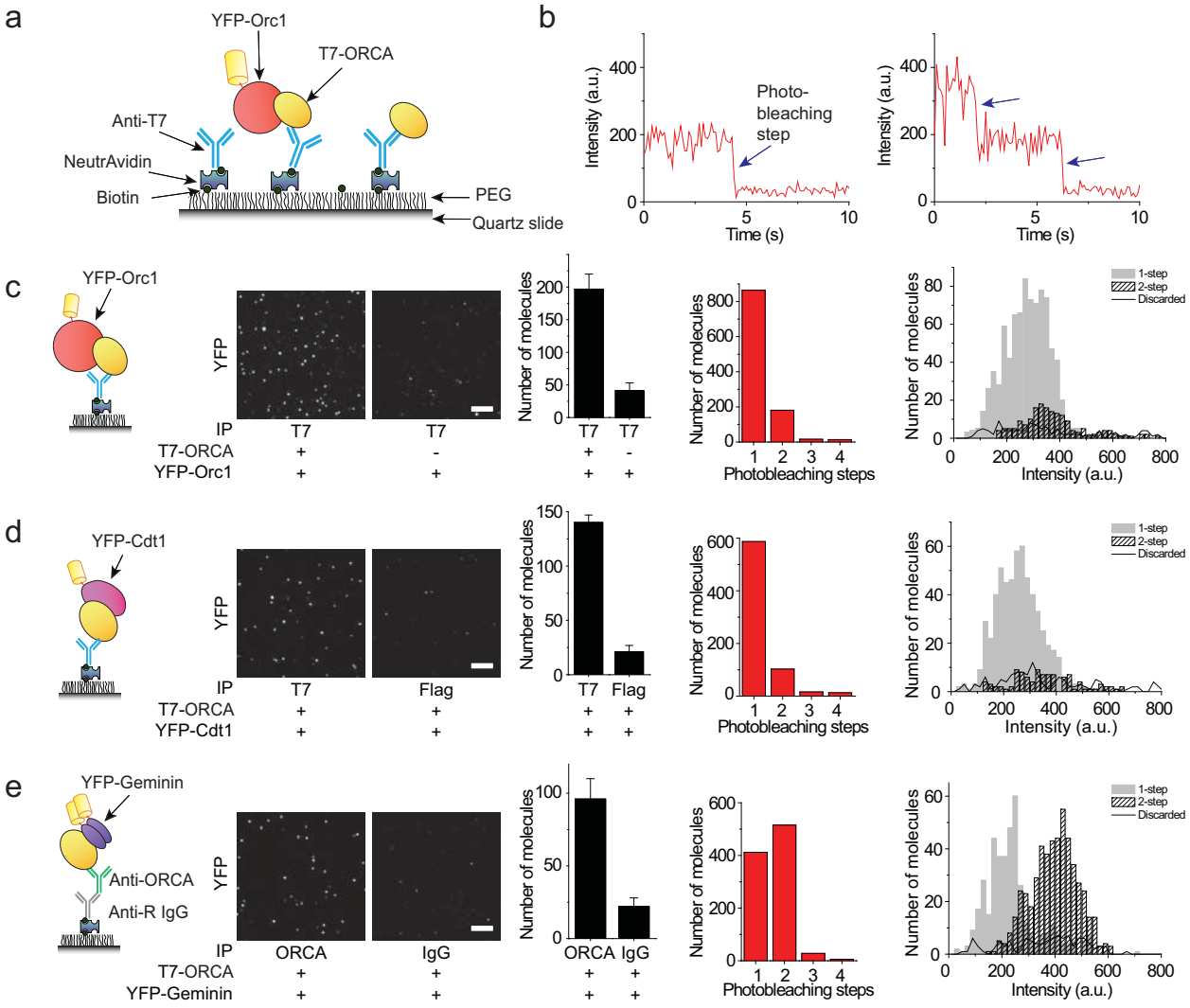

Figure 4.12 SiMPull on ORC binding proteins. (a) Schematic for ORC pull-down with ORCA. (b) Representative single-molecule fluorescence time trajectories of YFP-Geminin molecules that exhibit one-step and two-step photobleaching. (c) ORCA-Orc1 pull-down indicates that ORCA associates with one molecule of Orc1. (d) ORCA-Cdt1 pull-down shows Cdt1 bound to ORCA is monomeric (e) ORCA-Geminin pull-down; the photobleaching step distribution for Geminin-YFP is consistent with two copies of Geminin per complex ORCA-Geminin.

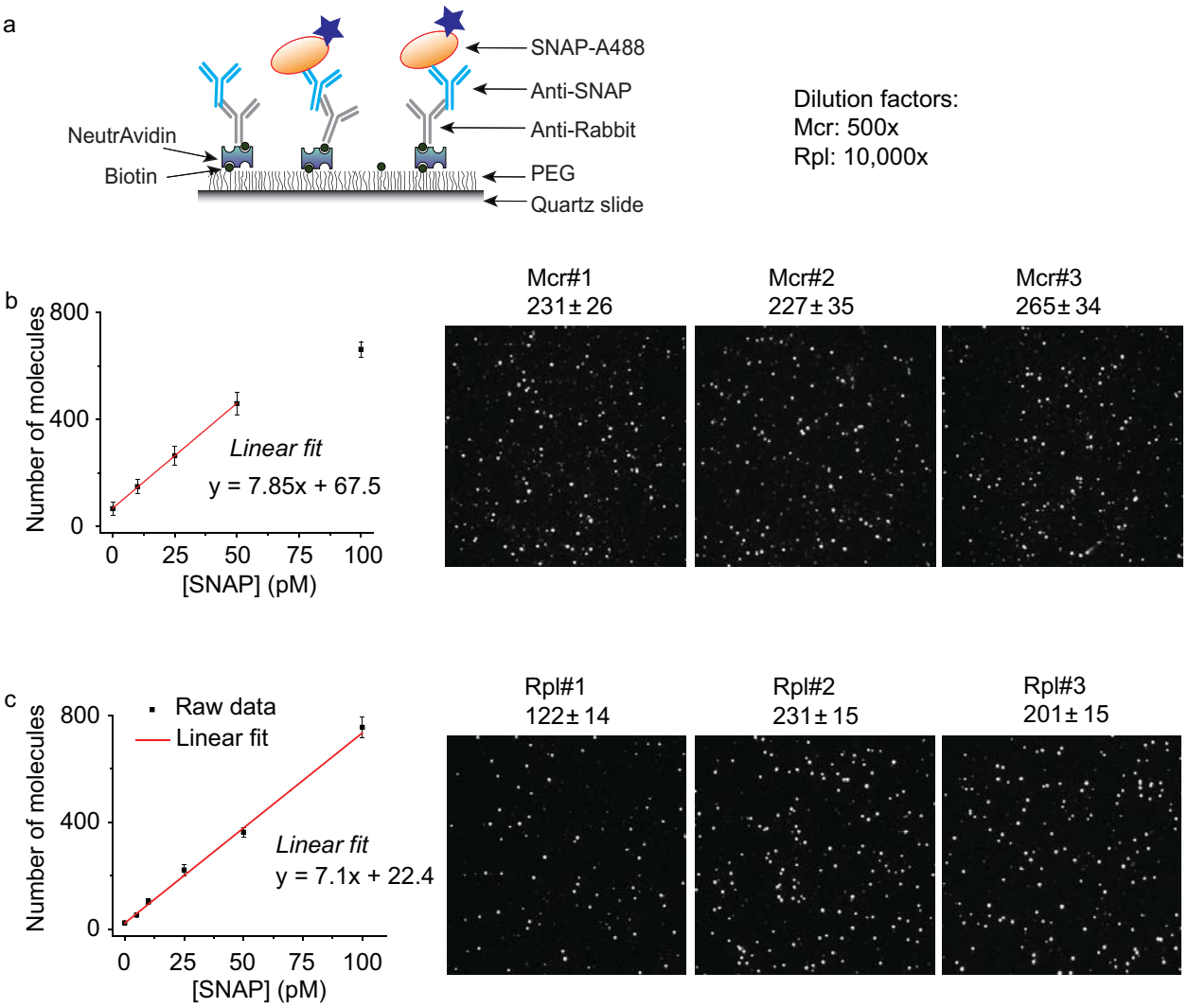

Figure 4.13 Copy-number determination for archeal proteins. (a) Schematic for SiMPull of SNAP tagged proteins. (b, c) Slides were calibrated using purified SNAP protein labeled with Alexa488. Triplicates of Mcr-SNAP or Rpl-SNAP culture with ~10^8 cells were labeled with Alexa488, and after free dye removal, samples were applied to SiMPull chambers with SNAP antibody. Comparison with the calibration curve yields the concentration of SNAP, which is converted to average copy number per cell.

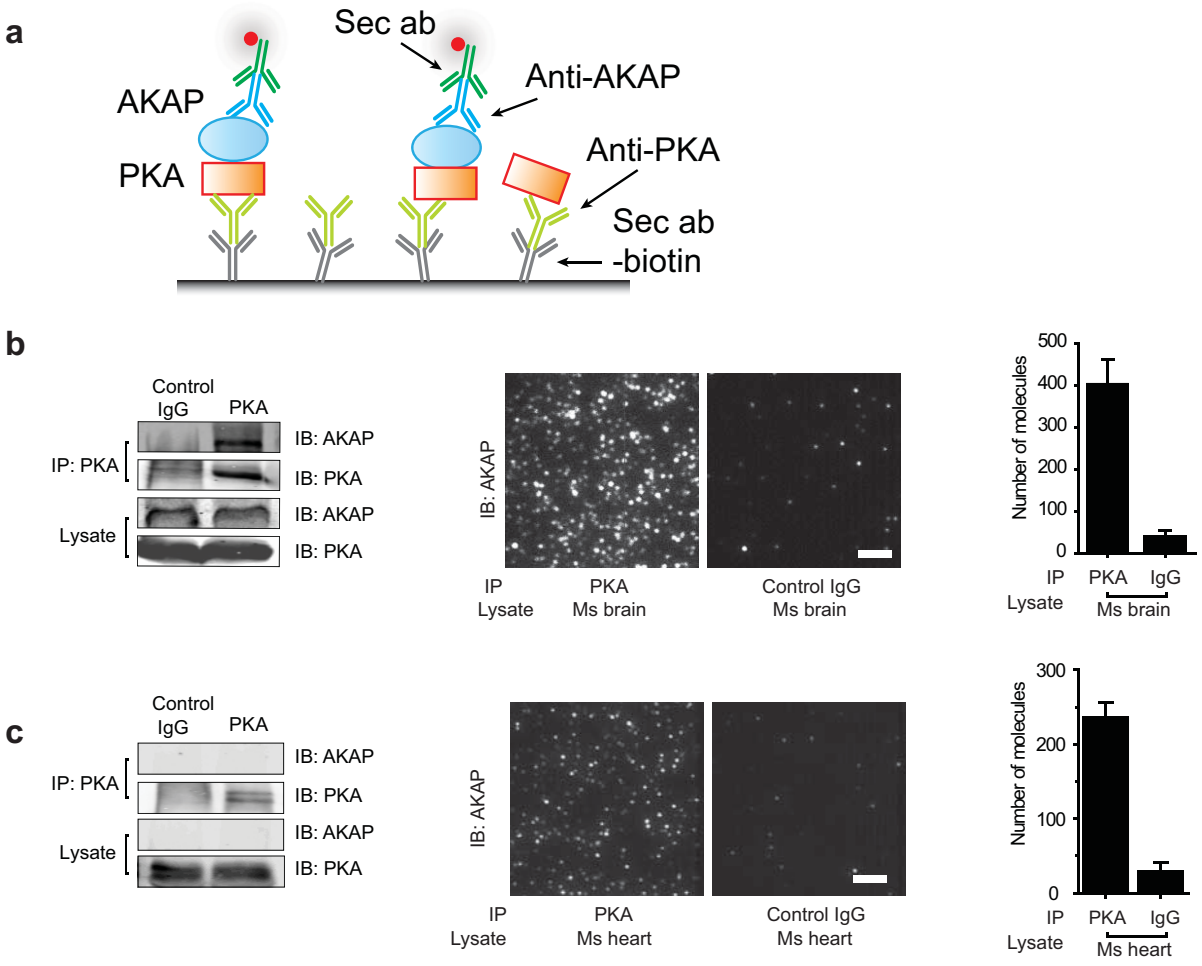

Figure 4.14 PKA-AKAP pull-down from tissue extracts. (a) Schematic for endogenous PKA-AKAP complex pull-down. (b) WB from mouse brain extract. AKAP is co-immunoprecipitated with antibody against PKA but not with control IgG. For SiMPull, antibody against PKA or control IgG is immobilized via a biotinylated secondary antibody. AKAP is detected using antibody against AKAP150 and a corresponding secondary antibody labeled with Alexa647. (c) Bulk immunoprecipitation of PKA from solubilized mouse heart extract. AKAP could not be detected in immunoblot from lysate due to its low abundance. Using SiMPull, we were able to detect PKA-AKAP association in heart lysate highlighting the sensitivity of the assay. Scale bar is 5 μm. Error bars represent standard deviation of the mean across 20 or more images.

Chapter 5*

Architecture and Assembly of mTOR Complexes

5.1 Background

The mechanistic (or mammalian) target of rapamycin (mTOR) is the master regulator of crucial cell and development processes such as cell growth, proliferation, differentiation, and metabolism. mTOR is a serine/threonine protein kinase belonging to the PI3K-related kinase family that integrates the sensing of nutrients, growth factors, oxygen, energy and different types of stress to regulate a myriad of biological processes such as cell growth, proliferation, differentiation and metabolism (Laplante and Sabatini, 2012).

In vivo, mTOR nucleates at least two biochemically and functionally distinct complexes – mTORC1 and mTORC2. mTORC1 is the rapamycin-sensitive complex and is composed of the proteins Raptor (Hara et al., 2002; Kim et al., 2002) and GβL (Kim et al., 2003), and the regulatory proteins PRAS40 (Fonseca et al., 2007; Oshiro et al., 2007; Sancak et al., 2007; Haar et al., 2007; Wang et al., 2007) and Deptor (Peterson et al., 2009) that function as inhibitors of mTORC1. A major function of mTORC1 is regulation of cell growth, and its activation depends on the availability of nutrients (in particular, amino acids) and growth factors (Laplante and Sabatini, 2012). The best-known substrates of the mTORC1 kinase are the ribosomal subunit S6 kinase S6K1 and the eIF4E binding protein 4EBP1, both regulators of protein translation (Ma and Blenis, 2009). mTORC2 consists of Rictor (Jacinto et al., 2004; Sarbassov et al., 2004), GβL, and mSin1

*This work in Chapter 5 has been published in the following paper, and is a part of a manuscript in preparation.

- Jain A, Liu R, Ramani B, Arauz E, Ishitsuka Y, Ragunathan K, Park J, Chen J, Xiang Y, & Ha T, "Probing cellular protein complexes using single-molecule pull-down", *Nature* **473**, 484-488 (2011).

(Frias et al., 2006; Jacinto et al., 2006; Yang et al., 2006), as well as the negative regulator Deptor (Peterson et al., 2009). The mTORC2 kinase substrates include Akt, SGK1, and cPKC, through which mTORC2 regulates a wide range of cellular and developmental processes (Oh and Jacinto, 2011). Originally defined as the rapamycin-insensitive complex, mTORC2 is inhibited by prolonged rapamycin treatment in some types of cells (Sarbassov et al., 2006).

Oligomerization of both mTORC1 and mTORC2 has been reported. A recent cryo-electron microscopy (cryo-EM) study has revealed that mTORC1 – containing mTOR, Raptor, and PRAS40 – self-associates as a dimeric structure (Yip et al., 2010). Detailed structural information about mTORC2 is currently lacking. Biochemical analyses over the years have also identified self-association of TOR/mTOR and mTORC1 (Wullschleger et al., 2005; Zhang et al., 2006; Wang et al., 2006; Takahara et al., 2006), but consensus is lacking on the oligomeric state of TORC2/mTORC2, which has been reported to be monomeric, dimeric, or multimeric (Takahara et al., 2006; Wullschleger et al., 2005; Tao et al., 2010; Frias et al., 2006).

Conventional biochemical methods have inherent limitations in deciphering protein complex assembly. Interaction assays such as pull-down and co-immunoprecipitation do not allow the determination of the copy numbers of each component in a complex. Size exclusion chromatography offers low-resolution estimates of the sizes of proteins complexes, but potential presence of unidentified proteins precludes confident assessment of oligomeric states of a complex by this method. Additionally, the lengthy procedures often associated with biochemical characterization could lead to loss or alteration of physiological protein complexes. Hence, an accurate understanding of mTOR complex assembly remains a formidable challenge.

We have used SiMPull to determine the oligomeric state and the possible assembly routes for mTORC1 and mTORC2. We systematically labeled individual mTORC1/mTORC2 components with a YFP fusion tag, and captured the intact complexes from whole cell extracts using antibody against non-YFP components (Figure 5.1a). All fusion constructs were tested for incorporation in the complexes via biochemical analysis; additionally, the fusion construct incorporated complexes were tested for their activity on S6K1 and/or Akt. We established a stable cell line expressing YFP-

mTOR at near endogenous level, and knocked down endogenous mTOR using shRNA. The modified cell line recapitulates the known functions of mTOR signaling and allowed us to implement SiMPull to investigate mTOR signaling in response to nutrients, growth factors and rapamycin.

5.2 mTORC1 is dimeric

mTORC1 is the rapamycin sensitive complex and is activated by nutrients (amino acids), anabolic growth factors (e.g., insulin and insulin-like growth factor), and cellular energy (ATP), and is better characterized of the two complexes. A cryo-electron microscopy study revealed that mTORC1 assembles in a two-fold symmetric structure with 2 copies each of mTOR, Raptor, GβL and PRAS40. We first validated our SiMPull assay for mTORC1 system.

Using an antibody against Raptor, we are able to pull-down YFP-mTOR from the cell line expressing YFP-mTOR at near endogenous level (Figure 5.1b), while a background level of fluorescence is observed in the control channel without Raptor antibody. We analyzed the fluorescence time-trajectories of each fluorescent spot. A vast majority of the molecules (97%) bleached in either 1 or 2-steps indicating that mTORC1 contains one or two molecules of YFP-mTOR (Figure 5.1b). 56% of the molecules exhibited 2-step bleaching, while 41% bleached in a single step. Previous reports by others and us have determined that fluorescent proteins may not mature to completion and the fraction of fluorescently active YFP is ~75% (Jain et al., 2011; Ulbrich and Isacoff, 2007). This observed distribution of photobleaching steps is consistent with two molecules of YFP-mTOR in each mTORC1, accounting for the active fraction of YFP. The intensity of the molecules bleaching in two steps was nearly twice that of single step bleachers; the discarded molecules did not exhibit any enrichment in intensities, indicating reliable scoring. Thus, each mTORC1 contains two copies of mTOR.

When we co-express YFP-mTOR and HA-Raptor, using an anti-HA antibody, we are able to pull-down YFP-mTOR (Figure 5.1c). On examining the fluorescence time-trajectories, we observe that nearly 37% of the molecules bleach in a single photobleaching step, while 56%

exhibited two-step bleaching indicating that each mTOR-Raptor complexes contain 2 copies of mTOR. Similar analysis was performed to determine the stoichiometry of Raptor in mTOR-Raptor complexes: we co-expressed YFP-Raptor together with Flag-mTOR and pulled down the complexes using anti-Flag antibody (Figure 5.1d). Nearly 48% of the YFP-Raptor molecules bleached in two steps, indicating that a majority of the complexes contain two Raptor molecules. Thus mTOR and Raptor co-expression is sufficient for a dimeric complex assembly.

mTORC1 activity is regulated by inhibitory proteins PRAS40(Oshiro et al., 2007; Sancak et al., 2007; Thedieck et al., 2007; Wang et al., 2007) and Deptor(Peterson et al., 2009). We sought to determine the stoichiometry of these inhibitors in mTORC1. We engineered YFP-PRAS40 and YFP-Deptor constructs that incorporate in mTORC1. PRAS40 directly interacts with Raptor (Thedieck et al., 2007); to ensure that we are capturing whole mTORC1, we pulled down YFP-PRAS40 using an antibody against mTOR (Figure 5.1e). Deptor binds to mTOR, and was captured using an antibody against Raptor to ensure that the observed YFP-Deptor molecules are in the mTORC1 complex. In either case, we observe a significant fraction of molecules bleaching in two steps, consistent with two molecules each of PRAS40 and Deptor in mTORC1.

Our attempts to label GβL with a fluorescent protein tag were not successful; a recent crystal structure of mTOR kinase domain shows that mTOR-GβL complex has 1:1 interaction stoichiometry (Yang et al., 2013). In summary, our results indicate that each protein component is present in 2 copies per mTORC1. The findings are consistent with the previous biochemical and cryo-electron microscopy data thus validating SiMPull and our fluorescent protein constructs for analysis of mTOR complexes.

5.3 mTORC2 is dimeric

Our current knowledge of mTORC2 assembly derives exclusively from traditional biochemical assays. Oligomerization of mTORC2 has been observed in gel-filtration and co-IP experiments (Pearce et al., 2007; Takahara et al., 2006; Tao et al., 2010), but the nature of the oligomers is unclear. We captured mTORC2 complexes from our YFP-mTOR cell line using an

antibody against endogenous Rictor. Intriguingly, once again we observed that 97% of the molecules bleached in one or two photobleaching steps, out of which 53% bleached in two-steps (Figure 5.2a). To corroborate our findings, we transiently expressed mTORC2 components in HEK293 cells. Co-expression of all mTORC2 core components, mTOR, Rictor, GβL and mSin1, was required to observe interaction between mTOR and Rictor, which is consistent with previous reports that mSin1 is essential for mTORC2 assembly (Frias et al., 2006). In this reconstitution system, we are able pull-down YFP-mTOR using antibody against Flag-Rictor. The observed fraction of molecules bleaching in two steps for YFP-mTOR (44%) is lower than that for our YFP-mTOR stable cell line, and may be due to endogenous mTOR which is not labeled with YFP, or due to incomplete assembly.

To determine the stoichiometry of Rictor in mTORC2, we prepared a YFP-Rictor construct, and co-expressed with Flag-mTOR, HA-mSin1 and HA- GβL. Assembly of mTORC2 was verified by ensemble pull-down. Using a Flag antibody, we are able to pull-down mTORC2 and determine the stoichiometry of YFP-Rictor (Figure 5.2 c). The observed photobleaching step distribution (38% 1-step and 55% 2-step bleaching) indicates that each mTORC2 contains two copies of Rictor. Finally, we co-expressed Deptor-YFP with core mTORC2 components and starved cells of serum to promote incorporation of Deptor in mTORC2; Deptor directly associates with mTOR and inhibits both mTORC1 and mTORC2 signaling (Peterson et al., 2009). Using antibody against Rictor, we specifically captured YFP-Deptor associated with mTORC2. The observed photobleaching step distribution corresponds to a mixture of monomers and dimers (54% dimer assuming 75% active YFP) indicating that each mTORC2 can harbor up to two copies of Deptor. Our attempts to fluorescently tag mSin1 were not successful. In summary our results indicate that both mTORC1 and mTORC2 exhibit a dimeric architecture where each subunit is present in 2 copies.

5.4 mTORC1 and mTORC2 are distinct

The observed dimeric organization of both mTORC1 and mTORC2 made us wonder if both Raptor and Rictor can be present in the same complex. Functional crosstalk between mTORC1 and mTORC2 at multiple levels is increasingly apparent (Huang and Manning, 2009;

Dibble et al., 2009; Julien et al., 2009; Laplante and Sabatini, 2009), and the current evidence cannot definitively rule out the existence of physical interaction between the two complexes in minor fractions. We used 2-color SiMPull to distinguish between the two complexes. As a positive control, we labeled Raptor with mCherry tag and mTOR with YFP. Upon GβL pull-down, we observe that ~46% of the YFP molecules co-localized with mCherry, significantly higher than the control (6%) (Figure 5.3). Incomplete co-localization between mCherry-Raptor and YFP-mTOR upon GβL pull-down may arise due to two reasons: first, not all mTOR-GβL complexes may bind to Raptor. Second, the chromophore in YFP and mCherry may not mature completely (~75% and < 40% respectively), and is discussed at length in Chapter 3 (Ulbrich and Isacoff, 2007; Dunne et al., 2009).

Next, we co-expressed mCherry-Raptor and YFP-Rictor together with Flag-mTOR and HA-mSin1 and HA-GβL. Using anti-Flag antibody we are able to capture both mTORC1 as well as mTORC2 as visualized by mCherry and YFP fluorescent spots respectively. When we overlay the two channels, ~12% of mCherry molecules co-localize with YFP, setting the upper limit of hybrid complexes containing both Raptor and Rictor. Out of 12% co-localization, 6% is likely false co-localization by chance due to simultaneous occurrence of two molecules in the same diffraction limited spot, as observed in the control. The probability of a molecule to contain a dark YFP is 0.25 for monomer and 0.06 for dimer. Thus, accounting for false co-localization and the dark YFP fraction, a maximum of 8% of the molecules contain both Raptor as well as Rictor. Thus a vast majority of mTORC1 and mTORC2 complexes are distinct and binding of Raptor and Rictor to mTOR is mutually exclusive, consistent with biochemical analyses.

5.5 mTORC1 and mTORC2 components are monomeric

Since both mTORC1 and mTORC2 are dimeric, we asked if mTOR or other core components of mTOR complexes can self-dimerize. We expressed individual components of the mTOR complexes tagged with YFP. When we express YFP-mTOR and capture it using anti-mTOR antibody, nearly 75% of the molecules bleached in a single-step, while 20% bleached in two steps,

indicating that 82% of YFP-mTOR is monomeric (Figure 5.4 a). Similar analysis for Raptor and Rictor revealed that these two proteins are also monomeric (88% and 93% respectively, Figure 5.4 b, c). Thus individually, mTOR, Raptor and Rictor are largely monomeric. The observed small dimer fraction may arise due to incorporation of YFP-tagged proteins in endogenous mTOR complexes.

It has been suggested that mTORC2 assembly depends on the interaction of two sub-complexes, mTOR-GβL and Rictor-mSin1. We tested if these sub-complexes are dimeric and form the interface for complex assembly. However, in each case we observed a monomer-like distribution (Figure 5.4 d, e). Finally, we also tested if Deptor can interact with mTOR, independent of the other mTOR components. YFP-Deptor associated with Flag-mTOR is also monomeric (Figure 5.4 f). Thus, individual mTOR components and sub-complexes are monomeric. Our data suggests that no single mTOR component serves as a dimerizing component, but rather sub-complexes interact to form the dimeric holocomplex.

5.6 Effect of rapamycin on mTOR complexes

We investigated the effect of rapamycin on the stoichiometry of mTOR complexes. Rapamycin is a potent inhibitor of mTOR. Short term treatment with rapamycin inhibits mTORC1 while on longer treatment mTORC2 activity is also affected. Despite numerous efforts, the mode of action of rapamycin is debated and it is not clear if rapamycin blocks activity by blocking access to the kinase domain or if it interferes with mTOR-Raptor interaction (Oshiro et al., 2004; Yang et al., 2013).

We used the YFP-mTOR stable cell line to study the effect of rapamycin treatment in mTOR complexes using SiMPull (Figure 5.5). Upon 30 min treatment of cells with 100 nM rapamycin, the number of YFP spots decreased by ~89%. Treatment with 2 nM rapamycin reduced the number of observed YFP-mTOR spots by ~50%. Thus, our data indicates that rapamycin directly disrupts the interaction between mTOR and Raptor and breaks the mTORC1 complexes. Next, when we analyzed the fluorescence time trajectories of rapamycin treated samples, we find that

the fraction of 2-step bleaching events decreases as the rapamycin dose is increased. At 2 nM rapamycin, about 45% of the molecules bleached in two steps, while at 10 nM, only 28% of the molecules exhibited 2-step bleaching. This observation of transient monomeric mTOR-Raptor complexes indicates that rapamycin disrupts mTORC1 in two steps: first dissociating the dimeric mTORC1 followed by mTOR-Raptor monomeric interaction (Yip et al., 2010). Furthermore, only about 40% of complexes are left intact after 2 nM rapamycin treatment: consistent with this fraction, in the biochemical assay measuring the kinase activity of mTORC1, we find that the kinase activity of mTORC1 is significantly reduced upon treatment with 2 nM rapamycin and is completely abrogated at 10 nM or higher concentrations of rapamycin. This correspondence between the intact mTORC1 fraction and the kinase activity indicates that disruption of mTORC1 significantly contributes to rapamycin mediated abrogation of mTORC1 signaling.

Of note, in vitro, even upon adding 250 nM rapamycin with 500 nM FKBP12 in whole cell lysates, we did not observe significant disruption of mTORC1 complexes in our SiMPull assay. It is possible that after lysis, the conformation of mTOR is different from that in vivo, and thus mTOR is not able to bind rapamycin as effectively as in vivo. As lysates are treated much gently in SiMPull as compared to the conventional immunoprecipitation assays, our results indicate that the observed disruption of mTORC1 complexes in in vitro biochemical assays (by addition of rapamycin after lysis) (Yip et al., 2010) may arise during biochemical purification steps. Thus, we find that rapamycin acts by disrupting mTOR-Raptor interaction, and breaks the complex by removing one mTOR-raptor sub-complex at a time.

Next, we investigated the effect of rapamycin on mTORC2. As expected, short term rapamycin treatment has no effect on mTORC2 complex (Figure 5.6). Upon prolonged treatment (> 6h) with 100 nM rapamycin, we find that the amount of mTORC2 that is captured with anti-Rictor antibody drops 4-fold after 24 hours. Interestingly, in contrast to the transient mTORC1 monomers, for mTORC2 we find that at each time point the fraction of molecules bleaching in two steps is nearly the same, and corresponds to two molecules of mTOR per complex. For the same sample, the amount of total mTOR remains constant, while mTORC1 is significantly disrupted at 6

h treatment. Thus, our results indicate that rapamycin does not break mTORC2 directly, but rather, it is an effect due to sequestration of free mTOR by rapamycin. Additionally, assembled mTORC2 complexes are exclusively dimeric.

5.7 Effect of glucose/glutamine starvation on mTOR complexes

mTOR is a key sensor for the energy status of the cell. A recent report (Kim et al., 2013a) identified the TTT-RUVBL1/2 complex as a mediator of mTORC1 oligomerization, which is inhibited in the energy depleted state, leading to mTORC1 disassembly. SiMPull allows us to directly quantify the number of assembled mTOR complexes against free mTOR or Raptor. We investigated the effect of the energy status of the cell on mTORC1 dimerization.

We starved YFP-mTOR cells of glucose and glutamine; combined glucose/glutamine deprivation for prolonged period (> 12 h) leads to severe energy depletion, and inhibition of mTORC1 signaling (Kim et al., 2013a). The inhibition is relieved by brief (1 h) stimulation by replenishing the growth medium with glucose and glutamine. In SiMPull, when we pull-down endogenous Raptor in starvation and stimulation conditions, we observe nearly equal number of mTORC1 complexes (Figure 5.7 a). When we analyze the stoichiometry of mTORC1, we find that the photobleaching step distribution of mTORC1 in starvation conditions corresponds to that of a dimer. Additionally, the photobleaching step distribution is not altered upon re-stimulation. Similarly, we find that the neither the number of mTORC2 complexes nor their stoichiometry is altered by energy stress (Figure 5.7 b). The level of mTOR expressed remains unchanged under energy depletion or re-stimulation (Figure 5.7 c). Thus, our results indicate that mTORC1 is dimeric upon energy depletion and the inhibition is not achieved by disassembling mTOR complexes.

Additionally, we analyzed the interaction of mTOR with the known inhibitors of mTORC1 signaling: PRAS40 and Deptor. When we pull-down endogenous Deptor, we do not observe any significant change in Deptor-mTOR binding or stoichiometry in response to energetic stress (Figure 5.7 d). We were not able to pull-down endogenous PRAS40 likely due to lack of suitable antibodies.

We co-expressed exogenous HA-tagged PRAS40 in our YFP-mTOR stable cell line. On surface immobilized anti-HA antibody, we observe YFP-mTOR binding, likely from inhibited mTORC1 complexes. The pulled down complexes are dimeric: this result further corroborates that mTORC1 is not disassembled in response to energy depletion.

In conjunction with previous reports, our results indicate that a complete inhibition of mTORC1 signaling can be achieved without requiring disassembly of mTORC1. Cellular energy levels are tightly coupled to mTOR activation and cells have evolved multiple pathways to regulate mTOR activity such as association with inhibitory proteins, inactivation of Rheb (by TSC2) (Sofer et al., 2005) or post-translational modifications (such as phosphorylation of Raptor via AMPK). Specialized regulators of mTORC1 activity in response to energy depletion such as PRAK have also been identified (Zheng et al., 2011). Kim et al. used $TSC2^{-/-}$ cells for demonstrating the mTORC1 disassembly in response to energy depletion (Kim et al., 2013a). TSC2 is a critical negative regulator of mTORC1 activity via Rheb; it is possible that the observed mTORC1 disassembly by Kim et al. in TSC2 knockout cells is a compensatory response to TSC2 depletion, and represents a second layer of regulation for mTORC1 signaling.

5.8 Effect of growth factors and amino acids

Multicellular organisms rely on growth factors such as insulin for long-range communication to coordinate the distribution of nutrients with cell-growth. Serum starvation inactivates mTORC2, which in turn, down-regulates Akt. Akt is upstream of mTORC1 and inactivation of Akt leads to increased activity of TSC1/TSC2, and thus down-regulation of mTORC1. This effect is reversed by insulin treatment. Amino acid signaling feeds directly to mTORC1, and in the absence of amino acids, mTORC1 is inactivated.

We explored the effect of growth factors on the architecture of mTOR complexes by depleting the medium of serum for prolonged time (24 h). The effect of serum starvation was reversed by stimulating the cells with insulin for 1 h. Finally, we explored the effect of amino acid starvation for 24 h.

Serum starvation had no effect on the number or integrity of mTOR complexes (Figure 5.8 a, b); the number of spots was similar upon serum depletion and upon stimulation with insulin. In each case, mTORC1 and mTORC2 were exclusively dimeric. We verified that the expression level of mTOR did not change under our experimental conditions (Figure 5.8 c), nor did its association with the inhibitory protein, Deptor (Figure 5.8 d). Furthermore, removal of amino acids followed by insulin treatment had no effect on the complexes or protein expression levels.

One hallmark of mTOR activation is the phosphorylation at Ser 2448 site. Activation of mTORC1 results in phosphorylation and activation of p70S6 kinase, which in turn, phosphorylates mTOR at Ser 2448 site (Holz and Blenis, 2005; Chiang and Abraham, 2005). We immobilized a Ser 2448 phospho-mTOR specific antibody on the surface and incubated it with the lysate from serum starved or insulin stimulated cells (Figure 5.8 e). We find that upon serum starvation, mTOR is dephosphorylated and the observed fluorescence is comparable to blank. However, upon 1 h stimulation with insulin, we observe phosphorylated YFP-mTOR as the number of spots is significantly (~600%) increased. When we analyze the stoichiometry of phosphorylated mTOR, we find that a majority of the molecules (73%) bleached in a single photobleaching step indicating that a majority of phosphorylated mTOR (75%) is monomeric. Since mTOR bound to Raptor or Rictor is exclusively dimeric, this result indicates that free mTOR can be phosphorylated by p70S6. The photobleaching step distribution is similar for both phospho-mTOR as well as total mTOR pull-down, thus indicating the p70S6 does not discriminate between free mTOR or mTOR complexes.

Metabolic stress leads to activation of AMPK that directly phosphorylates Ser 792 residue of Raptor, thus inactivating mTORC1. We used a Ser 792 phospho-Raptor antibody to pull-down inactivated mTORC1 complexes. For serum starved samples, we observed a 2-fold higher binding of YFP-mTOR as compared to insulin stimulated samples. Our antibody was not suitable for immuno-precipitation and we used undiluted lysates (as compared to 10-100 fold dilutions for other experiments, Figure 5.8 a-e), and it is possible that the binding observed in the insulin stimulated samples arises from non-specific binding of YFP-mTOR to the antibody or the surface. mTOR bound to phosphor-Raptor is also dimeric (73%), although the increased 1-step bleaching events

may arise due to increased background/non-specific binding with this antibody. Thus, Ser 792 phosphorylated Raptor although inactive in signaling, is a part of dimeric mTORC1. The analysis of post-translational modifications further suggests that mTOR signaling can be effectively inhibited without disassembling the complexes, and is likely mediated by post-translational modifications or association with other inhibitory proteins.

5.9 Discussion

SiMPull provides a direct platform to probe the oligomeric state of large complexes that cannot be readily purified. Using SiMPull we have determined the architecture of mTOR complexes. We find that both mTORC1 and mTORC2 have a dimeric architecture with two copies of each subunit. Interaction between mTOR and Raptor alone is sufficient to form mTORC1 dimers, however, mTORC2 assembly requires co-expression of mSin1 and GβL in addition to mTOR and Rictor. Individual subunits of mTOR complexes are monomeric. Thus no single protein acts as a dimerizing component. Rapamycin physically disrupts the interaction between mTOR and Raptor. The time-scale of dissociation is comparable to that for inhibition of the kinase activity. In low-dose and short term rapamycin treatment, we are able to capture transient monomeric mTOR-Raptor complexes.

Despite inflicting a variety of stress conditions, we were not able to find any evidence of a monomeric association between mTOR and Rictor. Our results indicate a model for mTOR complex assembly in which two copies of each sub-complex come together, likely facilitated by other proteins or lysosomal membranes, to assemble the holocomplex. This dimerization of complexes may allow mTOR to avoid physical cross-talk between mTORC1 and mTORC2 signaling: mTORC1 monomers are unstable and cannot physically interact with mTORC2 monomers. We find that the mTOR signaling can be completely abrogated without any change in the dimerization of mTOR complexes. Disassembly of mTORC1 likely provides reserve mechanism to regulate mTOR activation.

5.10 Figures

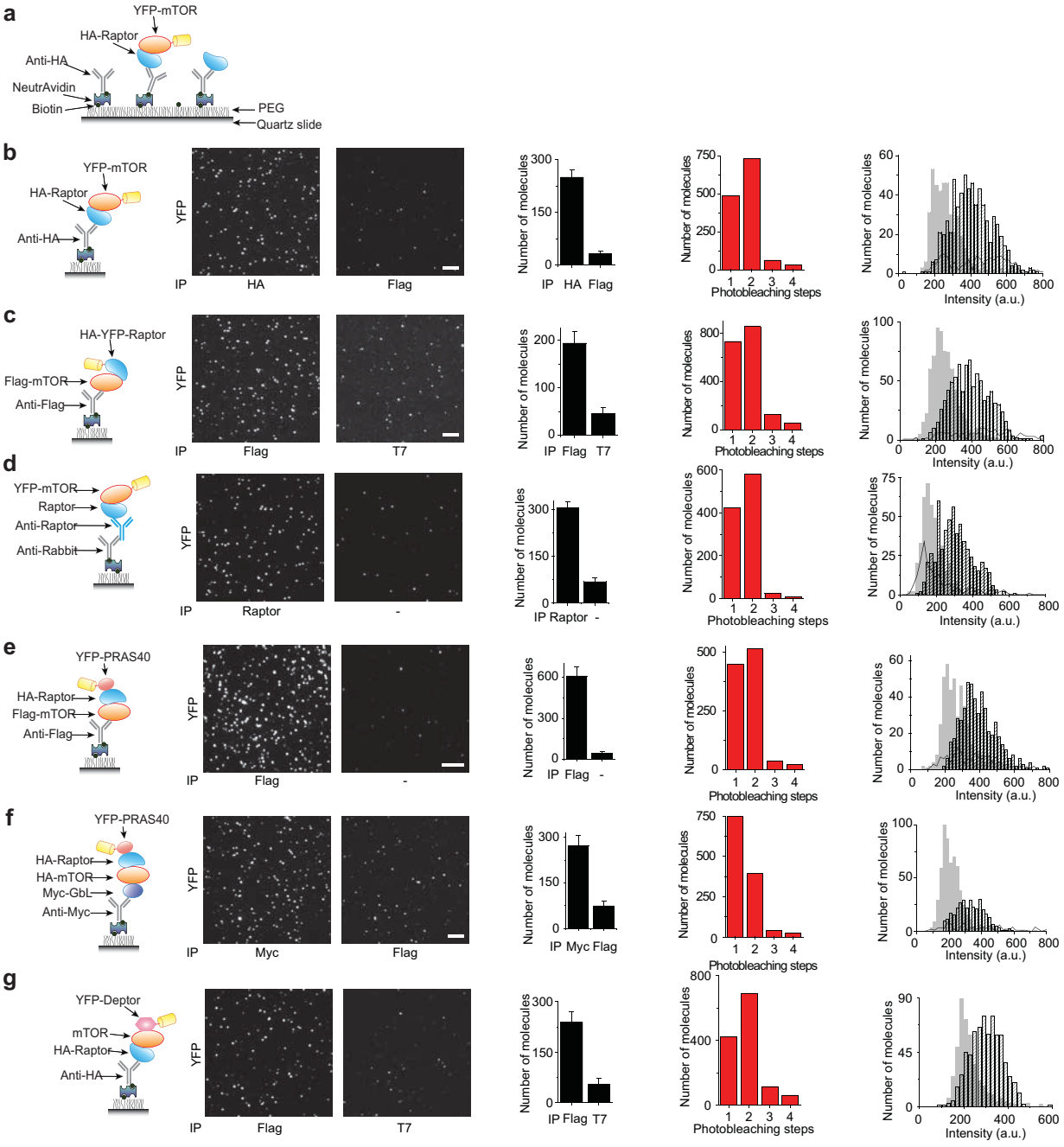

Figure 5.1 mTORC1 is dimeric. (a) Schematic for mTORC1 pull-down. (b, c) Raptor and mTOR when co-expressed, form dimers. (d) YFP-mTOR in complex with endogenous Raptor is dimeric. (e, f) PRAS40 when pulled down via mTOR shows a dimer like distribution and mixture of monomer and dimer in complex when pulled down via GβL (g) mTORC1 contains 2 copies of Deptor.

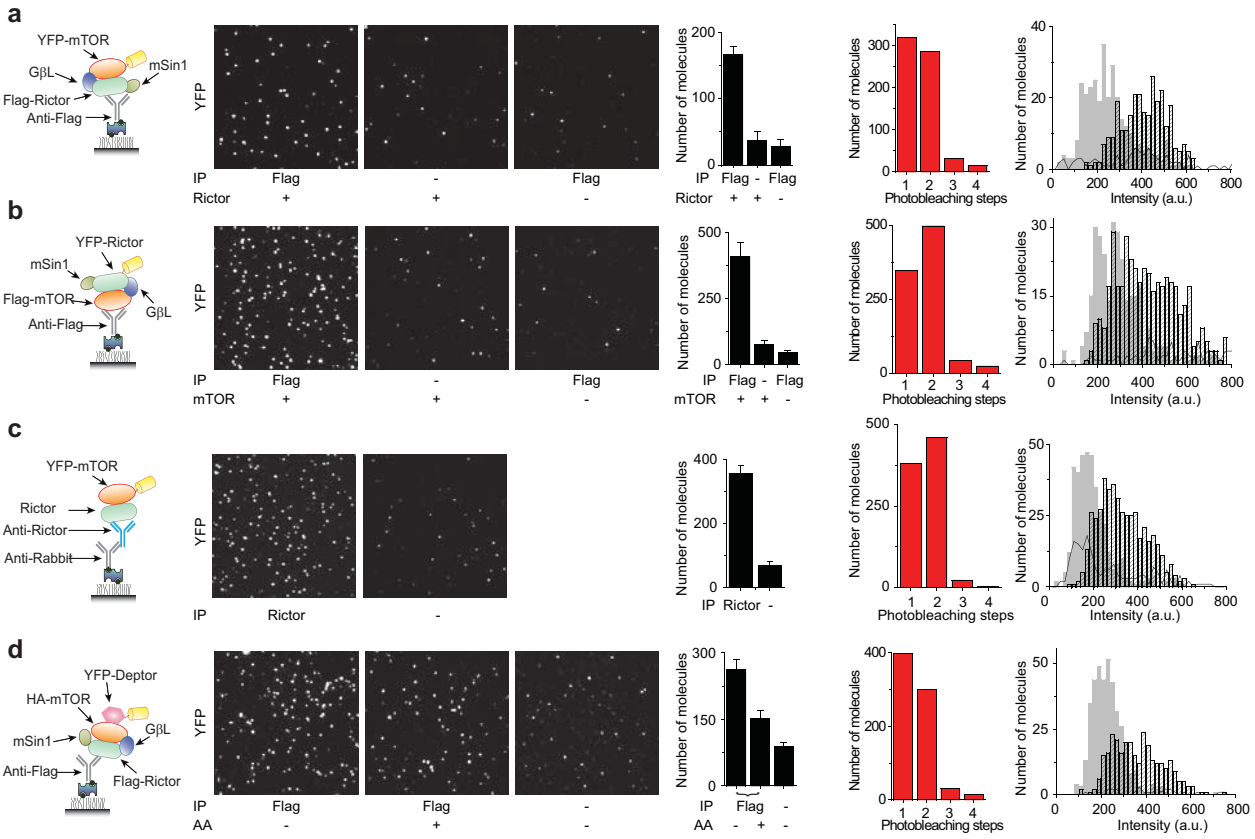

Figure 5.2 mTORC2 is dimeric. (a, b) All core subunits of mTORC2 are co-expressed (mTOR, GβL, Rictor and mSin1); each complex contains 2 copies of (a) mTOR and, (b) Rictor. (c) Endogenous Rictor associates with two molecules of mTOR. (d) mTORC2 can contain up to two copies of Deptor.

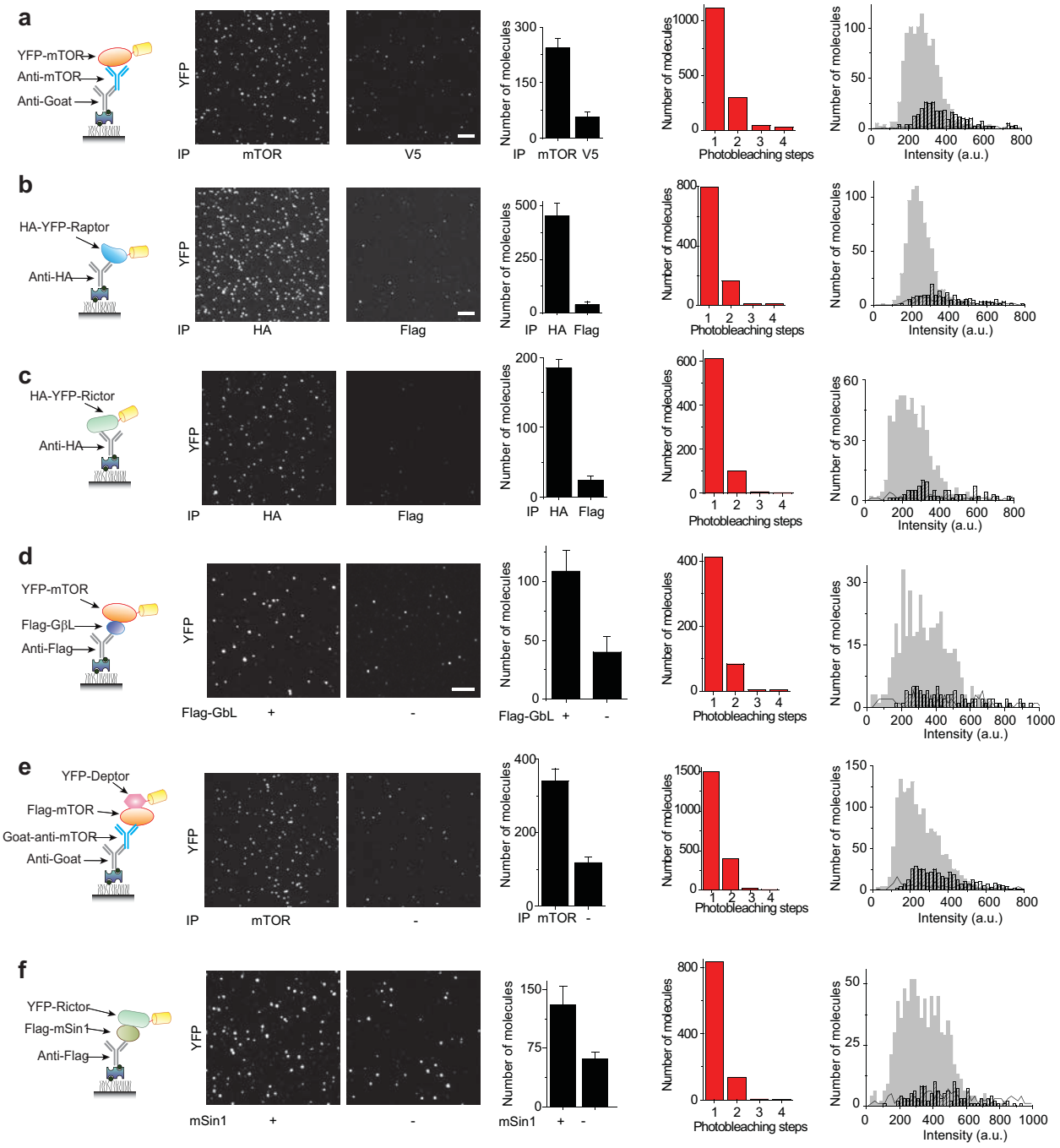

Figure 5.3 mTOR sub-complexes are monomeric. Individual subunits, (a) mTOR, (b) Raptor and (c) Rictor when expressed alone as YFP fusions, are monomeric. Sub-complexes (d) mTOR-GβL, (e) mTOR-Deptor and (f) mSin1-Rictor are monomeric and contain one copy of mTOR, Deptor and Rictor respectively.

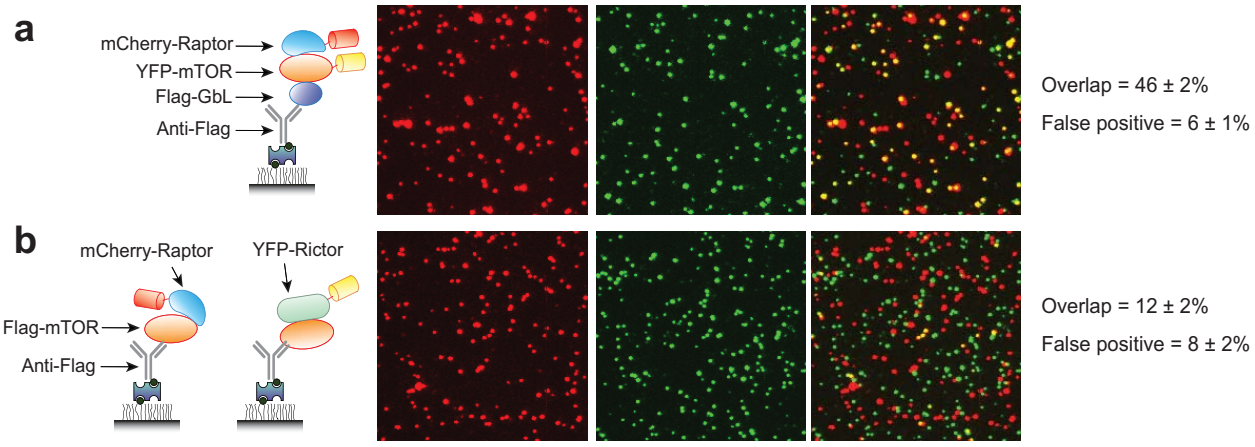

Figure 5.4 mTORC1 and mTORC2 are physically distinct. (a) YFP-mTOR, mCherry-Raptor and Flag-GβL are co-expressed. We are able to capture YFP-mTOR (center) and mCherry-Raptor (left) via antibody against Flag-Gβl. YFP-mTOR and mCherry-Raptor co-localize as depicted in the overlay of the two images (right). (b) mTORC1 and mTORC2 core components Flag-mTOR, mCherry-Raptor, YFP-Rictor, HA-GβL and HA-mSin1 are co-expressed. On capturing Flag-mTOR, we observe mCherry Raptor (left) and YFP-Rictor (center), but the two do not significantly overlap (right).

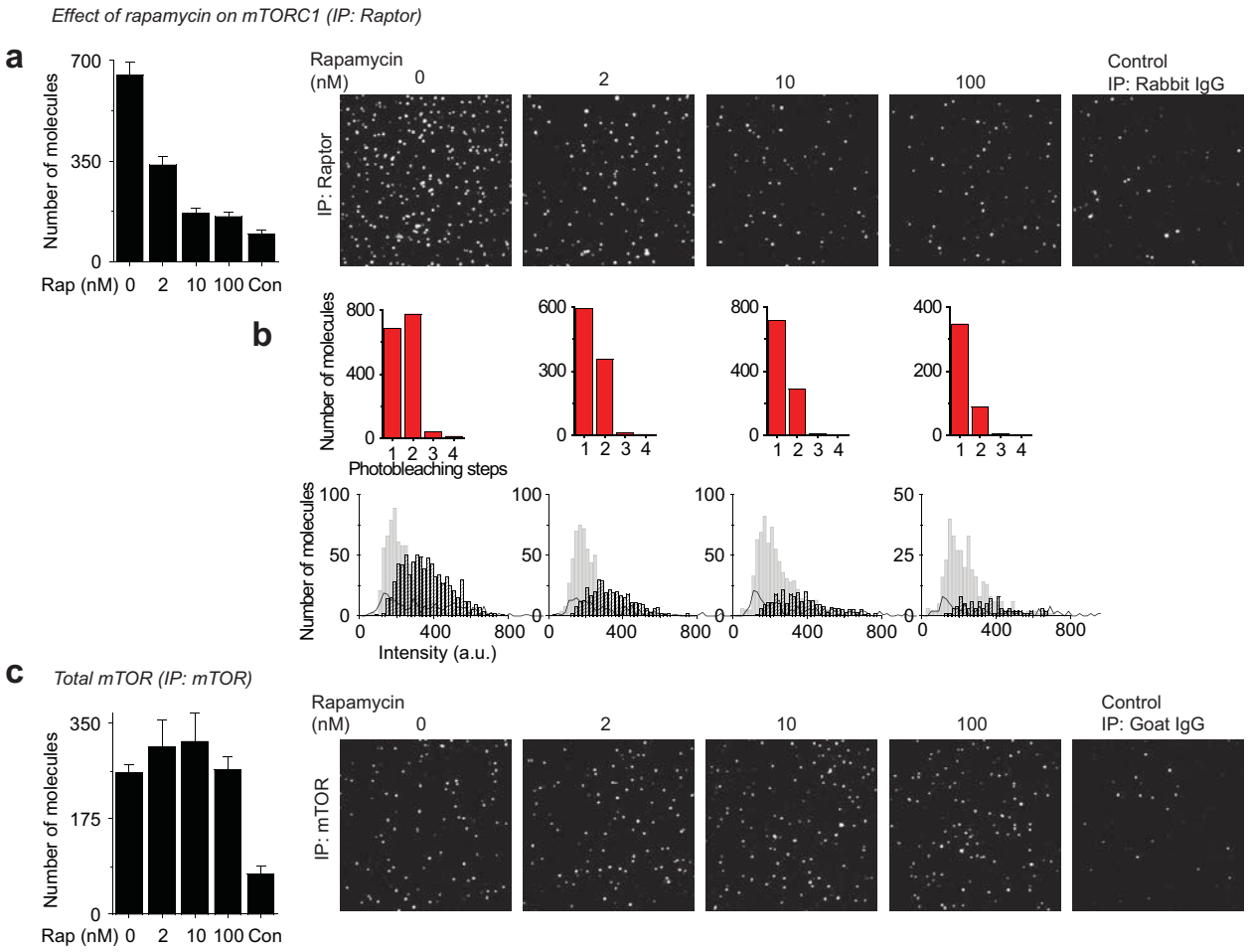

Figure 5.5 Effect of rapamycin on mTORC1. YFP-mTOR stable cells were treated with increasing dose of rapamycin for 30 min, and mTORC1 complexes were captured using an antibody against endogenous Raptor. (a) On increasing the concentration of rapamycin, the number of YFP-mTOR spots (mTORC1) decreases. (b) Stoichiometry distribution shifts from a dimer-like to a monomer-like distribution. (c) Expression level of mTOR is not significantly changed by rapamycin treatment.

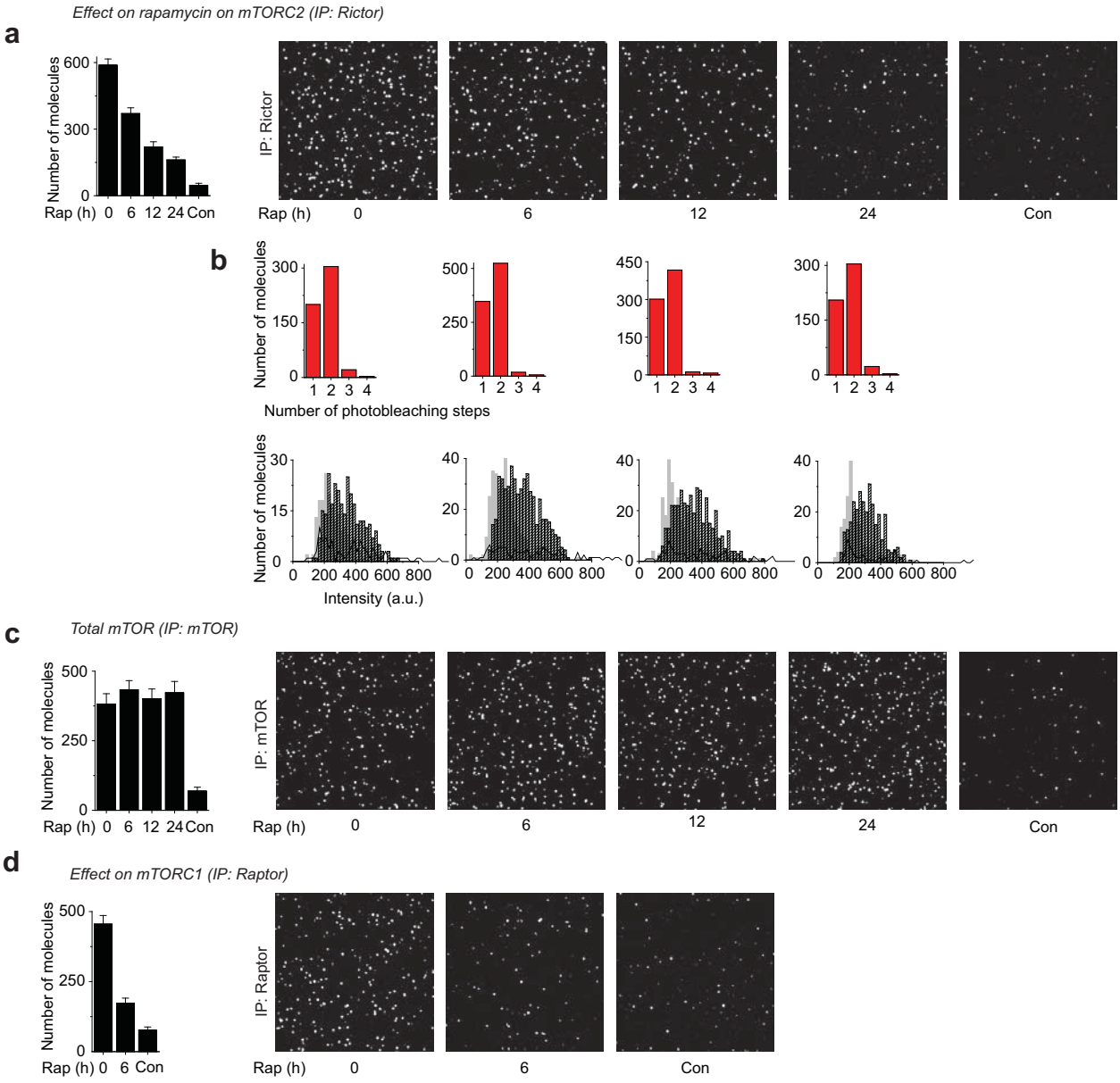

Figure 5.6 Effect of rapamycin on mTORC2. YFP-mTOR expressing cells were treated with 100 nM rapamycin for 0-24 hours and mTORC2 complexes were captured using an antibody against endogenous Rictor. (a) On prolonged treatment, the number of mTORC2 complexes decreases but (b) the stoichiometry of mTORC2 is not affected. (c) Treatment with rapamycin does not change overall mTOR expression level. (d) In the same samples, mTORC1 is disrupted.

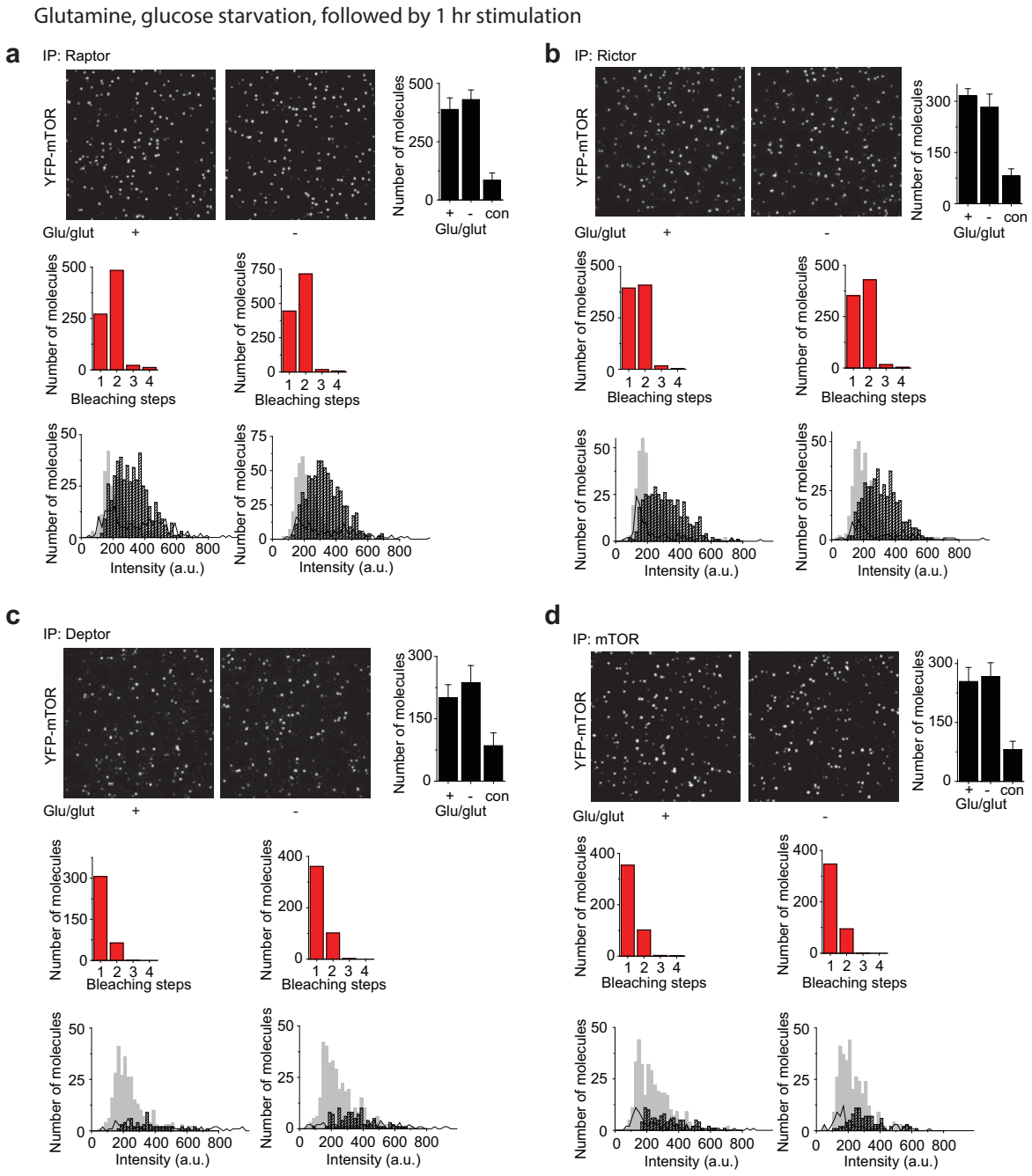

Figure 5.7 Effect of glucose and glutamine deprivation on mTOR complexes. YFP-mTOR expressing cells were starved of glucose and glutamine for 24 h and stimulated by replenishing the nutrients back in to the growth medium. Stoichiometry or the number of (a) mTORC1 and (b) mTORC2 complexes are not affected and both complexes are dimeric (c) In both conditions, mTOR-Deptor complexes are monomeric. (d) Expression level of mTOR is not changed by re-stimulation.

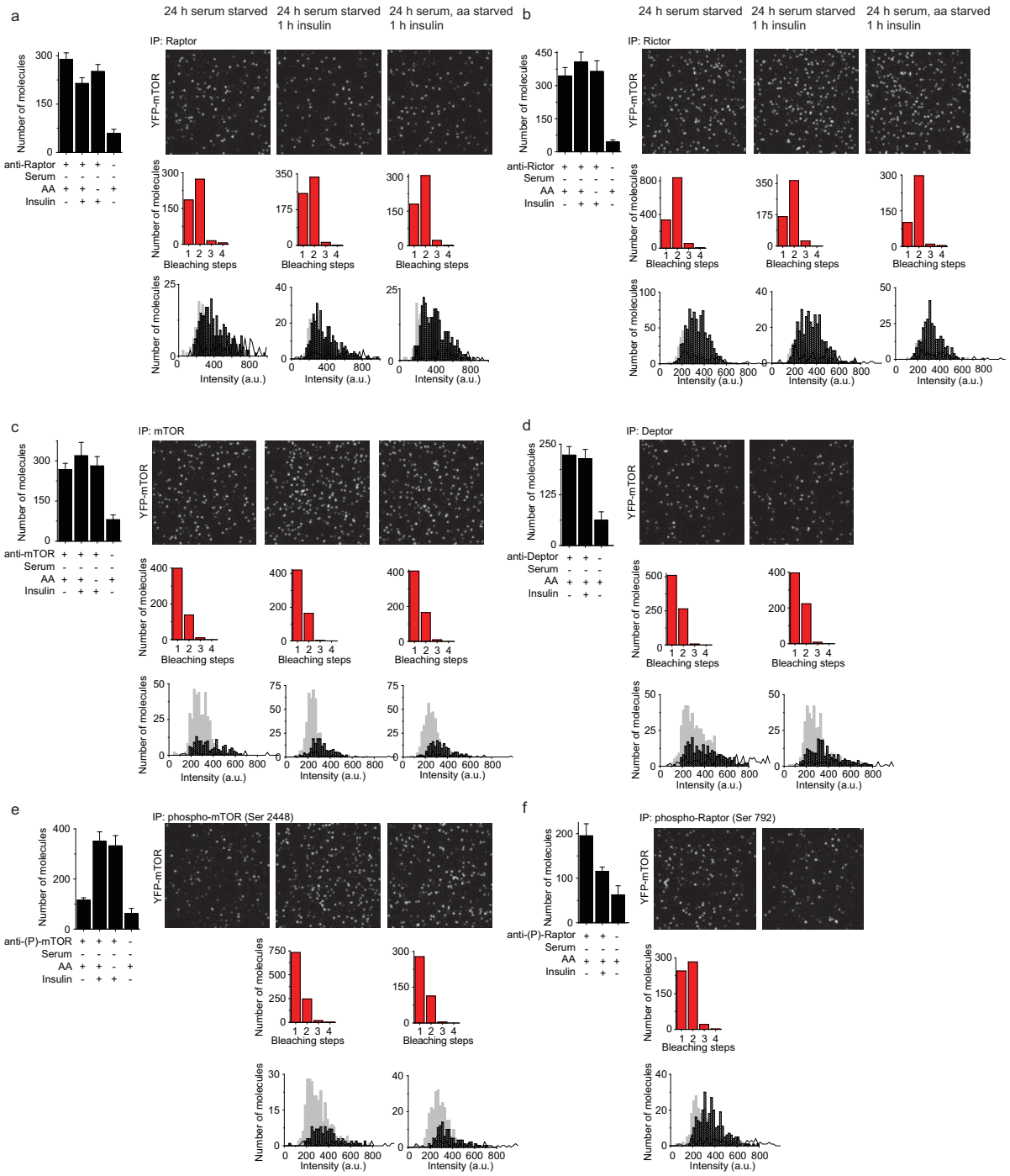

Figure 5.8 Effect of serum starvation on mTOR complexes. (a) mTORC1 & (b) mTORC2 stoichiometry is not affected. (c) YFP-mTOR expression levels & (d) association with Deptor is not affected. (e) mTOR is phosphorylated upon insulin stimulation; phosphorylated mTOR is monomeric. (f) Raptor is phosphorylated upon starvation; phosphorylated Raptor in mTORC1 is dimeric.

Chapter 6*

SiMPull as a Preparatory Method

A key advantage of SiMPull is that protein complexes can be directly observed from a fresh cell lysate, bypassing purification procedures. We tested if SiMPull can be used for functional analysis of pulled-down proteins. We demonstrate the use of SiMPull as a preparatory tool for two systems: PcrA and cGAS. Using SiMPull as a preparatory tool dramatically expands the repertoire of biological systems accessible to single-molecule technologies and can potentially have a far-reaching impact on the field.

6.1 PcrA helicase pull-down

PcrA is a superfamily 1 helicase: it is an ATP-driven motor protein that binds and translocates on single-stranded DNA (ssDNA) with a free 5' end. We expressed poly-histidine tagged PcrA in *E. coli*. Cells from 1 ml bacterial culture were pelleted down and were lysed using EasyLyse bacterial lysis solution (Epicenter Biotechnologies). Fresh lysate from these cells was applied to anti-His antibody on the SiMPull flow chambers. The captured protein was washed with 500 mM NaCl buffer to remove any bound endogenous DNA that may have been pulled down with PcrA. Next, we added a fluorescent labeled partial duplex DNA with a 5' tail to the immobilized protein. Fluorescent spots due to labeled DNA binding appeared in the flow channel with pulled-down PcrA, whereas the control channel showed minimal DNA binding (Figure 6.1 a-c). Thus, SiMPulled PcrA retains DNA binding activity.

*This work in Chapter 6 has been published as the following paper, and is a part of a manuscript in preparation.

- Jain A, Liu R, Ramani B, Arauz E, Ishitsuka Y, Ragunathan K, Park J, Chen J, Xiang Y, & Ha T, "Probing cellular protein complexes using single-molecule pull-down", *Nature* **473**, 484-488 (2011).

When PcrA binds to a partial duplex DNA with a 5′ overhang, it anchors itself to the junction and repetitively reels in the ssDNA and this activity can be monitored by via single-molecule fluorescence resonance energy transfer (FRET) when the DNA is appropriately labeled with a fluorescent donor and acceptor (Park et al., 2010). Similarly, in our SiMPull assay, when we added a FRET labeled DNA to the pulled down PcrA, in the presence of 1 mM ATP, we observed reeling-in activity as gradual increase in FRET. When PcrA reaches the end of the ssDNA tail, it runs off the ssDNA track and repeats the process from the junction over and over resulting in cyclic change in the observed FRET value (Figure 6.1 d). Nearly 86% of the bound FRET labeled DNA molecules exhibited repetitive cycling activity indicating a high activity yield of SiMPulled proteins. On increasing the ATP concentration, translocation became faster (Figure 6.2 a), and in the absence of ATP, DNA remained bound but no reeling-in activity was observed (Figure 6.2 b). The mean translocation time matched well with the data obtained with purified protein (Figure 6.1 e, f). Thus, SiMPull can pull-down functional macromolecules directly from cell extracts for subsequent single-molecule biochemistry.

6.2 Cyclic GMP-AMP synthetase

The power of using SiMPull as a preparatory tool is exemplified in our recent application to the enzyme cyclic GMP-AMP synthetase (cGAS). A recent study identified cGAS as a cytosolic immune receptor that recognizes cytosolic dsDNA and in response, produces a second messenger cyclic dinucleotide, cyclic GMP-AMP (cGAMP) that activates anti-viral signaling (Sun et al., 2013; Wu et al., 2013). The N-terminal domain of cGAS is unstructured and upon bacterial expression, the protein aggregates in the inclusion bodies. Hence, comprehensive biochemical analysis with the full-length protein has not been feasible. We used SiMPull to pull-down cGAS directly from human cells and used it for characterizing its DNA binding properties.

YFP-cGAS binds DNA

We prepared a YFP-cGAS construct and expressed in HEK293 cells. Using a surface immobilized GFP or cGAS antibody, we are able to pull-down YFP-cGAS as seen by the appearance of YFP spots (Figure 6.3). When we added a fluorophore labeled 45 base-pair double stranded (ds)

DNA to the chamber with SiMPulled cGAS, we did not observe any DNA binding. It is possible that the SiMPulled cGAS is bound to endogenous nucleic acids in the cell and hence may not be binding to additional DNA. To remove this endogenous DNA, we flushed the chambers with a high salt (500 mM NaCl) containing buffer. Indeed, after the high salt wash, we observed a 20-fold higher binding in the chamber with antibody against cGAS as compared to the control (Figure 6.4). The binding is dependent on the salt concentration in the buffer and decreases on increasing the salt concentration; in fact at concentrations higher than 150 mM, the binding of cGAS to DNA is comparable to blank.

We find that cGAS binds to both ssDNA as well as dsDNA (Fig 6.5). The binding of cGAS to ssDNA is length dependent: a 40mer ssDNA showed 5-fold higher binding when compared to 22mer ssDNA. The physiological role of binding to ssDNA is not understood as in vivo, cGAS is shown only to activate interferon signaling in response to dsDNA and is proposed to recognize only B-form DNA (Civril et al., 2013; Sun et al., 2013).

DNA binding to cGAS is transient

Next, we analyzed the fluorescence time-trajectories of DNA bound to cGAS. We find that DNA does not stably bind but dissociates within a few seconds from the surface immobilized cGAS. The duration of DNA binding is heterogeneous and varies significantly between molecules. Figure 6.6 depicts a typical time-trace of DNA binding and dissociating from immobilized cGAS. This transient binding may allow cGAS to screen multiple ligands within the crowded cytosol, and requires further investigation.

cGAS binds RNA

We investigated if SiMPulled cGAS can also bind to RNA. Although, in the activity assays, cGAS does not show cyclization activity with RNA, in our experiments, cGAS robustly bound to ssRNA as well as dsRNA oligonucleotides (Figure 6.7). In fact, the binding of RNA to cGAS was stable, and unlike DNA, bound RNA did not dissociate from the SiMPulled cGAS. The binding of RNA to cGAS is consistent with the expected biochemical results but the role of transient binding to DNA as against stable binding to RNA is not clear.

RNA competes off DNA from cGAS

When DNA and RNA are mixed together, the RNA can compete off DNA binding: the binding of DNA is 10-fold reduced in the presence of RNA (Figure 6.8). The physiological role of cGAS binding to RNA is not clear and our findings confound the problem: if RNA can compete off DNA from cGAS, how does cGAS recognize foreign DNA in the crowded cytosol where many RNA species including mRNA are present. Further investigation is required to understand the mechanism of specific DNA recognition by cGAS and it is a topic of ongoing research both via SiMPull as well as biochemical methods. In summary, SiMPull provides a rapid and robust platform for activity analysis of proteins that are not available from recombinant methods.

6.3 Figures

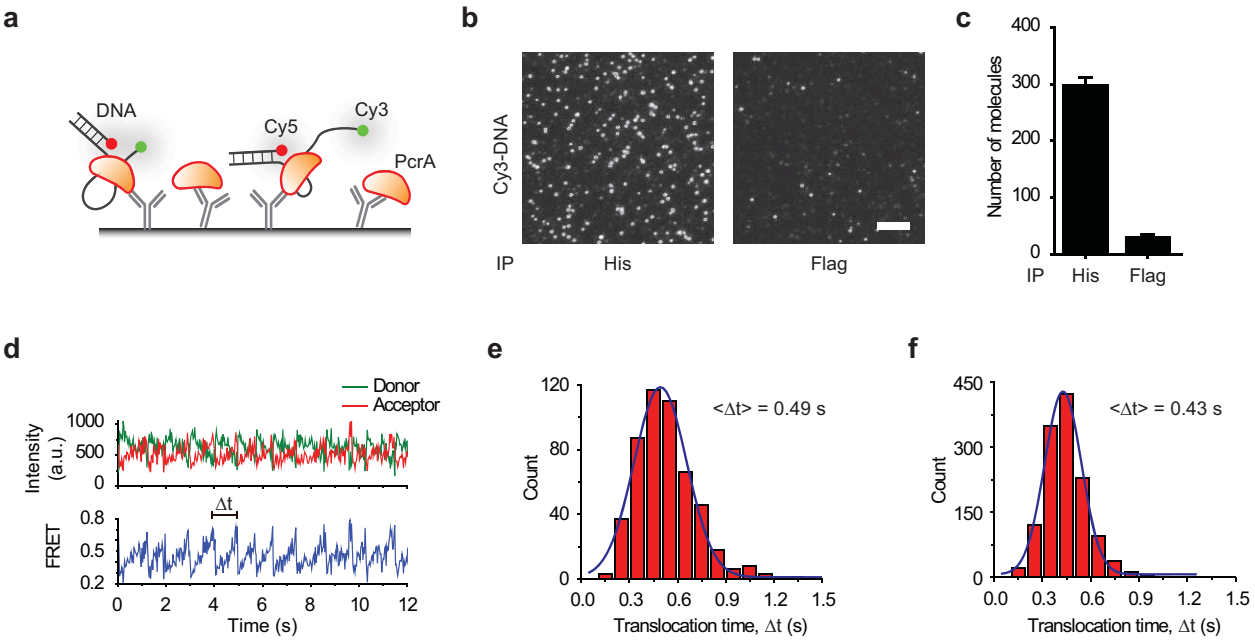

Figure 6.1 PcrA pull-down and activity. (a) Schematic of PcrA translocating on FRET-pair labeled DNA. (b) DNA binding to immunoprecipitated His-tagged PcrA. Scale bar is 5 μm. (c) Bar graph of number of bound DNA molecules. Error bars represent standard deviation of the mean across 20 or more images. (d) A typical time trace of repetitive reeling in activity of PcrA wherein in the donor and acceptor intensities show anti correlated changes and their associated FRET values. The distribution of translocation times (Δt) and its mean, <Δt>, (e) for purified PcrA and (f) for PcrA pulled down from cell extracts, at 1 mM ATP concentration.

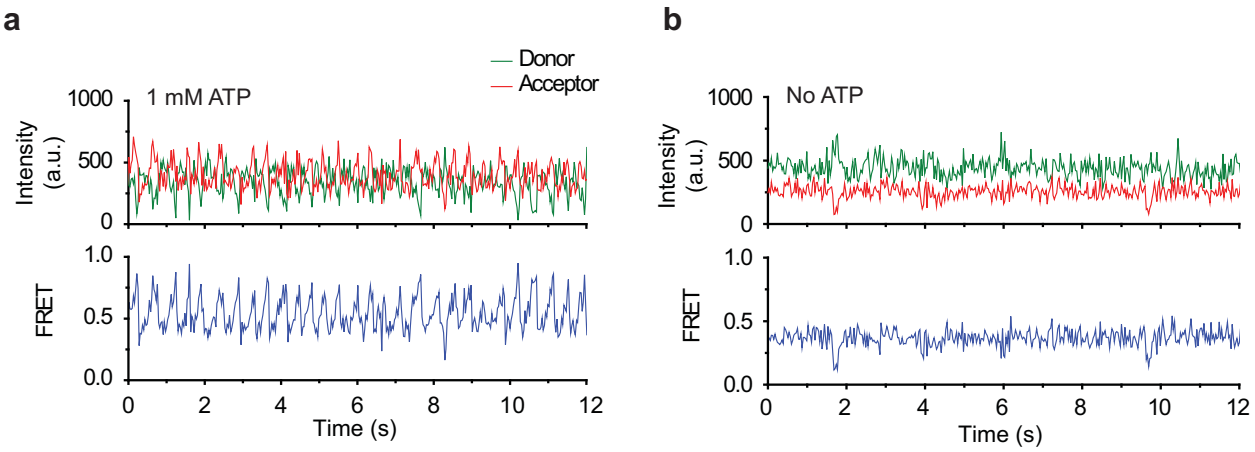

Figure 6.2 ATP dependence of pulled down PcrA activity. Sample traces for PcrA translocation on DNA. The saw-tooth pattern in FRET indicates repetitive reeling in of ssDNA by PcrA. (a) The rate of PcrA reeling in becomes faster at saturating (1 mM) ATP concentration compared to 5 μM used in Figure 6.1 (b) In the absence of ATP, no periodic change in FRET value is observed.

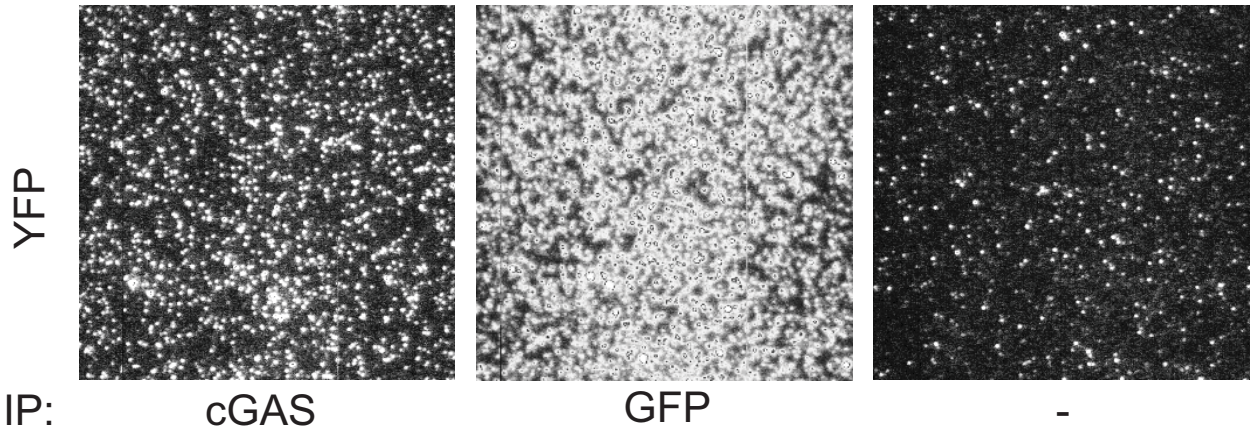

Figure 6.3 YFP-cGAS pull-down. HEK293T cells were transfected with YFP-cGAS. Using surface immobilized anti-cGAS or anti-GFP antibody, we are able to specifically capture YFP-cGAS from cell extracts as detected by YFP fluorescence.

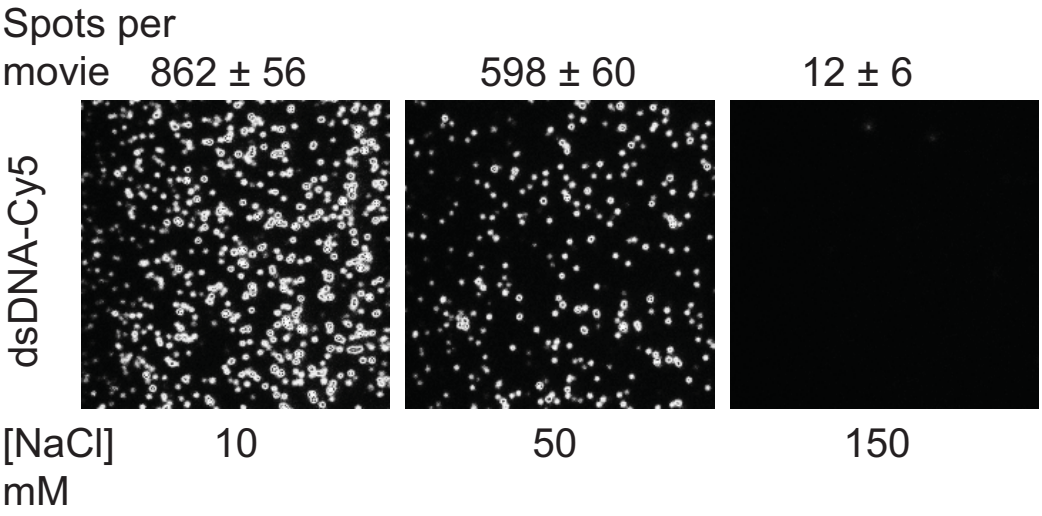

Figure 6.4 SiMPulled cGAS binds dsDNA. A 45 bp dsDNA labeled with Cy5 was added to SiMPull chambers after YFP-cGAS pull-down. DNA binding is dependent on the salt concentration and is abrogated at 150 mM NaCl concentration in the binding buffer.

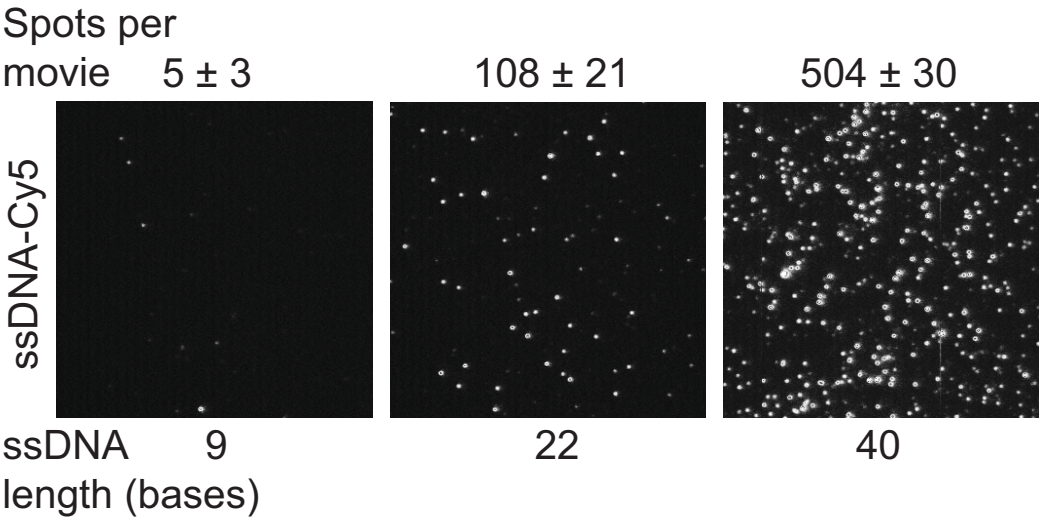

Figure 6.5 SiMPulled cGAS binds ssDNA. YFP-cGAS was exogenously expressed in HEK293 cells and was captured using anti-GFP antibody. On adding fluorophore labeled ssDNA, we observe a length dependent increase in binding.

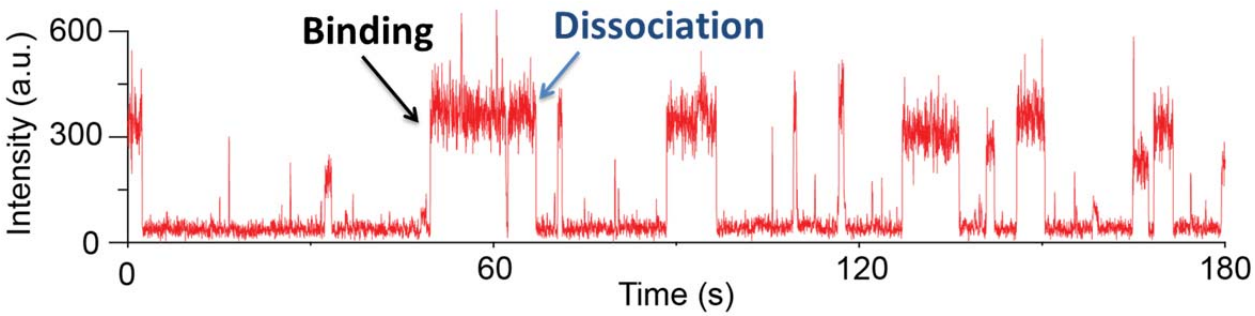

Figure 6.6 Sample time-trajectory. The binding of dsDNA to SiMPulled cGAS is transient with the mean off time ~ 1.5 s.

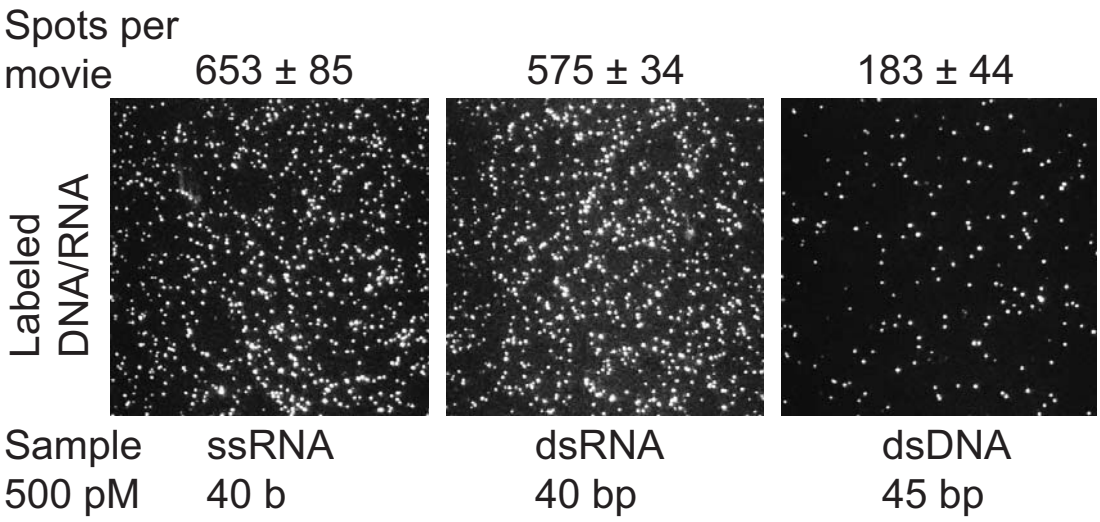

Figure 6.7 SiMPulled cGAS binds ssRNA & dsRNA. At the same concentration, 3-fold more spots are observed for RNA substrates as compared to dsDNA.

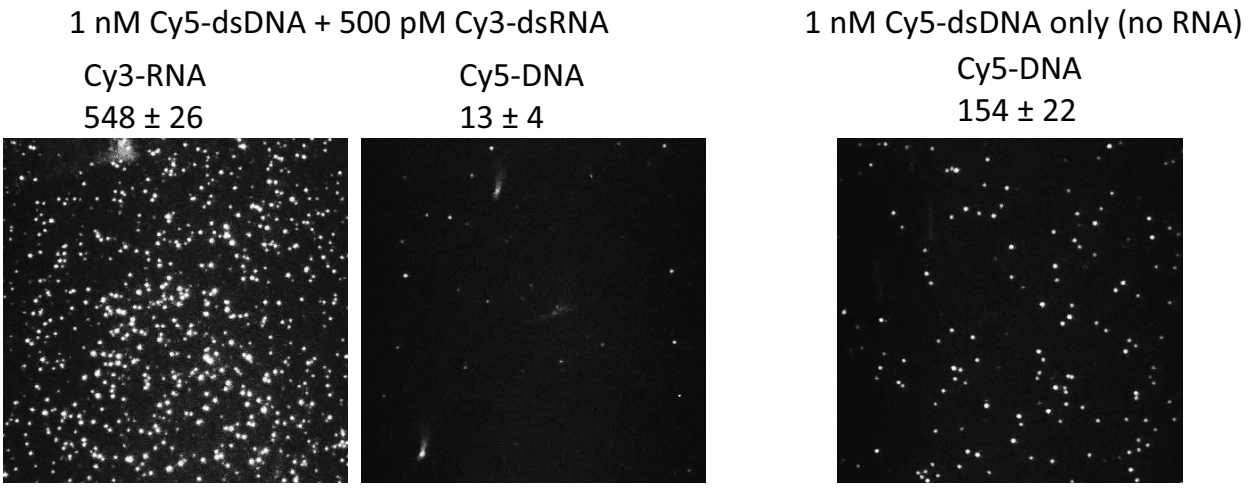

Figure 6.8 Competition between RNA and DNA for cGAS binding. YFP-cGAS was captured from cell extracts using anti-GFP antibody. (a) We added a mixture of 1 nM 45 bp DNA labeled with Cy5 and 500 pM 40 bp Cy3 labeled dsRNA. We observe RNA binding as Cy3 spots but a background level of fluorescence is observed upon imaging Cy5, indicating that DNA binding is abrogated in the presence of RNA. (b) When the same concentration of DNA is added to SiMPulled cGAS (without RNA), we observe 10-fold higher DNA binding.

Chapter 7*

SiMPull for Lipid-Protein Interactions

7.1 Background

Increasingly, researchers are identifying the key role of lipids in mediating and regulating cell signaling (Wymann and Schneiter, 2008). Lipids, in general, are weakly associated with proteins (Lee, 2003). Nevertheless, they play a significant role in modulating the spatiotemporal localization of the membrane bound proteins. Current research to study lipid-protein interactions involves either reconstitution of these interactions with purified proteins, or in vivo imaging based on the co-localization of proteins with lipids. Our SiMPull flow chambers are refractory to non-specific binding of proteins from the cell lysates. We tested if we can use lipid vesicles as bait for pull-down of proteins from cell extracts and thus develop a general approach to lipid-protein interactions.

7.2 Proof-of-concept

As a model system, we started with vesicles doped with the signaling lipid PI3P (phosphatidylinositol 3-phosphate) and as a protein of choice we used the PI3P sensor (FYVE domain of Akt) fused with GFP (Gillooly et al., 2000). We prepared vesicles with increasing amount of PI3P in a background of phosphatidyl choline (PC) and doped the vesicles with a biotinylated lipid (phosphatidyl ethanolamine labeled with biotin) for immobilization on avidin coated surfaces (Figure 7.1). When we add the lysate from cells expressing PI3P sensor to these vesicles, we observe GFP fluorescent spots only on the chamber which has the PI3P doped vesicles (Figure 7.1). Moreover, the binding of the sensor protein increased as we increase the concentration of PI3P in the vesicles.

*This work in Chapter 7 is a part of a manuscript in preparation.

Similarly, we immobilized vesicles doped with another signaling lipid, phosphatidic acid (PA) on the surface and added lysate from cells expressing a known PA binding protein tagged with GFP (PA sensor) (Figure 7.2). Once again, the binding is specific to the PA vesicles and the channel with PC only vesicles showed a background level binding of the PA sensor. Thus, using surface immobilized vesicles, we are able to pull-down proteins from cell extracts.

7.3 mTOR interacts with PA

mTOR signaling is modulated by PA and PA producing enzymes (Fang et al., 2001; Fang et al., 2003; Sun and Chen, 2008). Prof. Jie Chen's lab discovered that the FKBP12-rapamycin binding (FRB) domain of mTOR directly interacts with PA and the interaction between FRB domain and PA is abrogated by rapamycin-FKBP12 complexes (Fang et al., 2001). Though anticipated, thus far, it has not been possible to directly demonstrate the interaction between the mTOR protein and PA.

We applied our liposome based SiMPull approach for investigating the interaction between mTOR and PA. We immobilized PA containing vesicles on our microscope slides and infused lysate from cells expressing YFP-mTOR. As negative controls, we used vesicles containing PC only. PA is negatively charged and to rule out purely electrostatic interaction, we used phosphatidyl serine (PS) containing vesicles as an additional negative control. We observed 4-fold higher binding of YFP-mTOR to the PA vesicles, while the number of spots observed on PC only or PS vesicles was comparable to the background level of fluorescence (Figure 7.3 a), indicating a PA specific interaction. Next, we tested if the interaction between PA and mTOR can be modulated by rapamycin. On treating cells with rapamycin, for the same amount of cell extract, we observed nearly 3-fold reduced number of spots (Figure 7.3 b). Moreover, YFP only shows a background level of fluorescence and thus the binding is mTOR specific.

In summary, we have successfully extended the SiMPull assay to pull-down proteins from cell-extracts using surface immobilized lipid vesicles. Using this approach, we were able to verify a long-standing hypothesis that full-length mTOR binds to PA. A future direction is to understand

how PA modulates mTOR signaling and the effect of physiological stimulations (such as starvation) on the interaction between PA and mTOR.

7.4 Figures

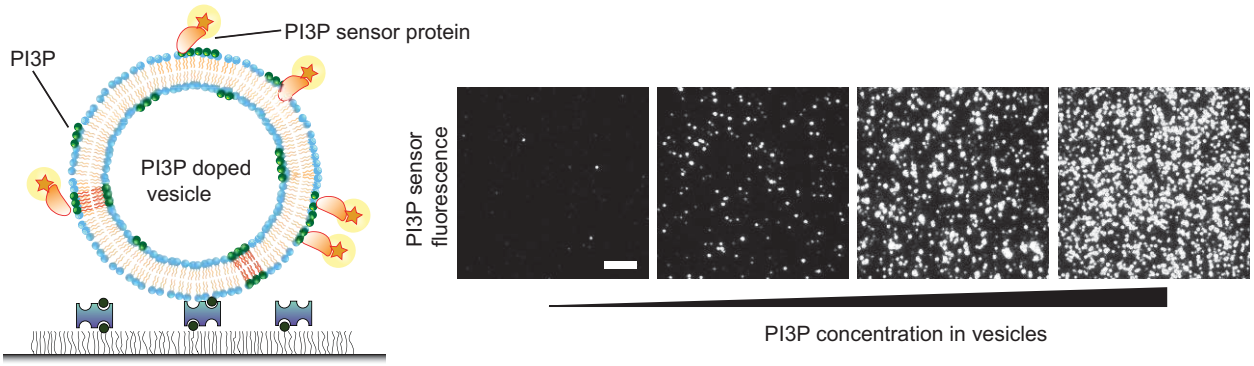

Figure 7.1 PI3P doped vesicles capture PI3P sensor from cell extracts. Vesicles with increasing fraction of PI3P (0 - 20%) are immobilized on passivated surface. Equal concentration of vesicles was immobilized in each case. To this, we added the PI3P sensor protein fused with GFP from cell extracts. The amount of sensor binding increases with the increasing concentration of the signaling lipid (PI3P) in the vesicles. Scale bar, 5 μm.

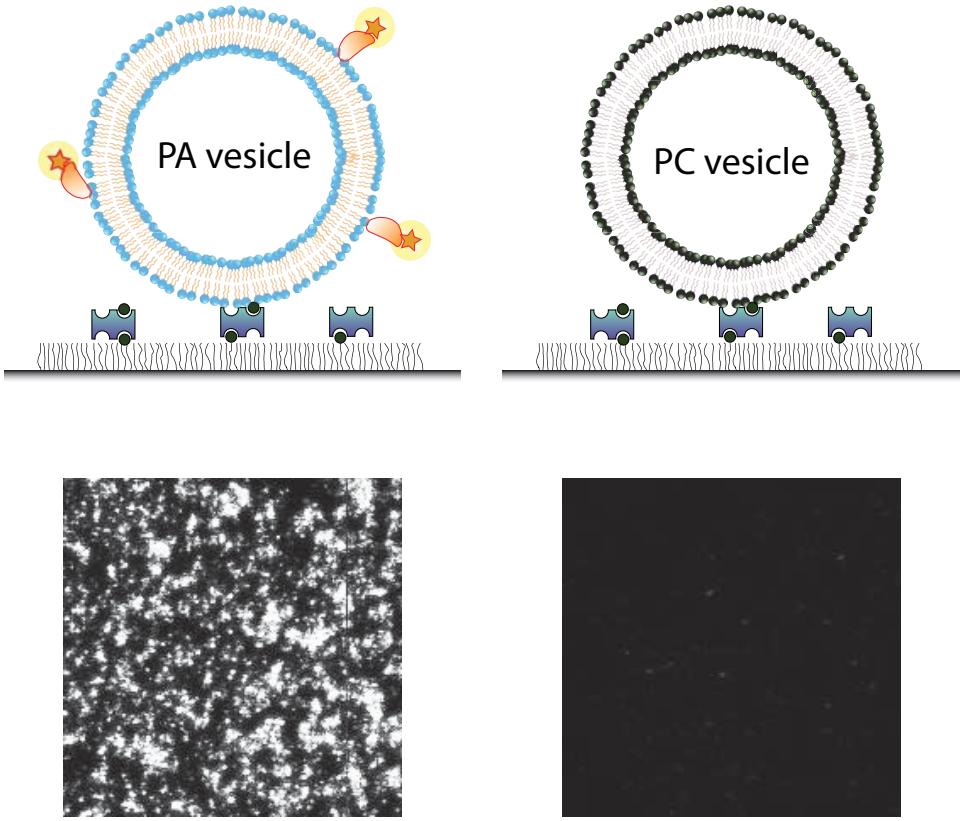

Figure 7.2 PA sensor from cell lysates binds PA vesicles. Vesicles containing 50% (left) or no PA (right) in the background of PC were immobilized on avidin coated SiMPull surfaces. When lysate from cells expressing PA-sensor tagged with GFP is flowed on to the immobilized vesicles, GFP fluorescent spots are observed only in the channel with the PA vesicles.

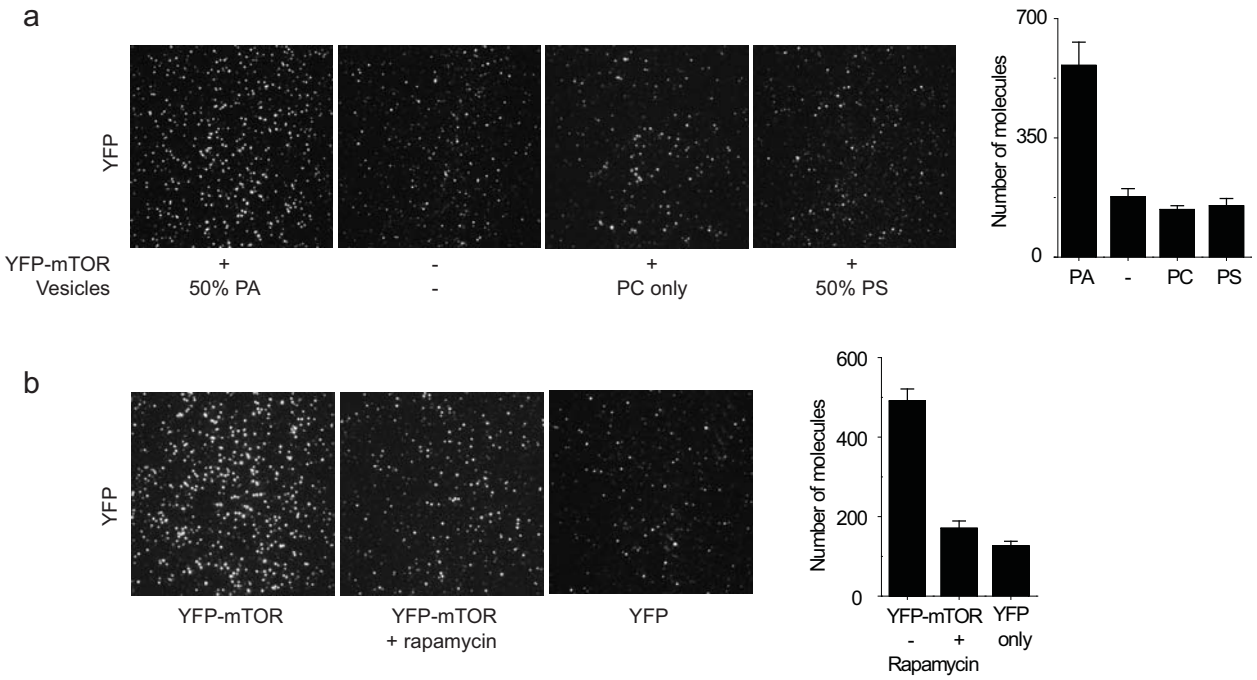

Figure 7.3 YFP-mTOR binds PA. (a) Vesicles with indicated lipid concentration in the background of PC were immobilized on the surface and the lysate from cells expressing YFP-mTOR was applied. YFP-spots due to capture of YFP-mTOR are enriched 3-fold in the chamber with PA vesicles. Binding on PC only and 50% PS vesicles is comparable to blank. (b)50% PA vesicles are immobilized on the flow chamber and YFP-mTOR with (center) or without (left) rapamycin treatment, or YFP only (right) lysates are added. The binding of YFP-mTOR is ~3-fold decreased upon rapamycin treatment and is comparable to the non-specific binding background for YFP-only lysate.

References

Adams, S. R., Campbell, R. E., Gross, L. A., Martin, B. R., Walkup, G. K., Yao, Y., Llopis, J. & Tsien, R. Y. (2002). New biarsenical ligands and tetracysteine motifs for protein labeling in vitro and in vivo: synthesis and biological applications. *Journal of the American Chemical Society,* **124**, 6063-76.

Aladjem, M. I. (2007). Replication in context: dynamic regulation of DNA replication patterns in metazoans. *Nature Reviews Genetics,* **8**, 588-600.

Alber, F., Dokudovskaya, S., Veenhoff, L. M., Zhang, W., Kipper, J., Devos, D., Suprapto, A., Karni-Schmidt, O., Williams, R., Chait, B. T., Rout, M. P. & Sali, A. (2007). Determining the architectures of macromolecular assemblies. *Nature,* **450**, 683-94.

Alberts, B. (1998). The cell as a collection of protein machines: preparing the next generation of molecular biologists. *Cell,* **92**, 291-4.

Ali, M. H. & Imperiali, B. (2005). Protein oligomerization: how and why. *Bioorganic & Medicinal Chemistry,* **13**, 5013-20.

Angers, S., Salahpour, A., Joly, E., Hilairet, S., Chelsky, D., Dennis, M. & Bouvier, M. (2000). Detection of beta 2-adrenergic receptor dimerization in living cells using bioluminescence resonance energy transfer (BRET). *Proceedings of the National Academy of Sciences of the United States of America,* **97**, 3684-9.

Bangia, N. & Cresswell, P. (2005). Stoichiometric tapasin interactions in the catalysis of major histocompatibility complex class I molecule assembly. *Immunology,* **114**, 346-53.

Barrios-Rodiles, M., Brown, K. R., Ozdamar, B., Bose, R., Liu, Z., Donovan, R. S., Shinjo, F., Liu, Y., Dembowy, J., Taylor, I. W., Luga, V., Przulj, N., Robinson, M., Suzuki, H., Hayashizaki, Y., Jurisica, I. & Wrana, J. L. (2005). High-throughput mapping of a dynamic signaling network in mammalian cells. *Science,* **307**, 1621-5.

Baum, A., Sachidanandam, R. & Garcia-Sastre, A. (2010). Preference of RIG-I for short viral RNA molecules in infected cells revealed by next-generation sequencing. *Proceedings of the National Academy of Sciences of the United States of America,* **107**, 16303-8.

Bell, S. P. (2002). The origin recognition complex: from simple origins to complex functions. *Genes & Development,* **16**, 659-72.

Benjamin, J. M., Torke, S. J., Demeler, B. & McGarry, T. J. (2004). Geminin has dimerization, Cdt1-binding, and destruction domains that are required for biological activity. *The Journal of Biological Chemistry,* **279**, 45957-68.

Bernlohr, D. A., Simpson, M. A., Hertzel, A. V. & Banaszak, L. J. (1997). Intracellular lipid-binding proteins and their genes. *Annual Review of Nutrition,* **17**, 277-303.

Blehm, B. H., Schroer, T. A., Trybus, K. M., Chemla, Y. R. & Selvin, P. R. (2013). In vivo optical trapping indicates kinesin's stall force is reduced by dynein during intracellular transport. *Proceedings of the National Academy of Sciences of the United States of America,* **110**, 3381-3386.

Chiang, G. G. & Abraham, R. T. (2005). Phosphorylation of mammalian target of rapamycin (mTOR) at Ser-2448 is mediated by p70S6 kinase. *The Journal of Biological Chemistry,* **280**, 25485-90.

Chung, H. S., McHale, K., Louis, J. M. & Eaton, W. A. (2012). Single-molecule fluorescence experiments determine protein folding transition path times. *Science,* **335**, 981-4.

Civril, F., Deimling, T., de Oliveira Mann, C. C., Ablasser, A., Moldt, M., Witte, G., Hornung, V. & Hopfner, K. P. (2013). Structural mechanism of cytosolic DNA sensing by cGAS. *Nature,* **498**, 332-7.

Coffman, V. C. & Wu, J. Q. (2012). Counting protein molecules using quantitative fluorescence microscopy. *Trends in Biochemical Sciences,* **37**, 499-506.

Collins, S., Caron, M. G. & Lefkowitz, R. J. (1991). Regulation of adrenergic receptor responsiveness through modulation of receptor gene expression. *Annual Review of Physiology,* **53**, 497-508.

Dibble, C. C., Asara, J. M. & Manning, B. D. (2009). Characterization of Rictor Phosphorylation Sites Reveals Direct Regulation of mTOR Complex 2 by S6K1. *Molecular and Cellular Biology,* **29**, 5657-5670.

Dunne, P. D., Fernandes, R. A., McColl, J., Yoon, J. W., James, J. R., Davis, S. J. & Klenerman, D. (2009). DySCo: quantitating associations of membrane proteins using two-color single-molecule tracking. *Biophysical Journal,* **97**, L5-7.

Edwards, A. S. & Scott, J. D. (2000). A-kinase anchoring proteins: protein kinase A and beyond. *Current Opinion in Cell Biology,* **12**, 217-21.

Emoto, K., Harris, J. M. & Van Alstine, J. M. (1996). Grafting Poly(ethylene glycol) Epoxide to Amino-Derivatized Quartz: Effect of Temperature and pH on Grafting Density. *Analytical Chemistry,* **68**, 3751-7.

Fang, Y., Park, I. H., Wu, A. L., Du, G., Huang, P., Frohman, M. A., Walker, S. J., Brown, H. A. & Chen, J. (2003). PLD1 regulates mTOR signaling and mediates Cdc42 activation of S6K1. *Current Biology,* **13**, 2037-44.

Fang, Y., Vilella-Bach, M., Bachmann, R., Flanigan, A. & Chen, J. (2001). Phosphatidic acid-mediated mitogenic activation of mTOR signaling. *Science,* **294**, 1942-5.

Fields, S. & Song, O. (1989). A novel genetic system to detect protein-protein interactions. *Nature,* **340**, 245-6.

Fleminger, G., Solomon, B., Wolf, T. & Hadas, E. (1990). Effect of polyethylene glycol on the non-specific adsorption of proteins to Eupergit C and agarose. *Journal of Chromatography,* **510**, 271-9.

Fonseca, B. D., Smith, E. M., Lee, V. H., MacKintosh, C. & Proud, C. G. (2007). PRAS40 is a target for mammalian target of rapamycin complex 1 and is required for signaling downstream of this complex. *The Journal of Biological Chemistry,* **282**, 24514-24.

Formstecher, E., Aresta, S., Colluar, V., Hamburger, A., Meil, A., Trehin, A., Reverdy, C., Betin, V., Marie, S., Brun, C., Jacq, B., Arpin, M., Bellaiche, Y., Bellusci, S., Benaroch, P., Bornens, M., Chanet, R., Chavrier, P., Delattre, O., Doye, V., Fehon, R., Faye, G., Galli, T., Girault, J. A., Goud, B., de Gunzburg, J., Johannes, L., Junier, M. P., Mirouse, V., Mukherjee, A., Papadopoulo, D., Perez, F., Plessis, A., Rosse, C., Saule, S., Stoppa-Lyonnet,

D., Vincent, A., White, M., Legrain, P., Wojcik, J., Camonis, J. & Daviet, L. (2005). Protein interaction mapping: A Drosophila case study (vol 15, pg 376, 2005). *Genome Research,* **15**, 601-601.

Frias, M. A., Thoreen, C. C., Jaffe, J. D., Schroder, W., Sculley, T., Carr, S. A. & Sabatini, D. M. (2006). mSin1 is necessary for Akt/PKB phosphorylation, and its isoforms define three distinct mTORC2s. *Current Biology,* **16**, 1865-70.

Funatsu, T., Harada, Y., Tokunaga, M., Saito, K. & Yanagida, T. (1995). Imaging of single fluorescent molecules and individual ATP turnovers by single myosin molecules in aqueous solution. *Nature,* **374**, 555-9.

Gandhi, T. K. B., Zhong, J., Mathivanan, S., Karthick, L., Chandrika, K. N., Mohan, S. S., Sharma, S., Pinkert, S., Nagaraju, S., Periaswamy, B., Mishra, G., Nandakumar, K., Shen, B. Y., Deshpande, N., Nayak, R., Sarker, M., Boeke, J. D., Parmigiani, G., Schultz, J., Bader, J. S. & Pandey, A. (2006). Analysis of the human protein interactome and comparison with yeast, worm and fly interaction datasets. *Nature Genetics,* **38**, 285-293.

Gavin, A. C., Aloy, P., Grandi, P., Krause, R., Boesche, M., Marzioch, M., Rau, C., Jensen, L. J., Bastuck, S., Dumpelfeld, B., Edelmann, A., Heurtier, M. A., Hoffman, V., Hoefert, C., Klein, K., Hudak, M., Michon, A. M., Schelder, M., Schirle, M., Remor, M., Rudi, T., Hooper, S., Bauer, A., Bouwmeester, T., Casari, G., Drewes, G., Neubauer, G., Rick, J. M., Kuster, B., Bork, P., Russell, R. B. & Superti-Furga, G. (2006). Proteome survey reveals modularity of the yeast cell machinery. *Nature,* **440**, 631-636.

Gillooly, D. J., Morrow, I. C., Lindsay, M., Gould, R., Bryant, N. J., Gaullier, J. M., Parton, R. G. & Stenmark, H. (2000). Localization of phosphatidylinositol 3-phosphate in yeast and mammalian cells. *The EMBO Journal,* **19**, 4577-88.

Gingras, A. C., Raught, B. & Sonenberg, N. (1999). eIF4 initiation factors: effectors of mRNA recruitment to ribosomes and regulators of translation. *Annual Review of Biochemistry,* **68**, 913-63.

Giot, L., Bader, J. S., Brouwer, C., Chaudhuri, A., Kuang, B., Li, Y., Hao, Y. L., Ooi, C. E., Godwin, B., Vitols, E., Vijayadamodar, G., Pochart, P., Machineni, H., Welsh, M., Kong, Y., Zerhusen, B., Malcolm, R., Varrone, Z., Collis, A., Minto, M., Burgess, S., McDaniel, L., Stimpson, E., Spriggs, F., Williams, J., Neurath, K., Ioime, N., Agee, M., Voss, E., Furtak, K., Renzulli, R., Aanensen, N., Carrolla, S., Bickelhaupt, E., Lazovatsky, Y., DaSilva, A., Zhong, J., Stanyon, C. A., Finley, R. L., White, K. P., Braverman, M., Jarvie, T., Gold, S., Leach, M., Knight, J., Shimkets, R. A., McKenna, M. P., Chant, J. & Rothberg, J. M. (2003). A protein interaction map of Drosophila melanogaster. *Science,* **302**, 1727-1736.

Gold, L., Ayers, D., Bertino, J., Bock, C., Bock, A., Brody, E. N., Carter, J., Dalby, A. B., Eaton, B. E., Fitzwater, T., Flather, D., Forbes, A., Foreman, T., Fowler, C., Gawande, B., Goss, M., Gunn, M., Gupta, S., Halladay, D., Heil, J., Heilig, J., Hicke, B., Husar, G., Janjic, N., Jarvis, T., Jennings, S., Katilius, E., Keeney, T. R., Kim, N., Koch, T. H., Kraemer, S., Kroiss, L., Le, N., Levine, D., Lindsey, W., Lollo, B., Mayfield, W., Mehan, M., Mehler, R., Nelson, S. K., Nelson, M., Nieuwlandt, D., Nikrad, M., Ochsner, U., Ostroff, R. M., Otis, M., Parker, T., Pietrasiewicz, S., Resnicow, D. I., Rohloff, J., Sanders, G., Sattin, S., Schneider, D., Singer, B., Stanton, M., Sterkel, A., Stewart, A., Stratford, S., Vaught, J. D.,

Vrkljan, M., Walker, J. J., Watrobka, M., Waugh, S., Weiss, A., Wilcox, S. K., Wolfson, A., Wolk, S. K., Zhang, C. & Zichi, D. (2010). Aptamer-based multiplexed proteomic technology for biomarker discovery. *PloS ONE,* **5**, e15004.

Grigoriev, A. (2003). On the number of protein-protein interactions in the yeast proteome. *Nucleic Acids Research,* **31**, 4157-61.

Ha, T., Kozlov, A. G. & Lohman, T. M. (2012). Single-molecule views of protein movement on single-stranded DNA. *Annual Review of Biophysics,* **41**, 295-319.

Haar, E. V., Lee, S.-i., Bandhakavi, S., Griffin, T. J. & Kim, D.-H. (2007). Insulin signalling to mTOR mediated by the Akt/PKB substrate PRAS40. *Nature Cell Biology,* **9**, 316-323.

Hara, K., Maruki, Y., Long, X., Yoshino, K., Oshiro, N., Hidayat, S., Tokunaga, C., Avruch, J. & Yonezawa, K. (2002). Raptor, a binding partner of target of rapamycin (TOR), mediates TOR action. *Cell,* **110**, 177-89.

Hendrix, J., Flors, C., Dedecker, P., Hofkens, J. & Engelborghs, Y. (2008). Dark states in monomeric red fluorescent proteins studied by fluorescence correlation and single molecule spectroscopy. *Biophysical Journal,* **94**, 4103-13.

Ho, Y., Gruhler, A., Heilbut, A., Bader, G. D., Moore, L., Adams, S. L., Millar, A., Taylor, P., Bennett, K., Boutilier, K., Yang, L. Y., Wolting, C., Donaldson, I., Schandorff, S., Shewnarane, J., Vo, M., Taggart, J., Goudreault, M., Muskat, B., Alfarano, C., Dewar, D., Lin, Z., Michalickova, K., Willems, A. R., Sassi, H., Nielsen, P. A., Rasmussen, K. J., Andersen, J. R., Johansen, L. E., Hansen, L. H., Jespersen, H., Podtelejnikov, A., Nielsen, E., Crawford, J., Poulsen, V., Sorensen, B. D., Matthiesen, J., Hendrickson, R. C., Gleeson, F., Pawson, T., Moran, M. F., Durocher, D., Mann, M., Hogue, C. W. V., Figeys, D. & Tyers, M. (2002). Systematic identification of protein complexes in Saccharomyces cerevisiae by mass spectrometry. *Nature,* **415**, 180-183.

Holz, M. K. & Blenis, J. (2005). Identification of S6 kinase 1 as a novel mammalian target of rapamycin (mTOR)-phosphorylating kinase. *The Journal of Biological Chemistry,* **280**, 26089-93.

Hoskins, A. A., Friedman, L. J., Gallagher, S. S., Crawford, D. J., Anderson, E. G., Wombacher, R., Ramirez, N., Cornish, V. W., Gelles, J. & Moore, M. J. (2011). Ordered and dynamic assembly of single spliceosomes. *Science,* **331**, 1289-95.

Hou, F., Sun, L., Zheng, H., Skaug, B., Jiang, Q. X. & Chen, Z. J. (2011). MAVS forms functional prion-like aggregates to activate and propagate antiviral innate immune response. *Cell,* **146**, 448-61.

Huang, J. & Manning, B. D. (2009). A complex interplay between Akt, TSC2 and the two mTOR complexes. *Biochemical Society Transactions,* **37**, 217-22.

Hulpke, S., Tomioka, M., Kremmer, E., Ueda, K., Abele, R. & Tampe, R. (2012). Direct evidence that the N-terminal extensions of the TAP complex act as autonomous interaction scaffolds for the assembly of the MHC I peptide-loading complex. *Cellular and Molecular Life Sciences,* **69**, 3317-27.

Ito, T., Chiba, T., Ozawa, R., Yoshida, M., Hattori, M. & Sakaki, Y. (2001). A comprehensive two-hybrid analysis to explore the yeast protein interactome. *Proceedings of the National Academy of Sciences of the United States of America,* **98**, 4569-4574.

Jacinto, E., Facchinetti, V., Liu, D., Soto, N., Wei, S., Jung, S. Y., Huang, Q., Qin, J. & Su, B. (2006). SIN1/MIP1 Maintains rictor-mTOR Complex Integrity and Regulates Akt Phosphorylation and Substrate Specificity. *Cell.,* **127**, 125-37. Epub 2006 Sep 7.

Jacinto, E., Loewith, R., Schmidt, A., Lin, S., Ruegg, M. A., Hall, A. & Hall, M. N. (2004). Mammalian TOR complex 2 controls the actin cytoskeleton and is rapamycin insensitive. *Nature Cell Biology,* **6**, 1122-8. Epub 2004 Oct 03.

Jain, A., Liu, R., Ramani, B., Arauz, E., Ishitsuka, Y., Ragunathan, K., Park, J., Chen, J., Xiang, Y. K. & Ha, T. (2011). Probing cellular protein complexes using single-molecule pull-down. *Nature,* **473**, 484-8.

Jiang, X., Kinch, L. N., Brautigam, C. A., Chen, X., Du, F., Grishin, N. V. & Chen, Z. J. (2012). Ubiquitin-induced oligomerization of the RNA sensors RIG-I and MDA5 activates antiviral innate immune response. *Immunity,* **36**, 959-73.

Joo, C., Balci, H., Ishitsuka, Y., Buranachai, C. & Ha, T. (2008). Advances in single-molecule fluorescence methods for molecular biology. *Annual Review of Biochemistry,* **77**, 51-76.

Julien, L. A., Carriere, A., Moreau, J. & Roux, P. P. (2009). mTORC1-Activated S6K1 Phosphorylates Rictor on Threonine 1135 and Regulates mTORC2 Signaling. *Molecular and Cellular Biology,* **30**, 908-921.

Kar, G., Gursoy, A. & Keskin, O. (2009). Human cancer protein-protein interaction network: a structural perspective. *PLoS Computational Biology,* **5**, e1000601.

Kerppola, T. K. (2006). Complementary methods for studies of protein interactions in living cells. *Nature Methods,* **3**, 969-71.

Kim, D. H., Sarbassov, D. D., Ali, S. M., King, J. E., Latek, R. R., Erdjument-Bromage, H., Tempst, P. & Sabatini, D. M. (2002). mTOR interacts with raptor to form a nutrient-sensitive complex that signals to the cell growth machinery. *Cell,* **110**, 163-75.

Kim, D. H., Sarbassov dos, D., Ali, S. M., Latek, R. R., Guntur, K. V., Erdjument-Bromage, H., Tempst, P. & Sabatini, D. M. (2003). GbetaL, a Positive Regulator of the Rapamycin-Sensitive Pathway Required for the Nutrient-Sensitive Interaction between Raptor and mTOR. *Molecular Cell,* **11**, 895-904.

Kim, S. G., Hoffman, G. R., Poulogiannis, G., Buel, G. R., Jang, Y. J., Lee, K. W., Kim, B. Y., Erikson, R. L., Cantley, L. C., Choo, A. Y. & Blenis, J. (2013a). Metabolic stress controls mTORC1 lysosomal localization and dimerization by regulating the TTT-RUVBL1/2 complex. *Molecular Cell,* **49**, 172-85.

Kim, Y., Kim, S. H., Tanyeri, M., Katzenellenbogen, J. A. & Schroeder, C. M. (2013b). Dendrimer probes for enhanced photostability and localization in fluorescence imaging. *Biophysical Journal,* **104**, 1566-75.

Krogan, N. J., Cagney, G., Yu, H. Y., Zhong, G. Q., Guo, X. H., Ignatchenko, A., Li, J., Pu, S. Y., Datta, N., Tikuisis, A. P., Punna, T., Peregrin-Alvarez, J. M., Shales, M., Zhang, X., Davey, M., Robinson, M. D., Paccanaro, A., Bray, J. E., Sheung, A., Beattie, B., Richards, D. P., Canadien, V., Lalev, A., Mena, F., Wong, P., Starostine, A., Canete, M. M., Vlasblom, J., Wu, S., Orsi, C., Collins, S. R., Chandran, S., Haw, R., Rilstone, J. J., Gandi, K., Thompson, N. J., Musso, G., St Onge, P., Ghanny, S., Lam, M. H. Y., Butland, G., Altaf-Ui, A. M., Kanaya, S., Shilatifard, A., O'Shea, E., Weissman, J. S., Ingles, C. J., Hughes, T.

R., Parkinson, J., Gerstein, M., Wodak, S. J., Emili, A. & Greenblatt, J. F. (2006). Global landscape of protein complexes in the yeast Saccharomyces cerevisiae. *Nature,* **440**, 637-643.

Lander, G. C., Estrin, E., Matyskiela, M. E., Bashore, C., Nogales, E. & Martin, A. (2012). Complete subunit architecture of the proteasome regulatory particle. *Nature,* **482**, 186-91.

Laplante, M. & Sabatini, D. M. (2009). mTOR signaling at a glance. *Journal of Cell Science,* **122**, 3589-3594.

Laplante, M. & Sabatini, David M. (2012). mTOR Signaling in Growth Control and Disease. *Cell,* **149**, 274-293.

Leake, M. C., Chandler, J. H., Wadhams, G. H., Bai, F., Berry, R. M. & Armitage, J. P. (2006). Stoichiometry and turnover in single, functioning membrane protein complexes. *Nature,* **443**, 355-8.

Lee, A. G. (2003). Lipid-protein interactions in biological membranes: a structural perspective. *Biochimica et Biophysica Acta,* **1612**, 1-40.

Lee, K. S., Balci, H., Jia, H., Lohman, T. M. & Ha, T. (2013). Direct imaging of single UvrD helicase dynamics on long single-stranded DNA. *Nature Communications,* **4**, 1878.

Li, X. D., Sun, L., Seth, R. B., Pineda, G. & Chen, Z. J. (2005). Hepatitis C virus protease NS3/4A cleaves mitochondrial antiviral signaling protein off the mitochondria to evade innate immunity. *Proceedings of the National Academy of Sciences of the United States of America,* **102**, 17717-22.

Loffredo, F. S., Steinhauser, M. L., Jay, S. M., Gannon, J., Pancoast, J. R., Yalamanchi, P., Sinha, M., Dall'Osso, C., Khong, D., Shadrach, J. L., Miller, C. M., Singer, B. S., Stewart, A., Psychogios, N., Gerszten, R. E., Hartigan, A. J., Kim, M. J., Serwold, T., Wagers, A. J. & Lee, R. T. (2013). Growth differentiation factor 11 is a circulating factor that reverses age-related cardiac hypertrophy. *Cell,* **153**, 828-39.

Loo, Y. M. & Gale, M., Jr. (2011). Immune signaling by RIG-I-like receptors. *Immunity,* **34**, 680-92.

Ma, X. M. & Blenis, J. (2009). Molecular mechanisms of mTOR-mediated translational control. *Nature Reviews Molecular Cell Biology,* **10**, 307-318.

Machleidt, T., Robers, M. & Hanson, G. T. (2007). Protein labeling with FlAsH and ReAsH. *Methods in Molecular Biology,* **356**, 209-20.

Maeder, C. I., Hink, M. A., Kinkhabwala, A., Mayr, R., Bastiaens, P. I. & Knop, M. (2007). Spatial regulation of Fus3 MAP kinase activity through a reaction-diffusion mechanism in yeast pheromone signalling. *Nature Cell Biology,* **9**, 1319-26.

Marsh, D. (2003). Lipid-binding proteins: structure of the phospholipid ligands. *Protein Science : a publication of the Protein Society,* **12**, 2109-17.

Maurel, D., Comps-Agrar, L., Brock, C., Rives, M. L., Bourrier, E., Ayoub, M. A., Bazin, H., Tinel, N., Durroux, T., Prezeau, L., Trinquet, E. & Pin, J. P. (2008). Cell-surface protein-protein interaction analysis with time-resolved FRET and snap-tag technologies: application to GPCR oligomerization. *Nature Methods,* **5**, 561-7.

Means, C. K., Lygren, B., Langeberg, L. K., Jain, A., Dixon, R. E., Vega, A. L., Gold, M. G., Petrosyan, S., Taylor, S. S., Murphy, A. N., Ha, T., Santana, L. F., Tasken, K. & Scott, J. D. (2011). An entirely specific type I A-kinase anchoring protein that can sequester two

molecules of protein kinase A at mitochondria. *Proceedings of the National Academy of Sciences of the United States of America,* **108**, E1227-35.

Mercier, J. F., Salahpour, A., Angers, S., Breit, A. & Bouvier, M. (2002). Quantitative assessment of beta 1- and beta 2-adrenergic receptor homo- and heterodimerization by bioluminescence resonance energy transfer. *The Journal of Biological Chemistry,* **277**, 44925-31.

Myong, S., Cui, S., Cornish, P. V., Kirchhofer, A., Gack, M. U., Jung, J. U., Hopfner, K. P. & Ha, T. (2009). Cytosolic viral sensor RIG-I is a 5'-triphosphate-dependent translocase on double-stranded RNA. *Science,* **323**, 1070-4.

Myong, S., Rasnik, I., Joo, C., Lohman, T. M. & Ha, T. (2005). Repetitive shuttling of a motor protein on DNA. *Nature,* **437**, 1321-5.

Nakajo, K., Ulbrich, M. H., Kubo, Y. & Isacoff, E. Y. (2010). Stoichiometry of the KCNQ1 - KCNE1 ion channel complex. *Proceedings of the National Academy of Sciences of the United States of America,* **107**, 18862-7.

Oh, W. J. & Jacinto, E. (2011). mTOR complex 2 signaling and functions. *Cell Cycle,* **10**, 2305-2316.

Oshiro, N., Takahashi, R., Yoshino, K., Tanimura, K., Nakashima, A., Eguchi, S., Miyamoto, T., Hara, K., Takehana, K., Avruch, J., Kikkawa, U. & Yonezawa, K. (2007). The proline-rich Akt substrate of 40 kDa (PRAS40) is a physiological substrate of mammalian target of rapamycin complex 1. *The Journal of Biological Chemistry,* **282**, 20329-39. Epub 2007 May 21.

Oshiro, N., Yoshino, K., Hidayat, S., Tokunaga, C., Hara, K., Eguchi, S., Avruch, J. & Yonezawa, K. (2004). Dissociation of raptor from mTOR is a mechanism of rapamycin-induced inhibition of mTOR function. *Genes to Cells : devoted to molecular & cellular mechanisms,* **9**, 359-66.

Padeganeh, A., Ryan, J., Boisvert, J., Ladouceur, A. M., Dorn, J. F. & Maddox, P. S. (2013). Octameric CENP-A nucleosomes are present at human centromeres throughout the cell cycle. *Current Biology,* **23**, 764-9.

Panter, M. S., Jain, A., Leonhardt, R. M., Ha, T. & Cresswell, P. (2012). Dynamics of major histocompatibility complex class I association with the human peptide-loading complex. *The Journal of Biological Chemistry,* **287**, 31172-84.

Park, J., Myong, S., Niedziela-Majka, A., Lee, K. S., Yu, J., Lohman, T. M. & Ha, T. (2010). PcrA helicase dismantles RecA filaments by reeling in DNA in uniform steps. *Cell,* **142**, 544-55.

Peaper, D. R. & Cresswell, P. (2008). Regulation of MHC class I assembly and peptide binding. *Annual Review of Cell and Developmental Biology,* **24**, 343-68.

Pearce, L. R., Huang, X., Boudeau, J., Pawlowski, R., Wullschleger, S., Deak, M., Ibrahim, A. F., Gourlay, R., Magnuson, M. A. & Alessi, D. R. (2007). Identification of Protor as a novel Rictor-binding component of mTOR complex-2. *Biochemical Journal,* **405**, 513-22.

Peterson, T. R., Laplante, M., Thoreen, C. C., Sancak, Y., Kang, S. A., Kuehl, W. M., Gray, N. S. & Sabatini, D. M. (2009). DEPTOR is an mTOR inhibitor frequently overexpressed in multiple myeloma cells and required for their survival. *Cell,* **137**, 873-86.

Przytycka, T. M., Singh, M. & Slonim, D. K. (2010). Toward the dynamic interactome: it's about time. *Briefings in Bioinformatics,* **11**, 15-29.

Puig, O., Caspary, F., Rigaut, G., Rutz, B., Bouveret, E., Bragado-Nilsson, E., Wilm, M. & Seraphin, B. (2001). The tandem affinity purification (TAP) method: a general procedure of protein complex purification. *Methods,* **24**, 218-29.

Rai, A. K., Rai, A., Ramaiya, A. J., Jha, R. & Mallik, R. (2013). Molecular Adaptations Allow Dynein to Generate Large Collective Forces inside Cells. *Cell,* **152**, 172-182.

Rehwinkel, J., Tan, C. P., Goubau, D., Schulz, O., Pichlmair, A., Bier, K., Robb, N., Vreede, F., Barclay, W., Fodor, E. & Reis e Sousa, C. (2010). RIG-I detects viral genomic RNA during negative-strand RNA virus infection. *Cell,* **140**, 397-408.

Revyakin, A., Zhang, Z., Coleman, R. A., Li, Y., Inouye, C., Lucas, J. K., Park, S. R., Chu, S. & Tjian, R. (2012). Transcription initiation by human RNA polymerase II visualized at single-molecule resolution. *Genes & Development,* **26**, 1691-702.

Reyes-Lamothe, R., Sherratt, D. J. & Leake, M. C. (2010). Stoichiometry and architecture of active DNA replication machinery in Escherichia coli. *Science,* **328**, 498-501.

Ries, J., Kaplan, C., Platonova, E., Eghlidi, H. & Ewers, H. (2012). A simple, versatile method for GFP-based super-resolution microscopy via nanobodies. *Nature Methods,* **9**, 582-4.

Roberts, M. J., Bentley, M. D. & Harris, J. M. (2002). Chemistry for peptide and protein PEGylation. *Advanced Drug Delivery Reviews,* **54**, 459-76.

Rose, R. J., Damoc, E., Denisov, E., Makarov, A. & Heck, A. J. (2012). High-sensitivity Orbitrap mass analysis of intact macromolecular assemblies. *Nature Methods,* **9**, 1084-6.

Roy, R., Hohng, S. & Ha, T. (2008). A practical guide to single-molecule FRET. *Nature Methods,* **5**, 507-16.

Rual, J. F., Venkatesan, K., Hao, T., Hirozane-Kishikawa, T., Dricot, A., Li, N., Berriz, G. F., Gibbons, F. D., Dreze, M., Ayivi-Guedehoussou, N., Klitgord, N., Simon, C., Boxem, M., Milstein, S., Rosenberg, J., Goldberg, D. S., Zhang, L. V., Wong, S. L., Franklin, G., Li, S. M., Albala, J. S., Lim, J. H., Fraughton, C., Llamosas, E., Cevik, S., Bex, C., Lamesch, P., Sikorski, R. S., Vandenhaute, J., Zoghbi, H. Y., Smolyar, A., Bosak, S., Sequerra, R., Doucette-Stamm, L., Cusick, M. E., Hill, D. E., Roth, F. P. & Vidal, M. (2005). Towards a proteome-scale map of the human protein-protein interaction network. *Nature,* **437**, 1173-1178.

Rufer, E., Leonhardt, R. M. & Knittler, M. R. (2007). Molecular architecture of the TAP-associated MHC class I peptide-loading complex. *Journal of Immunology,* **179**, 5717-27.

Sabatini, D. M. (2006). mTOR and cancer: insights into a complex relationship. *Nature Reviews Cancer,* **6**, 729-34.

Sancak, Y., Thoreen, C. C., Peterson, T. R., Lindquist, R. A., Kang, S. A., Spooner, E., Carr, S. A. & Sabatini, D. M. (2007). PRAS40 is an insulin-regulated inhibitor of the mTORC1 protein kinase. *Molecular Cell.,* **25**, 903-15.

Sarbassov, D., D., Ali, S. M., Kim, D. H., Guertin, D. A., Latek, R. R., Erdjument-Bromage, H., Tempst, P. & Sabatini, D. M. (2004). Rictor, a novel binding partner of mTOR, defines a rapamycin-insensitive and raptor-independent pathway that regulates the cytoskeleton. *Current Biology,* **14**, 1296-302.

Sarbassov, D. D., Ali, S. M., Sengupta, S., Sheen, J.-H., Hsu, P. P., Bagley, A. F., Markhard, A. L. & Sabatini, D. M. (2006). Prolonged Rapamycin Treatment Inhibits mTORC2 Assembly and Akt/PKB. *Molecular Cell,* **22**, 159-168.

Seth, R. B., Sun, L., Ea, C. K. & Chen, Z. J. (2005). Identification and characterization of MAVS, a mitochondrial antiviral signaling protein that activates NF-kappaB and IRF 3. *Cell,* **122**, 669-82.

Shen, Z., Chakraborty, A., Jain, A., Giri, S., Ha, T., Prasanth, K. V. & Prasanth, S. G. (2012). Dynamic association of ORCA with prereplicative complex components regulates DNA replication initiation. *Molecular and Cellular Biology,* **32**, 3107-20.

Shen, Z., Sathyan, K. M., Geng, Y., Zheng, R., Chakraborty, A., Freeman, B., Wang, F., Prasanth, K. V. & Prasanth, S. G. (2010). A WD-repeat protein stabilizes ORC binding to chromatin. *Molecular Cell,* **40**, 99-111.

Shi, X., Jung, Y., Lin, L. J., Liu, C., Wu, C., Cann, I. K. & Ha, T. (2012). Quantitative fluorescence labeling of aldehyde-tagged proteins for single-molecule imaging. *Nature Methods,* **9**, 499-503.

Sofer, A., Lei, K., Johannessen, C. M. & Ellisen, L. W. (2005). Regulation of mTOR and cell growth in response to energy stress by REDD1. *Molecular and Cellular Biology,* **25**, 5834-45.

Stelzl, U., Worm, U., Lalowski, M., Haenig, C., Brembeck, F. H., Goehler, H., Stroedicke, M., Zenkner, M., Schoenherr, A., Koeppen, S., Timm, J., Mintzlaff, S., Abraham, C., Bock, N., Kietzmann, S., Goedde, A., Toksoz, E., Droege, A., Krobitsch, S., Korn, B., Birchmeier, W., Lehrach, H. & Wanker, E. E. (2005). A human protein-protein interaction network: a resource for annotating the proteome. *Cell,* **122**, 957-68.

Sun, L., Wu, J., Du, F., Chen, X. & Chen, Z. J. (2013). Cyclic GMP-AMP synthase is a cytosolic DNA sensor that activates the type I interferon pathway. *Science,* **339**, 786-91.

Sun, Y. & Chen, J. (2008). mTOR signaling: PLD takes center stage. *Cell Cycle,* **7**, 3118-23.

Takahara, T., Hara, K., Yonezawa, K., Sorimachi, H. & Maeda, T. (2006). Nutrient-dependent multimerization of the mammalian target of rapamycin through the N-terminal HEAT repeat region. *The Journal of Biological Chemistry,* **281**, 28605-14.

Tao, Z., Barker, J., Shi, S. D., Gehring, M. & Sun, S. (2010). Steady-state kinetic and inhibition studies of the mammalian target of rapamycin (mTOR) kinase domain and mTOR complexes. *Biochemistry.,* **49**, 8488-98.

Thedieck, K., Polak, P., Kim, M. L., Molle, K. D., Cohen, A., Jeno, P., Arrieumerlou, C. & Hall, M. N. (2007). PRAS40 and PRR5-like protein are new mTOR interactors that regulate apoptosis. *PloS ONE,* **2**, e1217.

Tombola, F., Ulbrich, M. H. & Isacoff, E. Y. (2008). The voltage-gated proton channel Hv1 has two pores, each controlled by one voltage sensor. *Neuron,* **58**, 546-56.

Ulbrich, M. H. & Isacoff, E. Y. (2007). Subunit counting in membrane-bound proteins. *Nature Methods,* **4**, 319-21.

Veigel, C. & Schmidt, C. F. (2011). Moving into the cell: single-molecule studies of molecular motors in complex environments. *Nature Reviews Molecular & Cell Biology,* **12**, 163-76.

Wan, Q., Ramsey, C. & Baran, G. (2010). Thermal pretreatment of silica composite filler materials. *Journal of Thermal Analysis and Calorimetry,* **99**, 237-243.

Wang, L., Harris, T. E., Roth, R. A. & Lawrence, J. C., Jr. (2007). PRAS40 regulates mTORC1 kinase activity by functioning as a direct inhibitor of substrate binding. *The Journal of Biological Chemistry,* **282**, 20036-44. Epub 2007 May 17.

Wang, L., Rhodes, C. J. & Lawrence, J. C., Jr. (2006). Activation of mammalian target of rapamycin (mTOR) by insulin is associated with stimulation of 4EBP1 binding to dimeric mTOR complex 1. *The Journal of Biological Chemistry,* **281**, 24293-303. Epub 2006 Jun 23.

Wu, B., Chen, Y. & Muller, J. D. (2009). Fluorescence fluctuation spectroscopy of mCherry in living cells. *Biophysical Journal,* **96**, 2391-404.

Wu, J., Sun, L., Chen, X., Du, F., Shi, H., Chen, C. & Chen, Z. J. (2013). Cyclic GMP-AMP is an endogenous second messenger in innate immune signaling by cytosolic DNA. *Science,* **339**, 826-30.

Wullschleger, S., Loewith, R., Oppliger, W. & Hall, M. N. (2005). Molecular organization of target of rapamycin complex 2. *The Journal of Biological Chemistry,* **280**, 30697-704. Epub 2005 Jul 7.

Wymann, M. P. & Schneiter, R. (2008). Lipid signalling in disease. *Nature Reviews Molecular & Cell Biology,* **9**, 162-76.

Yamada, T. & Bork, P. (2009). Evolution of biomolecular networks: lessons from metabolic and protein interactions. *Nature Reviews Molecular & Cell Biology,* **10**, 791-803.

Yang, H., Rudge, D. G., Koos, J. D., Vaidialingam, B., Yang, H. J. & Pavletich, N. P. (2013). mTOR kinase structure, mechanism and regulation. *Nature,* **497**, 217-23.

Yang, Q., Inoki, K., Ikenoue, T. & Guan, K. L. (2006). Identification of Sin1 as an essential TORC2 component required for complex formation and kinase activity. *Genes & Development,* **20**, 2820-32.

Yao, J. Z., Uttamapinant, C., Poloukhtine, A., Baskin, J. M., Codelli, J. A., Sletten, E. M., Bertozzi, C. R., Popik, V. V. & Ting, A. Y. (2012). Fluorophore targeting to cellular proteins via enzyme-mediated azide ligation and strain-promoted cycloaddition. *Journal of the American Chemical Society,* **134**, 3720-8.

Yardimci, H., Loveland, A. B., van Oijen, A. M. & Walter, J. C. (2012). Single-molecule analysis of DNA replication in Xenopus egg extracts. *Methods,* **57**, 179-186.

Yeom, K. H., Heo, I., Lee, J., Hohng, S., Kim, V. N. & Joo, C. (2011). Single-molecule approach to immunoprecipitated protein complexes: insights into miRNA uridylation. *EMBO Reports,* **12**, 690-6.

Yip, C. K., Murata, K., Walz, T., Sabatini, D. M. & Kang, S. A. (2010). Structure of the Human mTOR Complex I and Its Implications for Rapamycin Inhibition. *Molecular Cell,* **38**, 768-774.

Yoneyama, M., Kikuchi, M., Natsukawa, T., Shinobu, N., Imaizumi, T., Miyagishi, M., Taira, K., Akira, S. & Fujita, T. (2004). The RNA helicase RIG-I has an essential function in double-stranded RNA-induced innate antiviral responses. *Nature Immunology,* **5**, 730-7.

Yu, Y., Ulbrich, M. H., Li, M. H., Buraei, Z., Chen, X. Z., Ong, A. C., Tong, L., Isacoff, E. Y. & Yang, J. (2009). Structural and molecular basis of the assembly of the TRPP2/PKD1 complex. *Proceedings of the National Academy of Sciences of the United States of America,* **106**, 11558-63.

Zhang, Y., Billington, C. J., Jr., Pan, D. & Neufeld, T. P. (2006). Drosophila target of rapamycin kinase functions as a multimer. *Genetics.,* **172**, 355-62. Epub 2005 Oct 11.

Zhao, G., Perilla, J. R., Yufenyuy, E. L., Meng, X., Chen, B., Ning, J., Ahn, J., Gronenborn, A. M., Schulten, K., Aiken, C. & Zhang, P. (2013). Mature HIV-1 capsid structure by cryo-electron microscopy and all-atom molecular dynamics. *Nature,* **497**, 643-6.

Zheng, M., Wang, Y. H., Wu, X. N., Wu, S. Q., Lu, B. J., Dong, M. Q., Zhang, H., Sun, P., Lin, S. C., Guan, K. L. & Han, J. (2011). Inactivation of Rheb by PRAK-mediated phosphorylation is essential for energy-depletion-induced suppression of mTORC1. *Nature Cell Biology,* **13**, 263-72.

Zhou, M., Morgner, N., Barrera, N. P., Politis, A., Isaacson, S. C., Matak-Vinkovic, D., Murata, T., Bernal, R. A., Stock, D. & Robinson, C. V. (2011). Mass spectrometry of intact V-type ATPases reveals bound lipids and the effects of nucleotide binding. *Science,* **334**, 380-5.